Dipl.-Ing. Philipp Schmid, BSc

# Germanium Trihydrides and their Nanoparticle Derivatives: Expanding the Scope of the Dehydrogenative Coupling Process

**DOCTORAL THESIS**

to achieve the university degree of

Doktor der technischen Wissenschaften

submitted to

**Graz University of Technology**

**Supervisor**

Univ.-Prof. Dipl.-Chem. Dr.rer.nat. Frank Uhlig

Institute of Inorganic Chemistry

Faculty of Technical Chemistry, Chemical and Process Engineering and Biotechnology

Graz, May 2025

# Acknowledgement

The first person I would like to thank is Frank Uhlig. Not only did he offer me the opportunity to research my PhD thesis in his working group, he also facilitated amazing international experiences, such as my research stay in Japan and several conferences. His organizational leadership prevented some of the financial worries often plaguing PhD candidates, and his scientific input made this thesis what it is today.

I owe a lot to Vladimir Yaroslav Lee. My visit to Tsukuba was by his invitation. The time abroad, the new research angle and the resulting break with old habits gave me back my motivation and love for science when I needed it most. During and after this time, Vladimir also provided me with invaluable insights and guidance.

Another important mentor was Ana Torvisco. She helped me settle into the institute during my first year and showed me the ropes of publishing. Her copy editing and tips improved all my written output. In addition, Ana performed the X-ray crystallography reported in this thesis.

I would have never had the stamina to see this work through without all my colleagues at the Institute of Inorganic Chemistry, be it through feedback, suggestions or just a few beers together. While there are too many to name them all, I want to particularly thank Christoph, Doris and Yaiza, who have been with me throughout most of my time in the working group and turned from colleagues to friends.

During my PhD thesis, I had the pleasure of supervising many great students. Their lab work enabled me to put more focus on the theoretical side of things, and some of their experiments have made it into this thesis. Thank you to Maria, Magdalena, Laura, Irisa, Anna Maria and Paula, as well as Florian, who never actually worked for me, but still gave me cake, which is almost as important.

This work, especially the materials characterization part, relied on the input of many people for various measurements and interpretations. I am very grateful for the contributions of Karin Bartl, Brigitte Bitschnau, Angela Chemelli, Matjaž Finšgar, Manfred Kriechbaum, Ilse Letofsky-Papst, Johannes Rattenberger, Klaus

Reichmann, Robert Saf, Max Schmallegger and Glen Smales. Additionally, I am thankful for the assistance and lab supplies provided by Babsi, Jakob, Moni, Paul and Yaiza.

I also want to thank all the friends who have accompanied and supported me throughout my years of study. You know who you are, and I appreciate you a lot. Thank you to my brother Dominik, the chance to finish slightly sooner than him (despite taking longer in total) was all that kept me from procrastinating even more, and my other brother Jakob, who often provided me with food on my longest days when I had no time to organize any myself. A huge thank you to Resl, who supported me in good times and in bad, both before the begin of our relationship and ever since. Here's to many more great years.

Last but most certainly not least, I want to thank my parents. For their unwavering support, for their willingness to always listen to my venting, for all of their advice and of course their monetary assistance. Without them, my chemistry aspirations would have probably died during the bachelor.

# Abstract

Dehydrogenative coupling of tin trihydrides is a known strategy for the production of decorated metal nanoparticles. However, the resulting materials are insoluble and highly air sensitive. Due to the higher element-hydrogen bond energy of germanium, it promised to be a more stable alternative. Additionally, germanium is an appealing basis for nanomaterials due to its low toxicity, small bandgap and large excitonic Bohr radius. This provided motivation to investigate the suitability of germanium trihydrides as precursors for dehydrogenative coupling towards germanium nanoparticles.

To this end, aryl-, alkyl-, and (trialkylsilyl)germanium trihydrides were prepared as starting materials. The suitability of these compounds for dehydrogenative coupling was investigated under varying conditions. Silylgermanes required the lowest amount of energy to induce coupling, producing solid polymers within a few hours at 110 °C. Arylgermanes were successfully coupled at 160 °C within a day, or in less than an hour at 270 °C inside a microwave oven. Alkylgermanium trihydrides did not form a solid material under any of the tested conditions.

The properties of the materials produced from arylgermanes were comprehensively investigated with a multitude of methods. These polymers were identified as Ge(0) nanoparticles, capped by decorating aryl groups. They have sizes of 1–6 nm, which can be shaped both *via* the reaction conditions and through etching. A key benefit is their full dispersibility in THF.

In addition, the ability to invert the reactivity of organolithium bases towards arylgermanium trihydrides through solvent choice was discovered. Screening reactions were used to further investigate this reaction system. Additional relevant factors, such as the steric bulk of the reagents, were found.

# Kurzfassung

Die dehydrierende Kopplung von Zinntrihydriden ist eine bekannte Strategie für die Herstellung von dekorierten Metallnanopartikeln. Die resultierenden Materialien sind allerdings unlöslich und höchst luftempfindlich. Aufgrund der höheren Element-Wasserstoff-Bindungsenergie von Germanium war dieses als stabilere Alternative vielversprechend. Germanium ist außerdem aufgrund seiner geringen Giftigkeit, seiner kleinen Bandlücke und seines großes exzitonischen Bohrradius eine attraktive Basis für Nanomaterialien. Dies lieferte die Motivation, die Eignung von Germaniumtrihydriden als Edukte für die dehydrierende Kopplung zu Nanopartikeln zu untersuchen.

Zu diesem Zweck wurden Aryl-, Alkyl- und (Trialkylsilyl)germaniumtrihydride als Ausgangsmaterialien hergestellt. Silylgermane benötigten die geringste Energie, um die Kopplung einzuleiten, und wurden innerhalb weniger Stunden bei 110 °C zu festen Polymeren. Arylgermane wurden bei 160 °C innerhalb eines Tages oder in weniger als einer Stunde bei 270 °C in einem Mikrowellenofen erfolgreich gekoppelt. Alkylgermaniumtrihydride bildeten unter den getesten Bedingungen keine festen Materialien.

Die Eigenschaften der aus Arylgermanen hergestellten Materialien wurden mit einer Vielzahl von Methoden eingehend untersucht. Diese Polymere wurden als Ge(0) Nanopartikel identifiziert, die mit dekorativen Arylgruppen überzogen sind. Sie haben eine Größe von 1–6 nm, die sowohl über die Reaktionsbedingungen als auch durch Ätzen beeinflusst werden kann. Ein wesentlicher Vorteil ist ihre vollständige Dispergierbarkeit in THF.

Darüber hinaus wurde die Möglichkeit entdeckt, die Reaktivität von Organolithiumbasen gegenüber Arylgermaniumtrihydriden durch die Wahl des Lösungsmittels zu invertieren. Zur weiteren Untersuchung dieses Reaktionssystems wurden Screening-Reaktionen durchgeführt. Weitere relevante Faktoren, wie etwa der sterische Anspruch der Reagenzien, wurden gefunden.

# Contents

# I. Introduction

Nanomaterials have drawn immense interest from the scientific community ever since Richard Feynman popularized the idea of nanoscale machines in 1959.[1] Their attraction lies in their unique properties which differ greatly from the bulk material. Nanomaterials have very high surface to volume ratios, increasing the relevance of surface properties. Additionally, the small size restricts the movement of subatomic particles and various quantum mechanical effects become noticeable. As a result, nanomaterials exhibit changes in reactivity, dispersibility, absorptivity and many other areas.[2,3]

A wide array of both potential and realized applications is known for group 14 nanoparticles. Their versatility has seen them included in all areas of modern life, such as agriculture, food safety, ecology, environmental protection, medicine, energy storage, solar cells, catalysis, security and fashion.[3,4,5–7] Consequently, these materials are an appealing research target. The focus of our working group is the preparation and characterization of germanium and tin nanoparticles, as knowledge about carbon- and silicon-based nanomaterials is quite comprehensive already.

There are a few different methods to choose from when polymerizing tin and germanium. Dehydrogenative coupling of the corresponding hydrides was chosen for our research due to the simplicity of the process and the comparably soft reaction conditions.[8,9] Considerable knowledge had previously been obtained on the preparation of aryl decorated tin nanoparticles from aryltin trihydrides ($ArSnH_3$) using a dehydrogenative coupling process. This reaction, particularly when catalyzed with an amine base, boasts high reaction speeds, low energy requirements and great yields. In addition, the workup is simple. The particles can be isolated through centrifugation, filtration or evacuation.[10] However, despite these advantages, the high reactivity of tin as center metal (caused by the weakness of the Sn-H bonds) comes with severe drawbacks. The trihydride precursors need to be stored at -80 °C to prevent degradation, and kept inert at all times.[11] While the nanoparticulate products are temperature stable, they are even more air sensitive, to the point of pyrophoricity. In addition, the obtained powder is completely insoluble in all common laboratory solvents. These disadvantages prevent a characterization of the obtained

nanomaterial beyond descriptions of size, composition and micromorphology.[10] The possibilities for further applications are also severely limited. While interesting insights were gained into the mechanism of the dehydrogenative coupling reaction and the relevant factors shaping the outcome, it was ultimately decided that germanium was the more promising candidate for further research into group 14 nanoparticles.

The goal of this work was to find a suitable method for the preparation of germanium nanoparticles through dehydrogenative coupling and to characterize the obtained materials. Various aryl- and silylgermanium trihydrides were to be prepared as starting materials. A simplified overview of the practical work presented in this thesis is shown in Scheme 1.

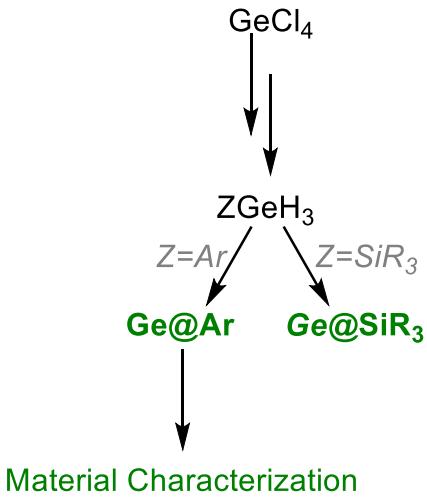


**Scheme 1:** Simplified project overview with original research shown in green

# II. Literature Review

## 2.1 Organogermanes

### 2.1.1 History

Organogermanes are defined as compounds with at least one carbon-germanium bond. Their first representative was prepared in 1887 by Clemens Winkler, after his discovery of germanium in 1886. He reacted $GeCl_4$ with $Et_2Zn$ to obtain $Et_4Ge$.[12] The following years, low germanium availability caused researchers to focus on its general properties, occurrences and extraction procedures over chemical aspects. Interest in the synthetic side of germanium finally picked up again in 1925 with the discovery of additional germanium sources. Morgan and Drew prepared the compounds $Ph_nGeBr_{4-n}$ (n=1–4) and $Ph_6Ge_2$.[13] Their work pioneered the use of Grignard reagents and Wurtz type couplings in organogermanium chemistry, both of which remain highly relevant to this day. More tetraorganogermanes,[14] organogermanium halides[15] and hydrides[16] soon followed. Kraus and Brown were the first to synthesize organogermanium polymers, also *via* a Wurtz type coupling.[17] Further advances were made by Schwarz *et al.*, who prepared optically active and heterocyclic germanes.[18] Arylgermanium trihydrides, central to this work, were not described until much later, in 1963.[19]

### 2.1.2 Organogermanium Halides

Germanium halides are the prevalent starting materials for organogermanium chemistry. A plethora of different reactions is known for the derivatization and further functionalization of germanium halides. In contrast to the related halosilanes, halogermanes are not as readily hydrolyzed by water. Only the fully halogenated $GeX_4$ (X=halogene) molecules show notable reactivity towards $H_2O$.[20,21] Organogermanium halides generally require an alkaline solution to undergo hydrolysis.[22,23] The halides are also temperature stable and can be purified through distillation.[22,24–26]

Preparation procedures typically start with the commercially available tetrahalides $GeX_4$. The most straightforward way to introduce organic groups is the use of either Grignard or organolithium reagents (Scheme 2). When used to prepare derivatives with three or four sterically demanding groups, these methods work selectively.[21,27]

However, if fewer or smaller organic substituents are desired, the reagents tend to substitute more halides than intended.

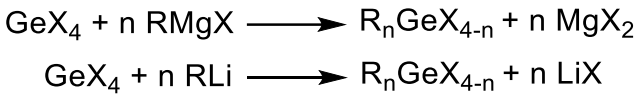


**Scheme 2:** Preparation of organogermanium halides *via* Grignard or organolithium reagents, n=1–3

Even with carefully optimized stoichiometry and reaction conditions, a product mixture can often not be avoided.[24,28,29,30] Reduced yields and a tedious workup are the consequences. Additionally, germanium halides are subject to spontaneous halogen exchange reactions. Reacting chlorogermanes with organic bromides, for example, results in the formation of mixed bromo(chloro)germanes.[22,23] Depending on the intended use of the reaction products, this might necessitate additional purification work, for example through conversion to the corresponding hydrides followed by chlorination.[21,31] A method for more selective preparation of arylated halogermanes *via* the Grignard route is the intentional generation of tri- or tetraarylgermanes. Superfluous aryl groups can then be cleaved off with several methods.[16,28,32] Selectivity can also be increased by replacing $GeX_4$ with $Ge(OEt)_4$ as starting material.[33–35] The resulting ethoxy(organo)germanes can be easily converted to the corresponding halogermanes, for example with acetyl chloride or HCl.[34,36] Despite the more selective product formation, $Ge(OEt)_4$ is not as popular as $GeX_4$ precursors, due to its lower accessibility.

The Kozeschkow redistribution, a standard procedure for the selective synthesis of organotin halides, is unfortunately more complicated in organogermanium chemistry.[37] The reaction requires either an $AlCl_3$ catalyst or extreme conditions.[38] Furthermore, because mono- and dihalides $R_3GeX$ and $R_2GeX_2$ form preferentially, attempts to synthesize trihalides $RGeX_3$ often lead to low yields and product mixtures.[38,39] Redistribution reactions between $GeCl_4$ and weaker group 14 reagents according to Scheme 3 have been developed as a workaround. However, because there is often no use for the secondary product, the atom efficiency of this process is low.[25,40,41]

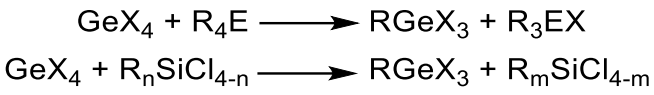

**Scheme 3:** Redistribution reaction towards organogermanium trihalides, E=Sn, Pb

Another approach for the selective synthesis of trihalides is the insertion reaction of $GeX_2$*1,4-Dioxane into an organic halide.[33,42] This offers a way to generate the target molecule in high yields without side reactions. However, the precursor is once again less accessible than $GeX_4$, preventing more widespread adoption.

Rochow, who developed the Müller-Rochow process, reported a very similar synthesis for dimethylgermanium dichloride from Ge(0) (Scheme 4). He also demonstrated its general applicability for other organic substituents and bromo derivatives.[43] However, this route is mostly outclassed by other procedures. Only $Me_2GeCl_2$ is still occasionally prepared *via* the Rochow process.

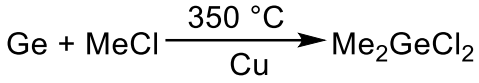

**Scheme 4:** Direct synthesis of $Me_2GeCl_2$ from Ge(0).

Over the past century, researchers have also experimented with some other synthetic approaches that found only limited adoption by the scientific community. The proliferation of cheaper, faster and less dangerous methods has rendered them largely obsolete. Scheme 5 provides an overview of these reactions.

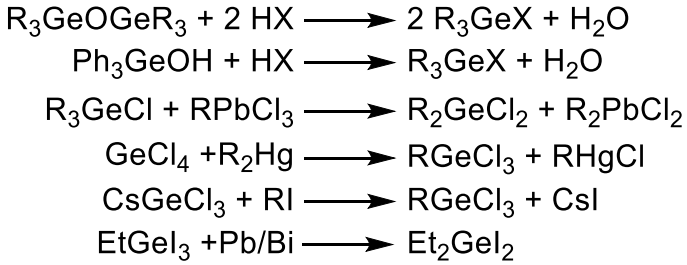

**Scheme 5:** Less common synthetic strategies towards organogermanium halides[14,16,25,44]

### 2.1.3 Organogermanium Hydrides

Germanium was crucial to the rise of the semiconductor industry through its role in the invention of the transistor and semiconductor production *via* chemical vapor deposition (CVD) is still the biggest commercial application of germanium hydrides.[45] Originally monogermane ($GeH_4$) had been the compound of choice for

thin film production.[46] However, its high toxicity and combustibility have increasingly lead to the investigation of organogermanes as less problematic replacement. Various organogermanes ($Me_nGeH_{4-n}$, $Et_nGeH_{4-n}$, *i*-$BuGeH_3$, *t*-$BuGeH_3$, $(GeH_3)_3CH$, $(GeH_3)_2CH_2$; n=1–3) have been reported in this role.[47] Other potential applications of organogermanium hydrides lie in hydrogen storage, as reducing agents and as starting materials for a variety of reactions, such as the lithiation and polymerization utilized in this work.[48]

Synthetic germanium hydride chemistry found its start in 1902 with the preparation of $GeH_4$. Voegelen used Zink and sulfuric acid as $H_2$ source to convert $GeCl_4$ to $GeH_4$.[49] The first organic germanium hydride was synthesized by reacting the sodium derivative with ammonium bromide (Scheme 6) or water.[16]

$$Ph_6Ge_2 + 2\ Na \longrightarrow 2\ Ph_3GeNa$$
$$Ph_3GeNa + NH_4Br \longrightarrow Ph_3GeH + NH_3 + NaBr$$

**Scheme 6:** Synthesis of the first organogermanium hydride

Alkali metal germanides remained the reagent of choice for hydride preparation for quite a while. In a procedure similar to Scheme 6, triethylgermane ($Et_3GeH$) was synthesized from $Et_6Ge_2$ and Li.[50] The first monoalkylgermanium trihydrides and various polyalkylgermanium hydrides were prepared with a slight variation of the method, by quenching alkali metal germanides with alkyl halogenides. An attempt to access arylgermanium trihydrides *via* this route failed.[51]

The most important breakthrough in germanium hydride chemistry was the discovery of lithium aluminum hydride ($LiAlH_4$) by Finholt, Bond and Schlesinger in 1947.[52] $LiAlH_4$ is an easily synthesized reducing agent. It is also able to convert various functionalized germanes, including halogermanes, to hydrides according to Scheme 7. Many new compounds became accessible due to this advancement.[25,53,54] Hydrogenation with $LiAlH_4$ remains the preferred method for lab scale preparation of organogermanium hydrides to this day.[55]

$$R_nGeX_{4-n} + LiAlH_4 \xrightarrow[-LiX,\ -AlX_3]{} R_nGeH_{4-n}$$

**Scheme 7:** Reduction of halogermanes with $LiAlH_4$

The stability of hydrides $R_nGeH_{4-n}$ towards thermal decomposition, hydrolysis and oxidation increases with the number and steric demand of the R substituents. Their reactivity in various applications consequently decreases in the same direction. Due to the very similar electronegativities of Ge and H, the polarity of the bond largely depends on the other substituents. As such the hydrogen atom can exhibit either protic or hydridic character.[45,55,56]

Almost all of this work relies on arylgermanium trihydrides ($ArGeH_3$), a subclass of organogermanium hydrides, as precursors. It should come as no surprise that the most basic representative of the class, $PhGeH_3$, was the first to be synthesized.[19] It is also by far the most common representative (102 references indexed by SciFinder as of January 2025, followed by 13 for mesityl$GeH_3$). A variety of arylgermanes are known, almost all of which have been prepared using $LiAlH_4$ (Table 1). Nevertheless, the overall amount of research into these compounds is relatively low, as they have not found any widespread applications yet. Many of the available publications focus on basic properties, such as preparation methods, reactivity, structure and spectra.[28,33,57,58] Others only utilized them for halide purification (see 2.1.2). Among the synthetic applications of trihydrides, hydrogermylation, transition metal complexes and catenation are the most prominent.[29,59,60,61]

**Table 1:** Synthetic strategies for the first reported preparation of selected Arylgermanes $ArGeH_3$

| Aryl Group | First Reported | Original Preparation Method |
|---|---|---|
| Ph | 1963[19] | $Ar_2Hg + GeCl_4$; $LiAlH_4$ |
| *p*-MeOPh | 1968[62] | $ArI + GeI_2$; $LiAlH_4$ |
| *p*-XPh (X=F, Cl) | 1972[57] | $ArMgBr + GeCl_4$; $LiAlH_4$ |
| *p*-tolyl | 1973[63] | $ArMgBr + GeCl_4$; $LiAlH_4$ |
| $C_6F_5$ | 1974[64] | $ArGeBr_3 + LiAlH_4$ |
| mesityl | 1979[65] | $ArMgBr + GeCl_4$, $LiAlH_4$ |
| *i*-$Pr_3$Ph | 1997[21] | $ArMgBr + GeCl_4$, $LiAlH_4$ |
| 8-MeO-1-naphthyl | 1998[66] | $Ar_2Mg + GeCl_4$; $LiAlH_4$ |
| *t*-$Bu_3$Ph | 2001[67] | $ArLi + GeCl_4$; $LiAlH_4$ |
| 2,6-(2,6-*i*-$Pr_2$Ph)$_2$Ph | 2005[68] | *a)* $(ArGeH_2)_2 + H_2$<br>*b)* $ArGe(OMe)_3 + LiAlH_4$ |
| 2,6-mesityl$_2$Ph | 2008[69] | $ArLi + GeCl_4$; $LiAlH_4$ |
| 2,6-(2,4,6-*i*$Pr_3$)Ph | 2019[70] | $ArLi + GeCl_4$; $LiAlH_4$ |
| 1-naphthyl, *p*-*n*-BuPh, (2,5-; 2,6-; 3,5-)-xylyl | 2022[28] | $ArMgBr + GeCl_4$; $LiAlH_4$ |
| 2-naphthyl, *o*-tolyl, *p*-$CF_3$Ph, *p*-$CH_3$SiPh | 2022[61] | $ArMgBr + GeCl_4$; $LiAlH_4$ |

## 2.2 Silylgermanes

### 2.2.1 General aspects

Silylgermanes (or, less common, germylsilanes) are compounds of the nature $R_3SiGeR_3$ with at least one single bond between germanium and silicone. The name and basic structure are derived from silylgermane $H_3SiGeH_3$. Like Ge-H compounds (Chapter 2.1.3), the bond polarity is strongly influenced by the other substituents attached to both Si and Ge, owing to their similar electronegativities. The inclusion of silicon into germanium compounds can be used to fine tune the band gap and create new types of semiconducting materials.[71]

Ge-C bonds are the backbone of organogermanium chemistry. As a Group 14 element, the potential of germanium for catenation was also expected and confirmed early on.[13] Naturally, investigations into Ge-E bonds with the neighboring group 14 elements followed soon. The first silylgermane, $Et_3SiGePh_3$, was isolated in 1934 from the reaction of sodium triphenyl germanide with triethylsilicon bromide.[72] This is yet another example of a compound class where the original synthetic strategy remains prevalent throughout its history (Scheme 8).

$$R_3EX + R'_3E'M \longrightarrow R_3EE'R'_3 + MX$$

**Scheme 8:** Basic method for forming Ge-Si bonds; E,E'=Ge,Si; X=halogene; M=alkali metal

Over the next three decades, silylgermane chemistry generated only limited interest. $(Ph_3Ge)_3SiH$[73] and $Ph_3GeSiPh_3$[74] were the only newly prepared compounds, reported in the 50s. Synthesis of the eponymous silylgermane $H_3SiGeH_3$ was hindered by the more complicated process and the hazardous nature of the involved chemicals. It was not isolated until 1963.[75] This coincided with a resurgent interest in silylgermanes. Over the next decades, the classic coupling of halogenides with alkali metal derivatives, as well as direct Wurtz type couplings, were used to expand the number of published silylgermanes.[76] More recent preparation strategies include the use of Grignard type reagents[77], germylzinc chloride[78] and electroreduction[79], or the insertion of a tetrylene species into E-Cl and E-H bonds[80]. The wide variety of uzilized synthetic strategies and obtained compounds showcase the scope and diversity of the field.

### 2.2.2 Sterically Encumbered Alkylsilylgermanes

Alkylsilanes with low steric encumbrance, like $Me_3SiX$, are labile groups prone to solvolysis and other degradation reactions.[81] This limits their applications. The stability can be improved considerably with bulkier substituents, for example a *tert*-butyl group. The steric shielding hinders access to the silicon. Degradation reactions are slowed or stopped entirely.

The first *tert*-butyl silicon compound, *t*-$BuSiCl_3$, was synthesized in 1947 by Tyler and Sommer. They confirmed it was more stable than other known alkyltrichlorosilanes.[82] Their continued research led to the inclusion of the *tert*-butyl group in a trialkylsilane: *tert*-butyl-di-methyl-silyl (henceforth abbreviated as TBDMS) chloride (Scheme 9).[83]

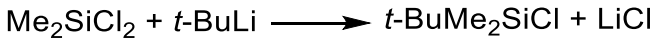


**Scheme 9:** Synthesis of TBDMSCl by Tyler and Sommer[83]

TBDMSGe($Me_2$)Ph, synthesized in 1996, was the first reported silylgermane containing the group. Sharma *et al.* used it to stabilize their silyl substituent and allow for selective replacement of a Ge-Ph bond with Ge-Cl through HCl/$AlCl_3$ (Scheme 10).[84] The crucial role of the *tert*-butyl group in stabilizing silylgermanes during aryl cleavage was later demonstrated in experiments with with triflic acid (TfOH).[71] TBDMS is also used to stabilize digermenes, germyllithiums and strained Ge containing rings.[85]

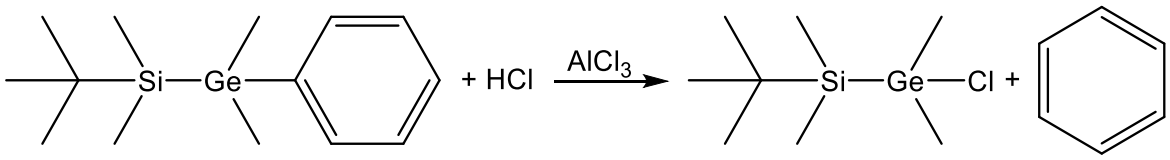


**Scheme 10:** Use of a sterically encumbered (trialkylsilyl)germane by Sharma *et al.*[84]

Trialkylsilanes with two *tert*-butyl groups are markedly harder to obtain. Attempts to react *t*-$Bu_2SiCl_2$ with MeLi or *t*-BuMe$SiCl_2$ with *t*-BuLi failed even under harsh conditions. The enormous steric bulk prevents the substitution of the chloride. The challenge was solved in 1975, when Doyle and West succeeded in preparing di-*tert*-butylmethylsilyl (henceforth abbreviated as DTBMS) hydride DTBMSH alongside the similarly elusive *t*-$Bu_3SiH$.[86] They demonstrated that, while electronically beneficial, the steric demand of the second chlorine atom in

*t*-$Bu_2MeSiCl_2$ blocks access of the MeLi. Replacing one chlorine with hydrogen solves the issue, and *t*-$Bu_2SiClH$ readily reacted with both MeLi and even *t*-BuLi. The method was soon improved upon by reversing the order of alkyl substitutions, reacting $MeSiCl_2H$ with *t*-BuLi.[81] DTBMSH is easily brominated with $Br_2$ to enable further reactions.[87] The first use of the group in silylgermane chemistry was once again to facilitate selective Ge-Ph cleavage.[88] Other applications of DBTMS are unsurprisingly also similar to those of TBDMS (see above). Especially Lee, Sekiguchi and varying coworkers have made use of its stabilizing effect to synthesize new digermenes, germyllithiums and strained rings like the one in Scheme 11.[89,90,91]

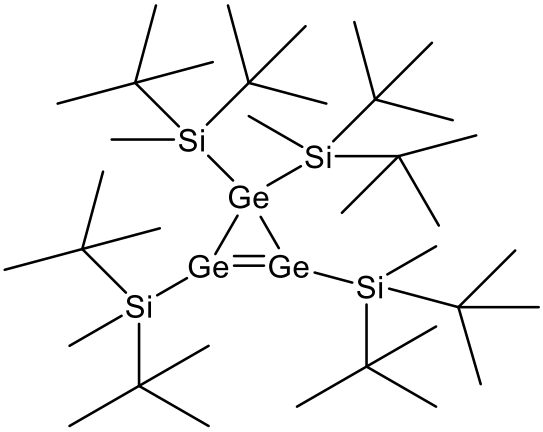


**Scheme 11:** Cyclo trigermene with bulky trialkylsilyl groups for stabilization[91]

## 2.3 Germanium Nanomaterials

### 2.3.1 Properties and Applications

Germanium is a semiconducting material with a narrow bandgap. Semiconductor nanocrystals dimensioned smaller than their excitonic Bohr radius experience quantum confinement. The band gap increases with decreasing size. Optical and electronic properties become size dependent as a result, making it possible to fine-tune them.[92] Germanium has a relatively large excitonic Bohr radius, leading to strong quantum confinement effects.[93] As a result, increasing nanocrystal sizes causes a red shift in their absorption, with the larger particles often absorbing the entire visible spectrum and beyond.[94–96] In addition, germanium nanocrystals often feature size dependent photoluminescence.[93,96–98] The low quantum yields observed in some of these publications are attributed to surface passivation, defects and impurities.[96,99,100] The unique optical and electronic properties of germanium have led to its inclusion in devices such as solar cells, photodetectors and field effect transistors.[6,101,102]

As bulk material, germanium is considered non-toxic. Toxicity research into germanium nanoparticles has produced conflicting results so far.[98,99,103] The surface chemistry appears to play a major role, with cationic particles being more dangerous, partly due to higher cellular uptake.[104] However, the overall amount of research into the biocompatibility of nanogermanium is still low.[105] Functionalized particles that combine high cellular uptake and low toxicity would have high potential in bioimaging and drug delivery applications.[104]

Germanium nanoparticles could also possibly overcome a longstanding problem with lithium ion batteries: The achievable energy density is limited by the 372 mAh/g maximum capacity of commercial graphite anodes.[106] While germanium has a much higher theoretical limit of 1600 mAh/g, its 370% volume increase during lithium intercalation prevents the manufacture of commercial devices. Nanoscale germanium materials could overcome this problem through buffering the volume expansion in an encapsulating matrix. The practical viability of this approach was demonstrated in many experiments.[7,107]

### 2.3.2 Preparation

Due to their high importance for modern life, production methods for nanoscale semiconductors have long drawn immense research interest. As such, plenty of different methods to generate germanium nanoparticles are known. All nanomaterials are either assembled from smaller molecules in so called “bottom-up” processes or freed from the bulk with “top-down” methods. In the case of germanium, top-down methods are rare. Only a few techniques have been described. For example, germanium nanoparticles have been prepared by laser ablation and bead milling, with photoetching being used to further decrease particle size.[108] Bottom-up procedures can be further categorized into two general approaches: Gas phase and solution methods, with the gas phase techniques being developed considerably earlier.

Germanium nanoparticles were reported at least as early as 1977. In a very straightforward approach, bulk germanium was evaporated in an inert atmosphere. As the vapor cooled, nanoparticles of varying sizes started to form.[109] The first particles with confirmed crystallinity were produced soon after with a very similar process.[110] However, the technique is limited to pure germanium. Using sputtering made it possible to generate decorated (Ge@H), alloyed ($Si_xGe_{1-x}$@H) and matrix embedded ($Ge:SiO_2$) nanoparticles.[111] The $Ge:SiO_2$ in particular drew immense interest for the study of quantum effects in nanoparticles.[94,112] Another way towards matrix embedded Ge-NPs is chemical vapor deposition.[113] All these techniques have in common that they rely heavily on gas phase processes.

Finally, in 1994, Heath *et al.* reported an inorganic solution phase synthesis of germanium nanoparticles through the reduction of chlorogermanes (Scheme 12). The use of $PhGeCl_3$ in the reaction mixture served to limit particle growth and prevent formation of bulk Ge(0).[114] Reduction of germanium halides has remained a popular synthetic choice ever since.

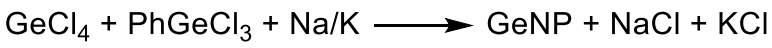


**Scheme 12:** Reduction of chlorogermanes to germanium nanoparticles as reported by Heath *et al.*[114]

$GeCl_4$ and $GeI_4$, as well as $GeBr_2$ and $GeI_2$ have all been reduced under a variety of conditions. Most researchers added surfactants rather than substituted germanes to

limit growth, because it affords higher size and shape control. While halide reduction usually produces monodisperse particles with narrow size distributions, the need for strong reducing agents or high reaction temperatures is a considerable disadvantage. When hydridic reducing agents are used, the unavoidable formation of the hazardous byproduct $GeH_4$ also significantly reduces the yield.[96,98,102,115]

A second widespread approach for liquid phase synthesis of germanium nanoparticles is the thermal decomposition of various germane precursors. Here, the dissolved or neat precursor is subjected to high temperatures either in pressurized reactors or under reflux. Inclusions of organic decomposition products in the final material can pose a problem with this method, as they are often difficult to remove.[116,117]

In sol gel processes, only some steps occur in solution. Dissolved precursors are first hydrolyzed to a polymer. Upon thermal or reductive decomposition, nanoparticles form inside an encapsulating matrix. If necessary, the matrix can be removed through etching processes to liberate the particles .[118]

There are also some less common approaches. Subjecting Zintl salts to metathesis with $GeCl_4$ or reaction with $NH_4Br$ and the spontaneous disproportionation of GeBr have only seen a handful of uses each.[119,120] Dehydrogenative coupling is even rarer. Despite being well established for the production of tin nanomaterials, only some preliminary attempts towards germanium nanomaterials have been reported. They are discussed in greater detail in chapter 2.4.3.

## 2.4 Dehydrogenative Coupling

### 2.4.1 Overview

Dehydrogenative coupling is a versatile condensation reaction. Both homo- and hetero-couplings are possible with many elements, including those of group 14. In carbon-carbon couplings, hydrogen acceptors such as oxygen or peroxides are used to overcome the high C-H bond energy and increase the thermodynamic favorability.[121] The higher group 14 homologues can be coupled while allowing $H_2$ evolution due to their progressively weaker E-H bonds (Scheme 13).[45]

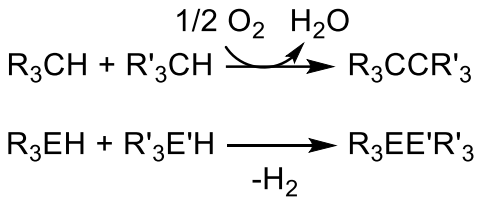


**Scheme 13:** Dehydrogenative coupling between group 14 elements; E, E' = Si, Ge, Sn

While the low bond strengths of higher group 14 elements, especially tin, enable catalyst free dehydrogenations,[8,122,123] catalyzed syntheses are more common. By far the most prevalent class of catalysts are transition metal complexes. Initially only $(Ph_3P)_3RhCl$, Wilkinson's Catalyst, was used in this role.[124] However, after the polymerization of $RSiH_3$ with titanocene was reported to be "orders of magnitude more active"[125], metallocenes quickly surpassed the rhodium complex in popularity.[126,127,128] Their dominance notwithstanding, numerous other complexes have been investigated.[129] The catalytic mechanism depends on the type of complex, the center metal and the used trihydride and is still ambiguous in some cases.[130]

Amine bases also represent a noteworthy group of dehydrogenation catalysts. They were first used by Neumann and König in the polymerization of $Ph_2SnH_2$.[131] Although far less common than transition metals, several benefits make their consideration worthwhile. Amine bases are cheap, ubiquitous compounds. They are often volatile liquids, and as such easy to remove during workup. Different catalyst types also enable conversion of a wider variety of precursors. For example, a comparative study found that tetramethylethylenediamine (TMEDA) is vastly superior to Wilkinson's Catalyst in the polymerization of diaryl- and (alkylaryl)tin dihydrides.[9] The donor capabilities of amine bases were also used to prepare and

stabilize divalent organostannanes.[132] Two different mechanisms for amine base catalysis in tin dehydrocouplings have been proposed. According to mechanism **I**, the amine initially coordinates to the metal center to promote hydrogen cleavage. Mechanisms **II** proposes that $H^+$ abstraction by the amine base is the initial step. Although some data points towards mechanism **II**, a definite conclusion cannot be drawn at this time.[10,132]

In an interesting contrast to the base catalyzed coupling of stannanes, the polymerization of monophenyl silane $PhSiH_3$ is promoted by the Lewis acidic catalyst $(B(C_6F_5)_3$. The initiation is proposed to occur through abstraction of a hydridic $H^-$ by the borane, mirroring the above described mechanism **II**. The propagation results in Ph-H elimination, a further parallel to the corresponding stannanes (see below).[133]

### 2.4.2 Aryl Decorated Tin Nanoparticles Sn@Ar

The successful utilization of TMEDA to promote dehydrogenative coupling generated additional interest into amine base catalysts. Especially aryltin trihydrides sparked the interest of various groups, as they had been largely neglected at that time. Sindlinger *et al.* used the very bulky terphenyl as aryl group. The large steric shield prevented the abstraction of more than one hydrogen. Depending on the reaction conditions, distannane $ArH_2SnSnH_2Ar$, adduct ArSnH(base) or free, dimeric stannylene $[ArSnH]_2$ were observed.[132]

Smaller aryl groups were investigated by Zeppek as part of her doctoral thesis. Adding TMEDA to *o*-tolyl$SnH_3$ in $Et_2O$ produced black, insoluble powder, highly susceptible to oxidation. An observed lack of powder XRD signals was attributed to insufficient particle size. The reported correlation length supports this, giving particle size estimates around 1.5 nm. Of particular note was the discovery of toluene in the reaction supernatant. The only possible source was elimination of *o*-tolyl, a stark mechanistic difference to the polymerization of diaryltin dihydrides. The removal of aromatic substituents in addition to $H_2$ suggested the presence of “naked” tin atoms, bound only to other tin atoms. A sub stoichiometric amount of C and H shown by elemental analysis (EA) and a phase transition at the melting point of Sn(0) in thermogravimetric analysis (TGA) provided further evidence for this theory. Based on these results, the obtained material was not reported as polymer network $[o\text{-tolySn}]_n$, but rather as *o*-tolyl decorated nanoparticles Sn@*o*-tolyl.[10]

DFT calculations and *in situ* UV/Vis were employed to propose a mechanism: Removal of $H_2$ leads to a dimeric intermediate (detected using $^1H$ NMR). It can undergo either toluene elimination or hydrogen rearrangement and heterolytic cleavage. The resulting divalent tin species is unstable and inserts into an Sn-Sn bond, growing the polymer (Scheme 14).[10]

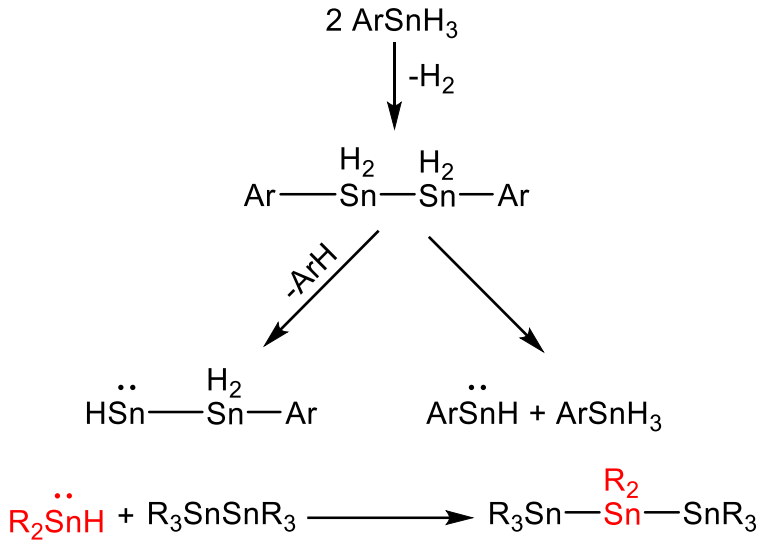


**Scheme 14:** Dehydrogenative coupling mechanism of aryltin trihydrides as proposed by Zeppek,[10] formation of the transition states demonstrated for bulky arylgermanes by Sindlinger *et al.*[132]

The properties of the obtained nanomaterials could be shaped *via* the reaction parameters. For example, larger aryl substituents produced bigger particles. Both solvent and catalyst choice also influenced the size. Lower donor capabilities and less basic amines were loosely associated with increased aryl cleavage, leading to additional coupling sites and larger nanoparticles. However, this was sometimes overshadowed by other factors that were not identified. For example, Pyridine catalysis resulted in almost complete dearylation, producing by far the largest particles (2.1 nm) of all investigated bases. A similarly drastic effect was only reproduced by omitting the catalyst altogether. These thermal dehydrocoupling reactions lasted anywhere from one (50 °C) to four (RT) weeks. The larger particles were sufficient in size to produce crystalline scattering signals. Their diffraction pattern matches that of β-Sn. This demonstrates the presence of ordered Sn(0) domains within each particle.[10,123,134]

Unfortunately, the high air sensitivity and lack of solubility prevented the use of many important analytical techniques. GPC, DLS, MS, NMR and UV/Vis were all not

suitable for the nanoparticles. While TEM was attempted the results were unsatisfactory. In addition to characterization, the potential for material processing or functionalization is also hampered by these hurdles. Consequently, research into aryl decorated tin nanoparticles has lain dormant in recent years.

### 2.4.3 Dehydrogenative Coupling in Germanium Chemistry

The coupling of monogermane $GeH_4$ in an ozonizer by Drake and Jolly in 1962 represents arguably the first use of dehydrogenative coupling in germanium chemistry (Scheme 15). They obtained degrees of polymerization up to n=9.[135]

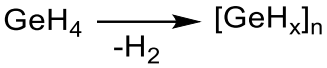


**Scheme 15:** Dehydrogenative coupling of monogermane

Dehydrocoupling of organogermanes was first reported in 1973. The approach is remarkably similar to the one used for nanoparticle generation in this work (see below. An amine base was used to abstract both hydrogen and aromatic groups from an arylgermanium trihydride (Scheme 16). Both oligomers and orange polymer were obtained, albeit the polymer was not characterized.[136] Two further coupling attempts, refluxing of $Et_2GeH_2$ over stainless steel wool and heating of $Ph_2GeH_2$ in the presence of titanocene only resulted in small oligomers with n≤4.[126,137]


**Scheme 16:** Dehydrocoupling of cyclopentadienyl germane

Pairing a zirconocene catalyst with *n*-BuLi in the polymerization of $PhGeH_3$ finally produced a polymer with high molecular weights ($M_w = 4*10^3–7*10^3$ Da). The product was a soluble yellow powder. However, characterization data suggested that the degree of cross-linking remained low. The material properties were very similar to those of linear polymers.[128]

Wolf attempted to apply the process developed for tin nanoparticle synthesis (Chapter 2.4.2) to germanium. However, this only resulted in colorless powder, which was not characterized.[138] Further experiments into the dehydrogenative coupling of arylgermanium trihydrides were undertaken by Traxler as part of his master's thesis. Theorizing that the lack of appreciable yield obtained by Wolf was

due to the higher bond energies of organogermanes compared to organostannanes (*e.g.* E-H: 335 kJ/mol in $Ph_3GeH$[139] *vs.* 290 kJ/mol in $Ph_3SnH$[140]), considerably harsher conditions were chosen. 1-Naphthyl$GeH_3$ was successfully decomposed by heating it to 220 °C for 68 hours to yield ~50% of orange-brown powder. The color change, as well as the identification of cleaved naphthalene, were taken as strong indications of successful synthesis of Ge@1-naphthyl nanoparticles (Scheme 17).[141]

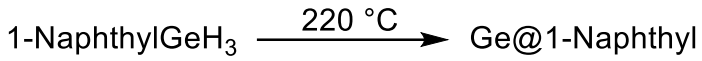


**Scheme 17:** Thermal dehydrocoupling of 1-naphthyl$GeH_3$

The catalytic properties of TMEDA were investigated in pressurized microwave reactions, as its boiling point (121 °C) made it unsuitable for thermal decomposition at 220 °C at room pressure. However, the yields of microwave reactions remained considerably below those achieved with conventional heating. The presence of leftover starting material confirmed an incomplete reaction. Full conversion could not be achieved.[141]

The work of Traxler established important baseline facts about the thermal dehydrocoupling of arylgermanes. The reaction proceeds similar to the process established for Sn@Ar (see above): In addition to dehydrogenation, aryl groups are partially eliminated as ArH. Particle sizes can be increased through the use of bulkier aryl substituents. While TMEDA acts as catalyst, the effect is drastically weaker than in the tin-based system. Most importantly however, Traxler demonstrated that Ge@Ar nanoparticles obtained with his process are at least partially dispersible in many common solvents.[141] Lack of dispersibility was one of the biggest obstacles in Sn@Ar studies. Overcoming this obstacle demonstrated the high potential of further research into aryl decorated germanium nanoparticles and was part of the motivation for my work. It aims to expand knowledge about this synthetic method and help establish it as a tool for nanomaterial scientists.

# III. Results

## 3.1 Synthesis of Organo- and Organo(halo)germanes

All the organogermanium trihydrides utilized in this work are literature known compounds. Their synthesis followed well-established procedures.[28] This chapter will therefore be kept brief.

### 3.1.1 Grignard Reaction

Preparation *via* the Grignard route was attempted at least once for all organogermanes. In the standard variant, aryl bromide was reacted with magnesium in $Et_2O$ or THF, and the resulting Grignard reagent dripped slowly into a cooled $GeCl_4$ solution (Scheme 18).[28,142]

$$RBr + Mg \xrightarrow[\text{reflux}]{THF/Et_2O} RMgBr$$

$$RMgBr + GeCl_4 \xrightarrow[\text{-70 °C}]{Et_2O} RGeX_3 + MgX_2$$

**Scheme 18:** Preparation of organogermanium trihalides *via* Grignard reaction

Yields for *p*-tolyl$GeX_3$ (10–20% after hydrogenation and purification) and *n*-Bu$GeX_3$ (traces) were so low that they were preferentially synthesized with different methods (Chapters 3.1.2 and 3.1.3). The yield for mesityl$GeX_3$ was similarly minuscule. After tracing the problem to insufficient formation of Grignard reagent, the Schlenk equilibrium was shifted through 1,4-dioxane addition.[143] This brought the yield in line with expectations.

### 3.1.2 Insertion of Germanium Dichloride into 4-Bromotoluene

Because the reaction of $GeCl_4$ with *p*-tolylMgBr resulted primarily in the formation of di- and tri-substituted derivatives, a more selective route was required. Insertion of $GeCl_2$ into *p*-tolylBr produced *p*-tolyl$GeX_3$ as sole product (Scheme 19).[33] Following this procedure, overall yields for *p*-tolyl$GeH_3$ were improved to 48%. However, the process is more time consuming than the Grignard reaction, and yields were found to be sensitive to small changes in temperature and reaction time. Consequently,

trihalide preparation *via* $GeCl_2$ insertion was not extended to the other aryl derivatives with more acceptable Grignard yields.

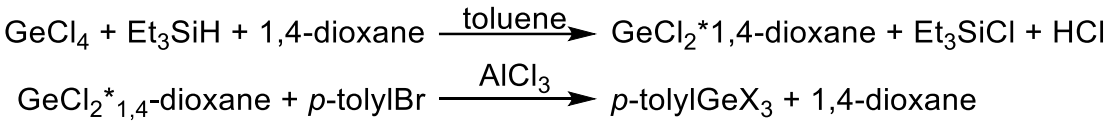


**Scheme 19**: Preparation of *p*-tolylgermanium trihalide *via* $GeCl_2$ insertion

### 3.1.3 Modified Kozeschkow Redistribution

Similar to *p*-tolyl$GeX_3$, *n*-Bu$GeX_3$ (X = Cl, Br) did not form in appreciable amounts when prepared *via* the Grignard route. The main issue was once again the prevalence of additional substitution reactions beyond the first. In this case, a modified Kozeschkow reaction was used to improve selectivity (Scheme 20).[40]

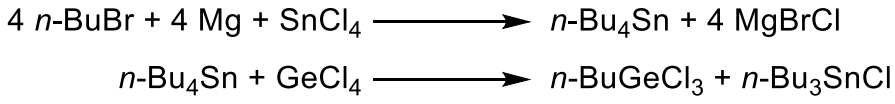


**Scheme 20:** Preparation of *n*-butylgermanium trichloride *via* alkyl halide exchange

### 3.1.4 Hydrogenation to Germanium Hydrides

Trihydrides were produced by reacting the obtained trihalides with excess $LiAlH_4$ in an etheric solvent (Scheme 21).[28] A comparison of trihydride yields obtained *via* the Grignard route can be found in Table 2, the different aryl groups are depicted in Scheme 22.

**Table 2:** Overview of arylgermanium trihydride yields obtained in this work *via* the Grignard route

| **Compound** | **Yield [%] (based on $GeCl_4$)** | **$^1$H shift of $GeH_3$ ($C_6D_6$)** |
|---|---|---|
| phenyl$GeH_3$ (**2**) | 9.4 | 4.24 ppm |
| *o*-tolyl$GeH_3$ (**3**) | 23 | 4.22 ppm |
| *p*-tolyl$GeH_3$ (**4**) | 12 | 4.28 ppm |
| 2,5-xylyl$GeH_3$ (**5**) | 66 | 4.26 ppm |
| 2,6-xylyl$GeH_3$ (**6**) | 38 | 4.17 ppm |
| mesityl$GeH_3$ (**7**) | 38 | 4.20 ppm |

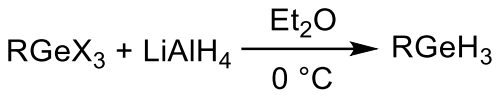


**Scheme 21:** Hydrogenation of crude organogermanium trihalides with $LiAlH_4$

The overall yield was found to depend mostly on steric factors. A methyl group in *ortho* position (**3**) provides shielding for the Ge center during the Grignard reaction, inhibiting formation of di- and triarylgermanes. A second *o*-$CH_3$ group (**6**, **7**) increases the hinderance and consequently the overall yield even further. The highest yield was recorded for the 2,5-xylyl derivative **5**. In comparison, the literature yield for 3,5-xylyl$GeH_3$ with two *m*-$CH_3$ group is more in line with **6** and **7**.[141] It appears that the the combination of an *o*-$CH_3$ with an *m*-$CH_3$ group provides optimal steric shielding to reduce unwanted substitution reactions. The melting point of **7** (>0 °C, relatively high compared to other arylgermanium trihydrides) made it possible to obtain the previously unreported crystal structure (Figure 1).

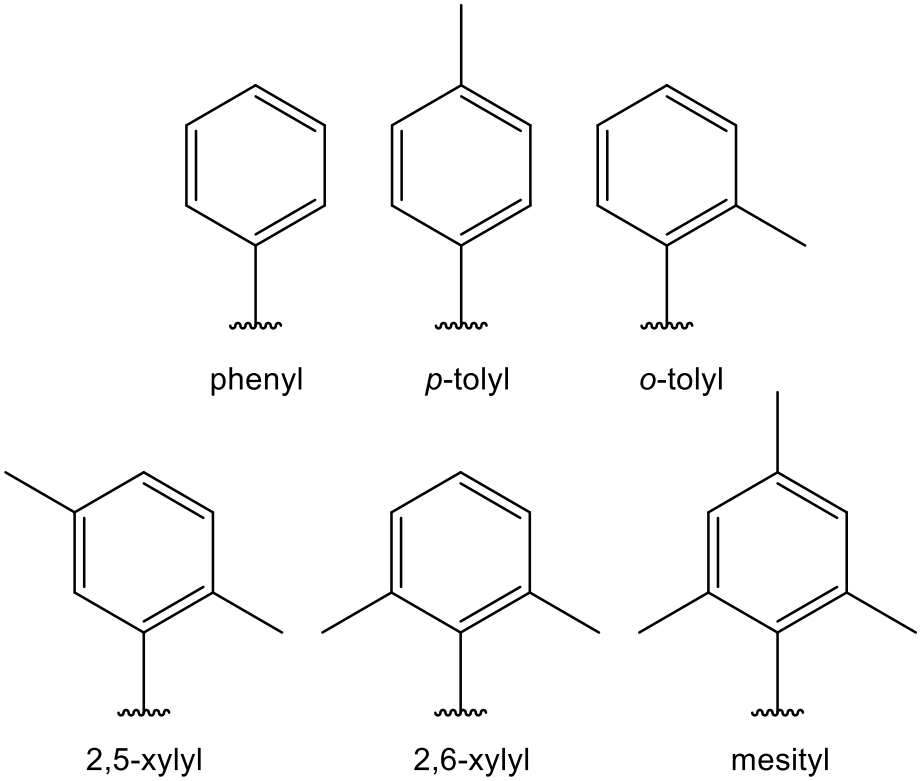


**Scheme 22:** The aryl substituents used in this work

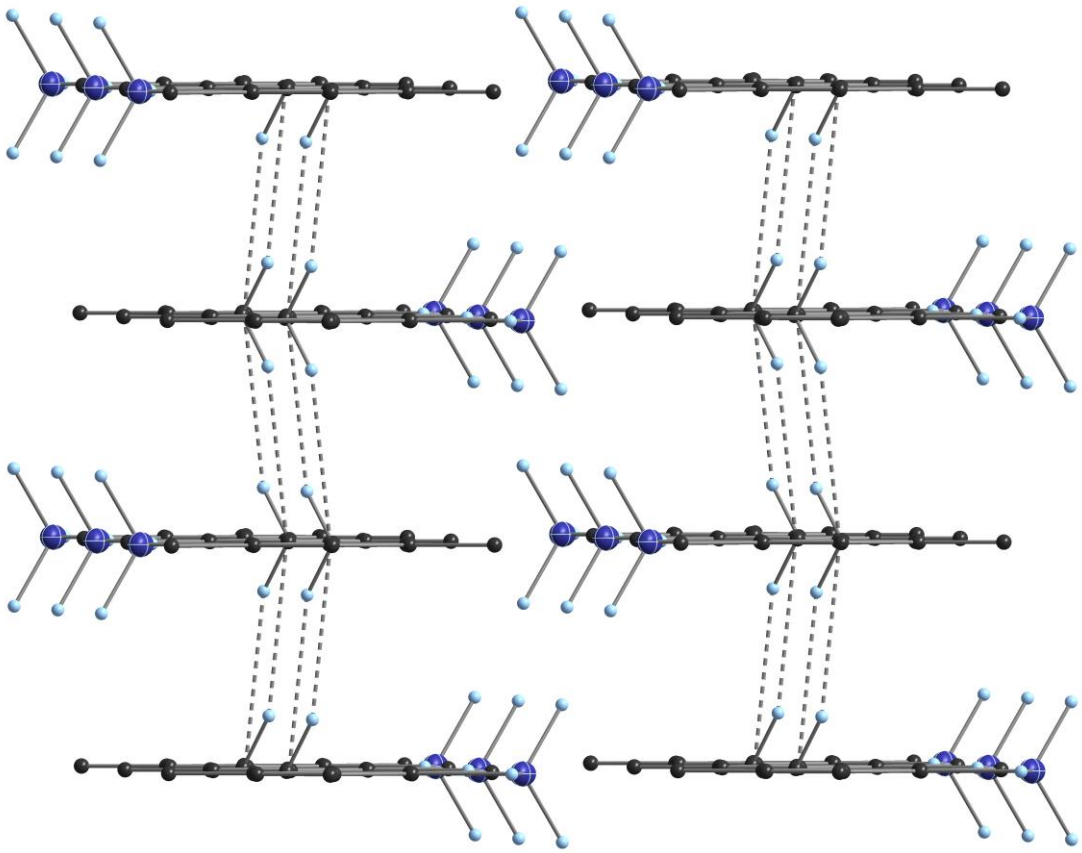

**Figure 1:** Extended crystal structure of **7**

### 3.1.5 Chlorination of Arylgermanium Trihydrides

Of the above-described routes towards organogermanium trihalides, only the modified Kozeschkow reaction (3.1.3) delivers a pure compound. Insertion (3.1.2) results in mixed chlorides and bromides $ArGeX_3$, and the Grignard route (3.1.1) produces an even more complicated mixture $Ar_nGeX_{4-n}$ (n=1–4, X=Cl, Br). While these crude mixtures generally suffice as intermediates for trihydride synthesis, a clean trichloride was sometimes desirable for other applications. The preparation of pure *o*-tolylGeCl$_3$ (**10**) as precursor for deuteration to **12** allowed for more economic use of the expensive reagent $LiAlD_4$. MesitylGeCl$_3$ (**9**), solid at room temperature, was crystallized from toluene to obtain its previously unreported crystal structure (Figure 2). Additionally, the partially chlorinated derivative *o*-tolylGe(Cl)H$_2$ (**11**) was prepared as starting material for dimerization.

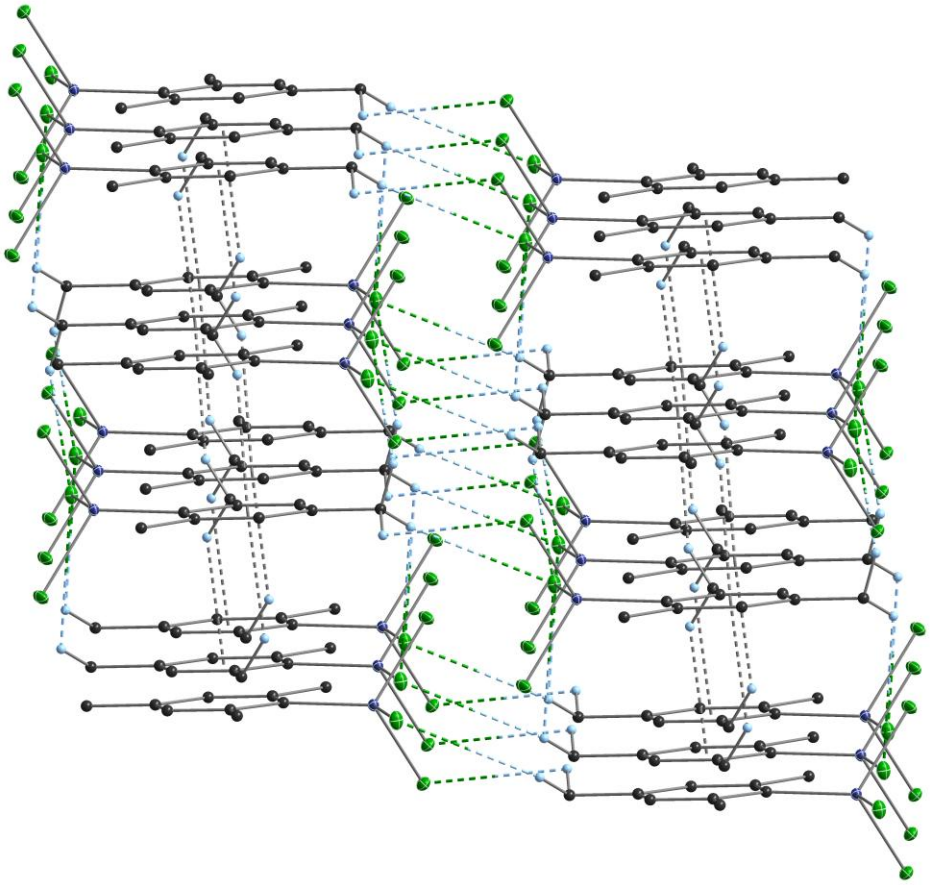

**Figure 2:** Extended crystal structure of **9**

Two different chlorination reagents were used. Reflux in $CCl_4$ with a palladium catalyst is a robust way for full chlorination (Scheme 23). The workup is simple. Catalyst removal *via* filtration followed by solvent evaporation provides the clean product.

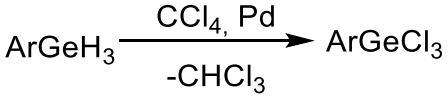


**Scheme 23:** Chlorination of arylgermanes with $CCl_4$

Alternatively, trichloroisocyanuric acid (TCCA) can be used as chlorination reagent, avoiding regulatory and ecological concerns over $CCl_4$. Additionally, this method enables selective monochlorination (Scheme 24).[144] However, side reactions such as the inadvertent chlorination of THF can occur if the reaction conditions are not carefully controlled. The workup is also more time consuming compared to

chlorination with $CCl_4$, because THF needs to be replaced with a nonpolar solvent like *n*-pentane before filtration.

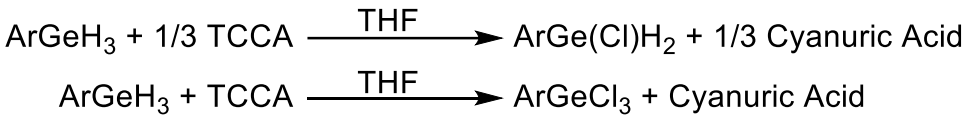


**Scheme 24:** Selective monochlorination (top) and full chlorination (bottom) of arylgermanes with TCCA

## 3.2 (Trialkylsilyl)germanes $R_3SiGeH_3$[145]

In addition to the above discussed alkyl- and arylgermanes, (trialkylsilyl)germanium trihydrides were synthesized as starting materials for dehydrogenative coupling. The lower Si-Ge bond stability compared to C-Ge had the potential to decrease the necessary reaction temperature and increase the Ge(0) ratio within the particles.[146] The influence of a silicone based substituent on the material properties was also of interest.

Because of the anticipated instability of the Si-Ge bond, the use of bulky trialkylsilyl substituents seemed prudent (chapter 2.2.2). $TBDMSGeH_3$ (TBDMS = *t*-$BuMe_2Si$-) and $DTBMSGeH_3$ (DTBMS = *t*-$Bu_2MeSi$-) were selected as target compounds. In addition to dehydrogenative coupling, these silylgermanes could find future use in transition metal complexes Ge=M or other doubly bonded derivatives Ge=E. Similar applications for bis(trialkylsilyl)germanes $(R_3Si)_2Ge$- have been previously reported.[147]

The preparation of the target molecules is not as straightforward as for arylgermanes. Silylgermanium halides have a known propensity towards α-elimination, increasing in the order $(R_3Si)_3GeX<(R_3Si)_2GeX_2<R_3SiGeX_3$.[90,148,149] This makes the silylation of $GeCl_4$ with subsequent $LiAlH_4$ reduction unfeasible. While the preparation of $Me_3SiGeH_3$ from $Me_3SiX$ and $NaGeH_3$ had been previously reported, the yields were very low.[150] The need to prepare $NaGeH_3$ by bubbling an excess of $GeH_4$ through sodium in $NH_3$ made this approach even less appealing. Inspired by the solution reported by Lee *et al.* for a similar problem,[149] a less direct route was chosen (Scheme 25).

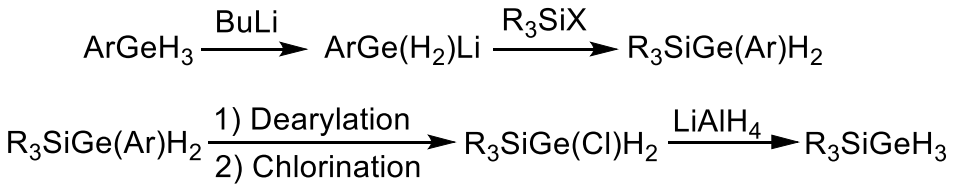


**Scheme 25:** Synthetic plan towards (trialkylsilyl)germanes $R_3SiGeH_3$

### 3.2.1 Silylation of Arylgermanes

A common strategy for the coupling of arylgermanes with silicon halides is metalation of the former (Scheme 26).[71,84,149] Due to the known instability of germyl lithium compounds,[151] isolation of this intermediate was not attempted. The full conversion of **4** to *p*-tolylGe($H_2$)Li was instead confirmed by *in situ* $^1$H NMR of a model reaction: First THF[$d_8$] and then *p*-tolylGe$H_3$ were condensed into a C. Young NMR tube charged with solid *t*-BuLi. Upon thawing, vigorous bubbling and a color change indicated the reaction start. When the gas formation ceased, a $^1$H NMR spectrum was taken (Figure 3). The considerable upfield shift of the characteristic Ge-H signal (2.65 ppm, THF[$d_8$]) when compared to that of **4** (4.28 ppm, $C_6D_6$) already provided strong support for lithiation at the germanium center. This was further demonstrated through derivatization with methyl iodide. The $^1$H NMR ($C_6D_6$) showed characteristic coupling pattern for both the Ge-H (4.29 ppm, q) and the Ge-$CH_3$ (0.50 ppm, t) signal.

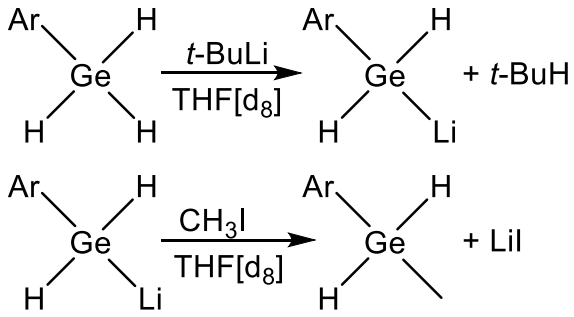


**Scheme 26:** Model reaction for the lithiation of arylgermanium trihydrides

The synthetic protocol was adjusted for subsequent reactions to facilitate a bigger scale. *t*-BuLi in *n*-pentane was dripped into *p*-tolylGe$H_3$ in THF under cooling. Slow addition and thorough mixing are important, because a local *t*-BuLi excess can cause nucleophilic substitution of H with *t*-Bu instead of the desired lithiation.[152,153] After stirring the clear, yellow solution for two hours, it was mixed with the silyl halide *t*-BuMeRSiX in THF and stirred overnight. The solvents were then removed from the now colorless solution and replaced with *n*-pentane. Salts were removed by filtration and the product purified through vacuum recondensation.

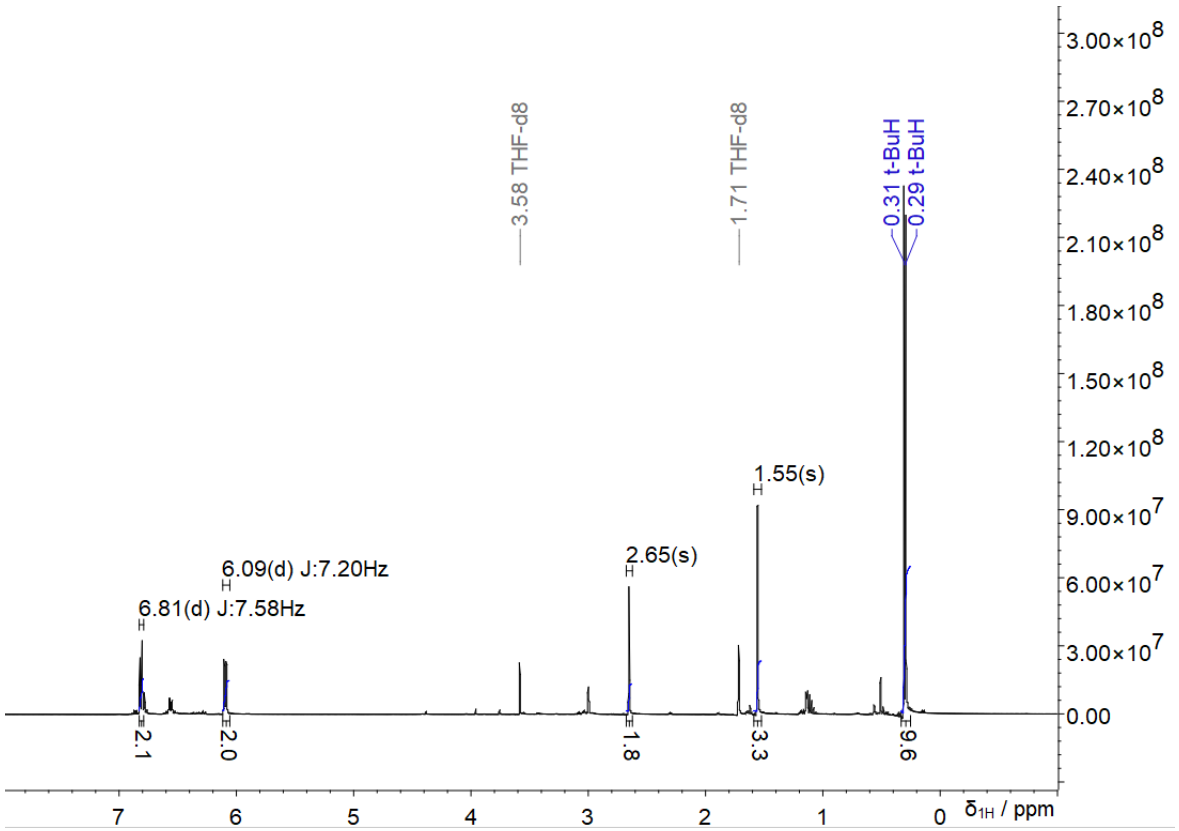


**Figure 3:** $^{1}H$ NMR (400 MHz, THF[$d_8$]) of *p*-tolylGe($H_2$)Li

For the preparation of TBDMSGe(mesityl)$H_2$, some additional adjustments were necessary. The steric bulk of the mesityl substituent reduces the reactivity with organolithium reagents to the point where the competing ether cleavage becomes an issue. To prevent this side reaction, *t*-BuLi was replaced with MeLi, which only reacts very slowly with THF. Of course, the weaker lithium base decreased the overall reaction speed even further, and the reaction was stirred for two full days at room temperature to allow for complete conversion of the reagents.

The silyl(aryl)germanes prepared as part of this work are listed in Table 3. They are air stable liquids with modest temperature stability. However, due to their high boiling points, decomposition temperatures can be reached even when recondensing under vacuum. This is especially true for **17** because of the heavy DTBMS substituent. It cannot be isolated without a high-powered vacuum pump. Even under the specified conditions, some amount of the decomposition product DTBMSGeH was always found in the condensate. Any small leakage in the vacuum apparatus can obliterate the yield. Expecting an even less favorable boiling point, no attempts to couple DTBMS with the heavier arylgermanes was made. Synthesis of

DTBMSGe(phenyl)$H_2$ was also skipped, as TBDMSGe(phenyl)$H_2$ (**14**) had already demonstrated the low suitability of the phenyl substitutent for the subsequent dearylation reaction (Chapter 3.2.2).

**Table 3:** Overview of the silyl(aryl)germanes prepared as part of this thesis

| **Compound** | **Yield [%]** | **Recondensation conditions** | **$^1$H shift of $GeH_2$ ($C_6D_6$)** |
|---|---|---|---|
| TBDMSGe(phenyl)$H_2$ (**14**) | 55 | 60 °C, 5.0*10$^{-3}$ mbar | 4.26 ppm |
| TBDMSGe(*p*-tolyl)$H_2$ (**15**) | 47 | 80 °C, 7.2*10$^{-3}$ mbar | 4.29 ppm |
| TBDMSGe(2,6-xylyl)$H_2$ (**16**) | 37 | 70 °C, 5.0*10$^{-3}$ mbar | 4.21 ppm |
| TBDMSGe(mesityl)$H_2$ (**18**) | 45 | 125 °C, 5.5*10$^{-3}$ mbar | 4.23 ppm |
| DTBMSGe(*p*-tolyl)$H_2$ (**17**) | 47 | 160 °C, 5.6*10$^{-3}$ mbar | 4.35 ppm |

The silyl(aryl)germanes have almost identical $^1$H NMR shifts to the corresponding arylgermanes (Figure 4). GC/MS is thus better suited to verify full conversion of the starting material.

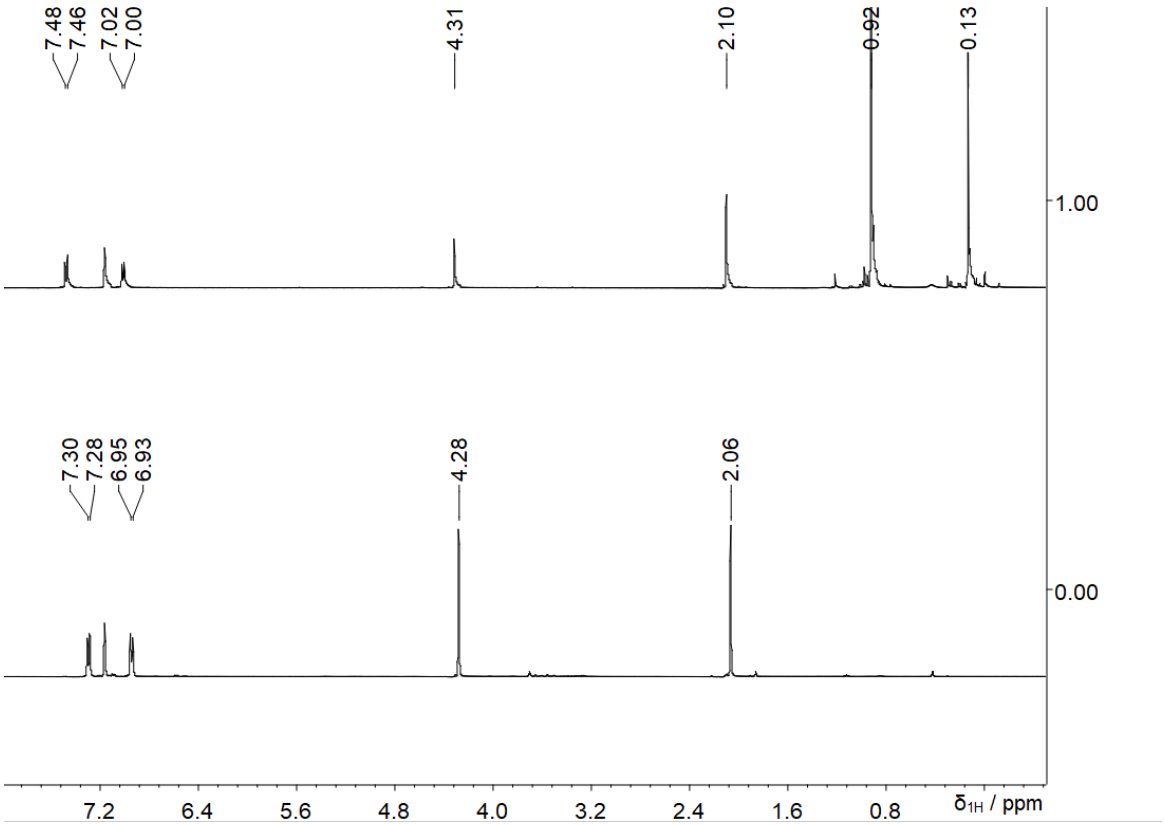


**Figure 4:** $^1$H NMR (400 MHz, $C_6D_6$) of **15** (top) and **4** (bottom)

Rare $^{73}$Ge NMR shifts of **15** (δ = -204.7 ppm) and **17** (δ = -207.3 ppm) were also obtained, despite the asymmetric nature of these compounds (Figure 5).

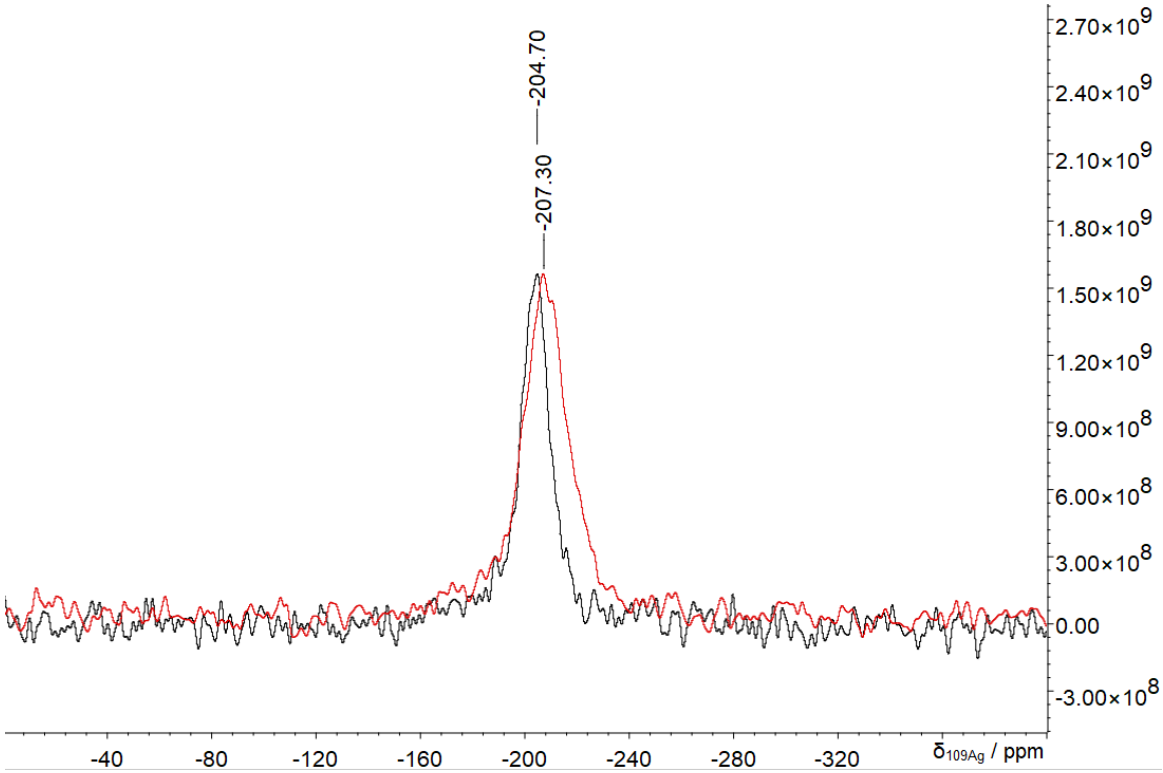


**Figure 5:** $^{73}$Ge NMR ($C_6D_6$, 24.4 MHz) of **15** (-204.7 ppm, black) and **17** (-207.3 ppm, red)

### 3.2.2 Chlorodearylation of Silyl(aryl)germanes

The first attempt at the dearylation reaction was once again made by following an established literature procedure for similar compounds, the selective Ge-$C_{Ar}$ bond cleavage of triaryl(silyl)germanes with trifluoromethanesulfonic acid (triflic acid or TfOH) (Scheme 27).[71,88,149]

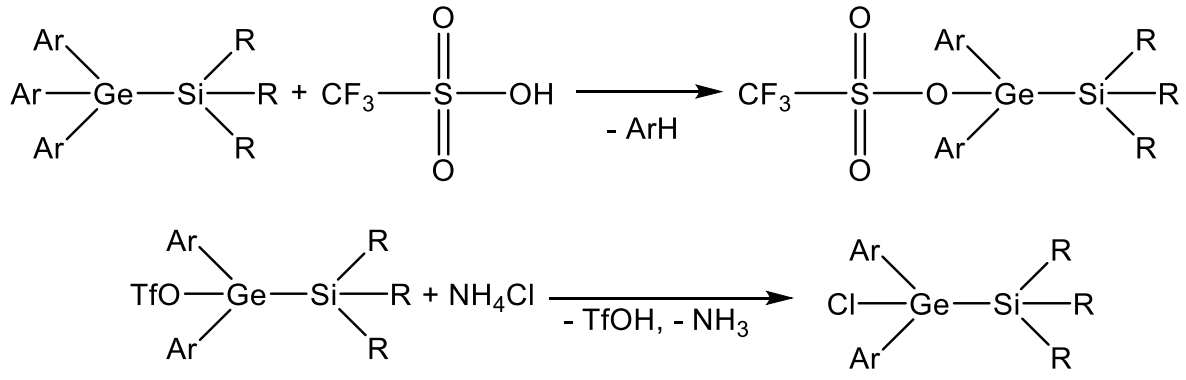


**Scheme 27:** Reaction of triaryl(trialkylsilyl)germanes with triflic acid and subsequent quenching

However, the reaction of TBDMSGe(*p*-tolyl)$H_2$ (**15**) with TfOH resulted in decomposition. Multiple attempts with different solvents ($CH_2Cl_2$, $CDCl_3$, toluene) and at different temperatures (-60 to 0 °C) all lead to the same outcome.

Using $^1$H NMR, both toluene and TBDMSOTf were identified as reaction products. The removal of these substituents from the germane likely produces a germylene which subsequently polymerizes and is not accessible to standard analytics anymore, explaining why no germanium containing decomposition product was found. The presence of toluene suggests that the intended dearylation reaction does indeed take place, but is then followed by Ge-Si cleavage. The low stability of silylgermanium triflates was previously noted by others. However, in these cases *in situ* derivatization of the triflate intermediates was sufficient to stabilize the dearylated products.[71,88] The even lower stability of TBDMSGe($H_2$)OTf observed in the present work can be explained by the lack of additional aryl groups at the Germanium. This necessitated a different strategy for dearylation.

HCl, combined with catalytic amounts of anhydrous $AlCl_3$, is another well-established reagent for selective Ge-$C_{Ar}$ bond cleavage.[84,149] To facilitate water exclusion, HCl is often supplied as gas. However, HCl solutions in $Et_2O$ can be commercially obtained as well. For this thesis, etheric HCl was used as it allows for more precise dosage and simplifies reaction setups. Initial experiments were conducted in $C_6D_6$ to allow for continuous NMR monitoring. It is important to note that charging the reaction vessel with $AlCl_3$ and TBDMSGe(*p*-tolyl)$H_2$ (**15**) prior to solvent addition resulted in degradation of the silylgermane and thus needs to be avoided. The Ge-H resonances allow for convenient identification of the different germane species, despite the large amounts of undeuterated $Et_2O$. Full conversion of **15** to TBDMSGe(Cl)$H_2$ (**19**) took approximately 5 hours. The $^1$H NMR signal of $GeH_2$ in the product exhibited an expected downfield shift (δ = 5.25 ppm) due to the vicinity of chlorine (Figure 6). The slight difference of the Ge-H shift recorded for **15** in Chapter 3.2.1(4.29 ppm) to the one observed here (4.25 ppm) is because of the $Et_2O$.

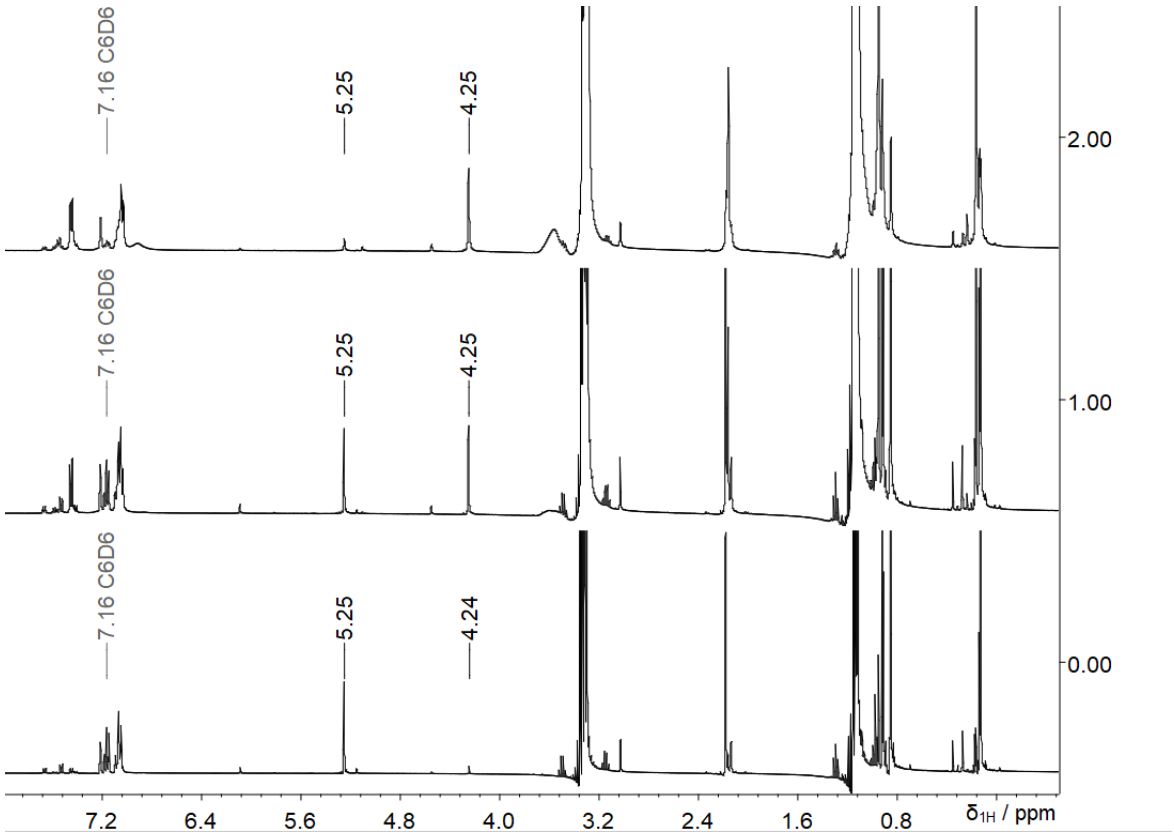


**Figure 6:** $^{1}$H NMR (400 MHz, $C_6D_6$) monitoring of the $AlCl_3$ catalyzed reaction between TBDMSGe(*p*-tolyl)$H_2$ and HCl (1 M $Et_2O$) after 10 min (top), 1 h (middle) and 5 h (bottom).

The isolation of the silyl(chloro)germanes turned out to be a challenge as well. While the pure product was observed in solution, solvent removal led to decomposition and formation of several additional compounds. An initial suspicion that this was caused by direct contact with $AlCl_3$ (as observed for the starting material) could not be confirmed. Even after $AlCl_3$ was precipitated with *n*-pentane and filtrated off with Celite®, a mixture formed upon concentrating a solution of TBDMSGe(Cl)$H_2$ (**19**). The mixture was subjected to vacuum (RT → 45 °C, 0.012 mbar) to isolate the more volatile components. The condensate consisted primarily of two distinct compounds, as shown by $^{1}$H (Figure 7) and $^{29}$Si NMR. One compounds was immediately identified as remainders of **19** by its $^{1}$H and $^{29}$Si NMR shifts. The second compound was indicated by GC/MS to be TBDMSGe$H_3$ (**21**). In order to verify this assumption, $Et_2O$ and $LiAlH_4$ was added to the mixture. After the resulting hydrogenation of **19** only the shifts of suspected **21** remained, confirming the assignment to be correct.

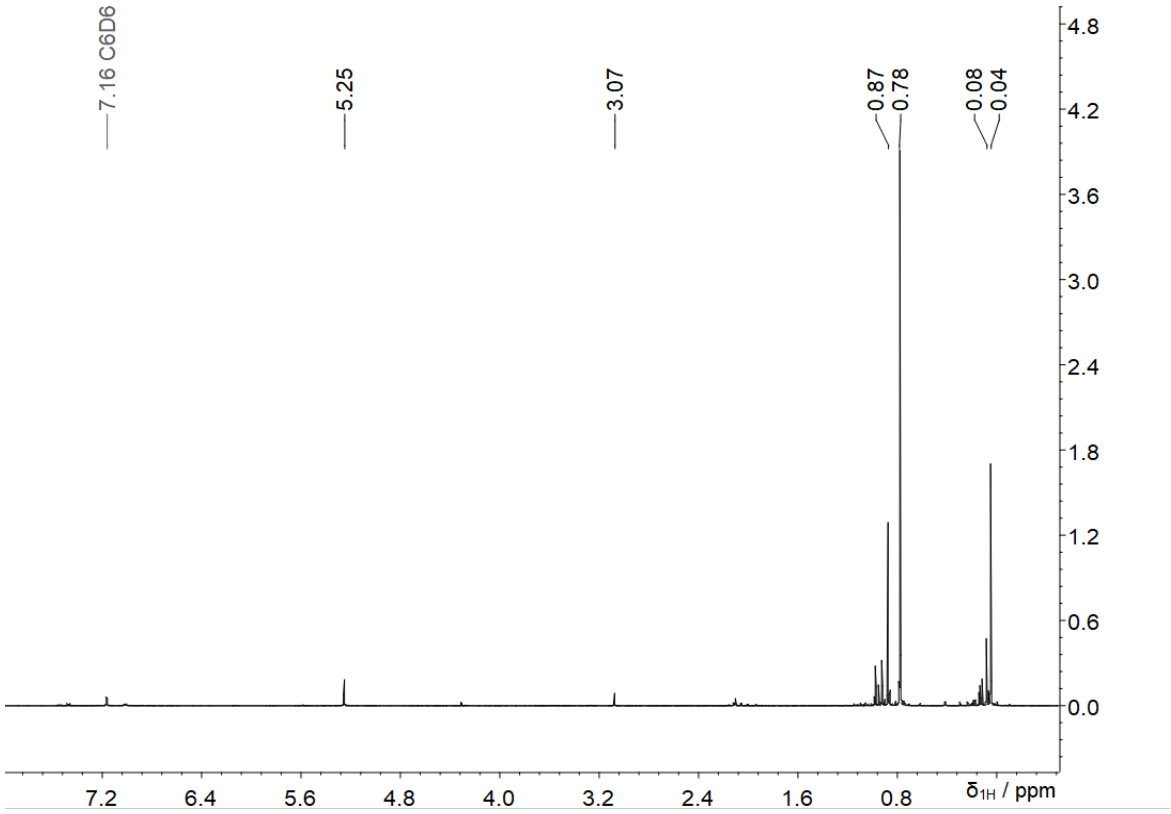


**Figure 7:** $^{1}$H NMR (400 MHz, $C_6D_6$) of **19** after solvent removal and recondensation

Based on these results, it seems likely that **19** decomposes through disproportionation (Scheme 28). The bimolecular process explains why the decomposition is concentration dependent. The dichloride TBDMSGe($Cl_2$)H which should form as a result of this reaction was not found. However, this can be explained with the low stability of silylgermanium dihalides, discussed in the introduction of this chapter. The α-elimination product of TBDMSGe($Cl_2$)H, TBDMSCl, was indeed identified in the reaction mixture.

$$2\ \text{TBDMSGe(Cl)H}_2 \longrightarrow \text{TBDMSGeH}_3 + \text{TBDMSGe(Cl}_2\text{)H}$$

**Scheme 28:** Proposed decomposition reaction for **19**

An attempt to find the predicted dichloride with DTBMSGe(Cl)$H_2$ (**20**) succeeded, thanks to the additional stability provided by the second *t*-Bu group. After solvent evaporation and recondensation of **20**, signals for Ge($Cl_2$)H (7.01 ppm) and $GeH_3$ (3.09 ppm) were found in the $^{1}$H NMR ($C_6D_6$, Figure 8). Their integrals exhibited the 1:3 ratio predicted by Scheme 28. The shifts for Ge-*t*-Bu and Ge-Me could not be assigned due to overlapping signals from the three similar silylgermanes. A $^{29}$Si NMR showed an expected downfield shift for DTBMSGe($Cl_2$)H (23.7 ppm) compared to **20** (16.4) and **22** (14.8).

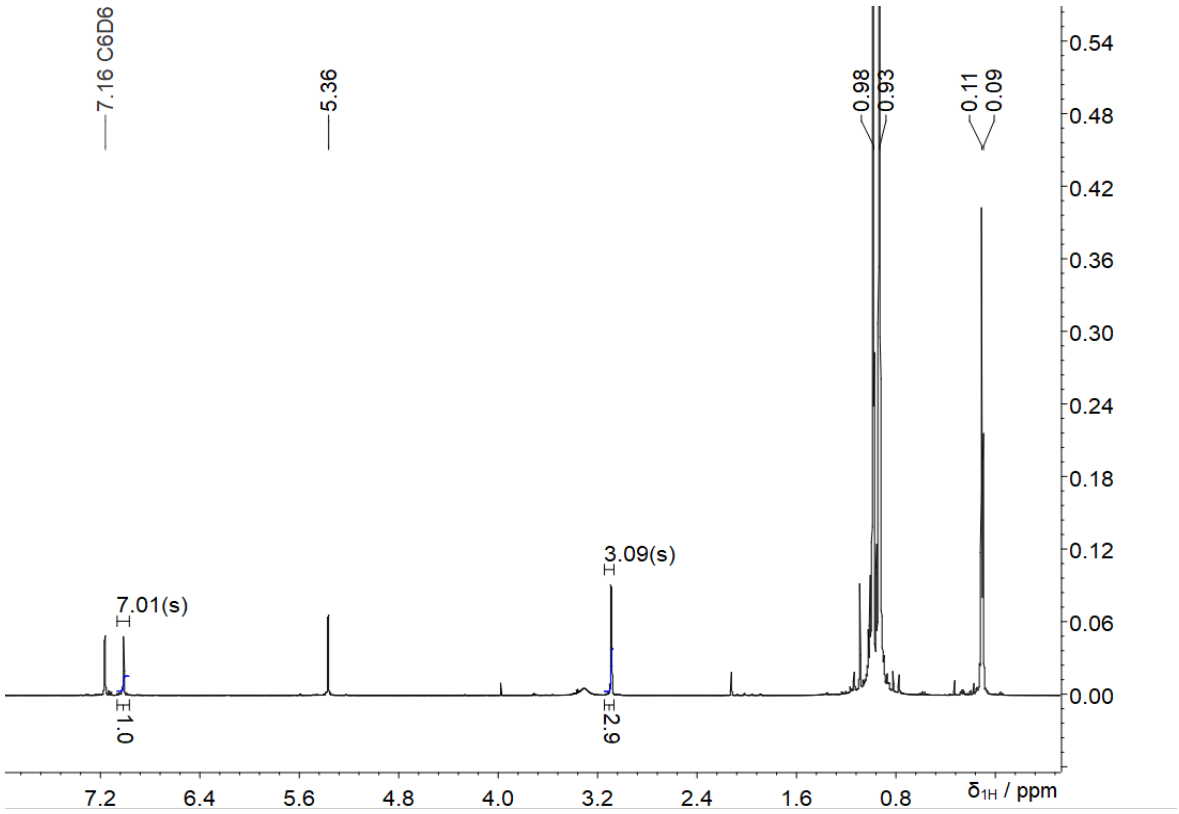


**Figure 8:** $^{1}H$ NMR (400 MHz, $C_6D_6$) of a mixture of DTBMSGe($Cl_x$)$H_{3-x}$ (x=0**–**2), obtained through recondensation

Although the decomposition mixture *t*-BuMeRSiGe($Cl_x$)$H_{3-x}$ (x=0–2) could theoretically be converted to *t*-BuMeRSiGe$H_3$ without loss of yield, there are some problems with that in praxis. *t*-BuMeRSiGe($Cl_2$)H decomposes due to its low stability. Additionally, the low boiling *t*-BuMeRSiGe$H_3$ is removed alongside solvents during evacuation. To prevent decomposition, the reaction solution was first cooled to between -20 and -30 °C. The solvents were then removed under vacuum. Either $Et_2O$ (for storage and follow-up reactions) or $C_6D_6$ (for NMR measurement of the monochloride) were immediately added before thawing. The lower boiling, less stable **19** proved impossible to isolate. Some toluene always remained in the mixture and attempts to remove it fully resulted in considerable product degradation. When **16** or **18** were used as starting material, the produced xylene and mesitylene were even more difficult to remove. Purification of **20** was considerably easier, and NMR spectra were obtained with only minor contamination remaining (Figure 9). Due to the need to immediately redissolve the compounds, yields could not be determined. Neither **19** nor **20** were stable enough to show up in mass spectra.

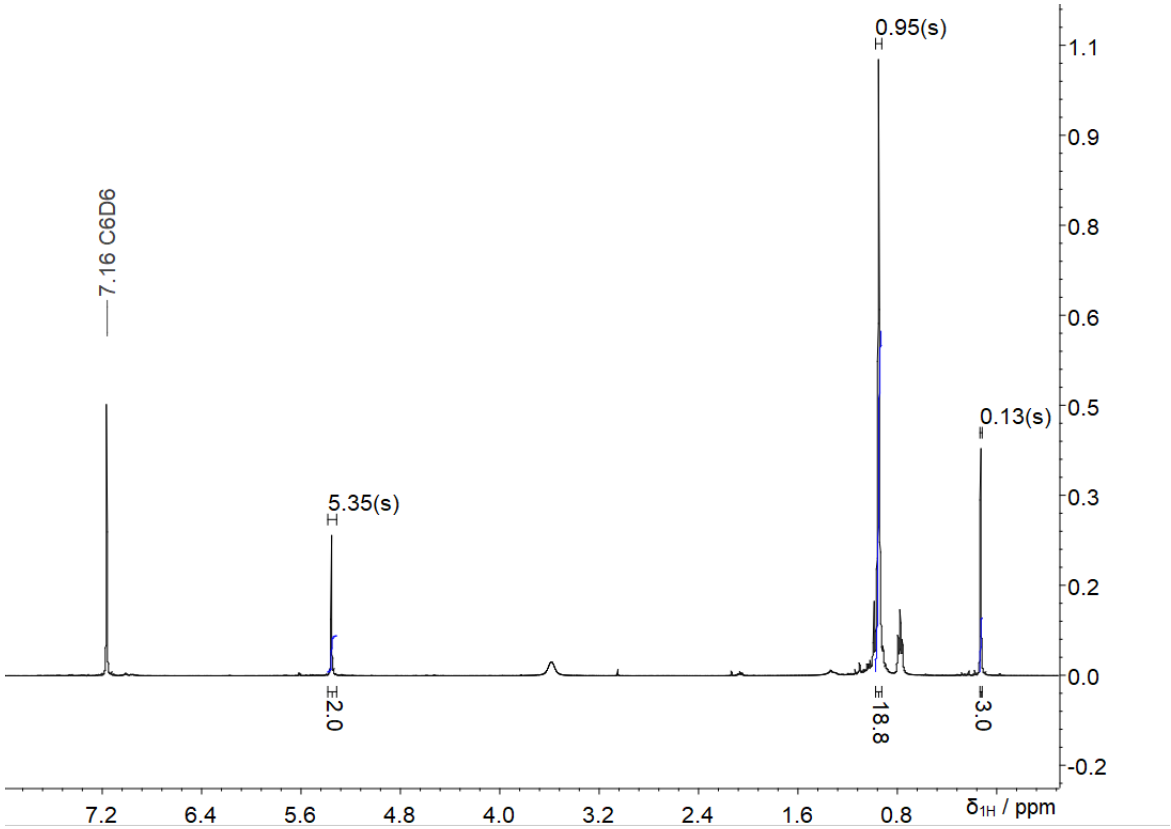


**Figure 9:** $^{1}$H NMR (400 MHz, $C_6D_6$) of **20** after solvent removal at low temperatures

The dearylation experiments were initially conducted in benzene, as described in the literature.[84,149] However, pure $Et_2O$ could be shown to be adequate as well. Avoiding benzene speeds up low temperature solvent removal, lowering the risk of decomposition (Scheme 29). While reaction solutions without benzene become biphasic upon HCl addition, full dearylation still occurs overnight under vigorous stirring. An attempt to further simplify the workup through omittance of $AlCl_3$ was unsuccessful. Albeit dearylation still occurred at slow rates (~75% conversion after 7 d), a competing decomposition reduced the yield and caused additional impurities.

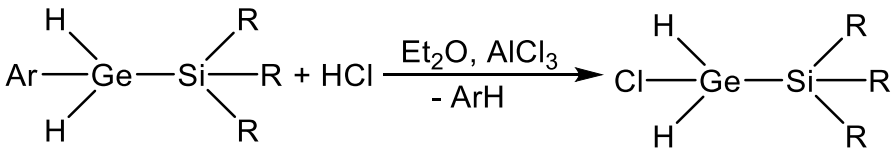


**Scheme 29:** Dearylation and chlorination of aryl(trialkylsilyl)germanium dihydrides

Substrates **15–18** were successfully dearylated to the corresponding silyl(chloro)germane. Only the phenyl derivative, **14**, proved to be unsuitable for this

reaction. Despite being subjected to the same conditions as the other compounds, only a minority was converted to the chloro derivative. Most of the starting material remained unchanged. The phenyl-Ge bond is well known to be more resistant towards acidic cleavage than other arylgermanes.[154] It appears that the present reaction condition are not sufficient to overcome this higher strength. As a consequence, DTBMSGe(phenyl)$H_2$ was no longer considered a suitable candidate for further research, and no attempts to synthesize it were made.

### 3.2.3 Hydrogenation of Silyl(chloro)germanes

The final step towards the target silylgermanes TBDMSGe$H_3$ (**21**) and DTBMSGe$H_3$ (**22**) was the well-established $LiAlH_4$ hydrogenation of germanium halides (Chapter 2.1.3). After adding an excess of $LiAlH_4$ to the cooled $Et_2O$ solution of **19** or **20**, the hydrogenation occurred without any issues (Scheme 30).

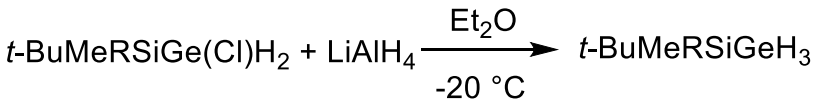


**Scheme 30:** $LiAlH_4$ reduction of **19** to **21** (R=Me) and **20** to **22** (R=*t*-Bu)

$LiAlH_4$ hydrogenations are commonly quenched with $H_2O$. However, as a new compound class, nothing is known yet about the hydrolytic stability of (trialkylsilyl)germanes. To avoid this risk factor, the reaction solution was first concentrated at reduced pressure (room temperature, 400 mbar) and then recondensed (30 °C, 0.1 mbar). Based on observations during the recondensation, the boiling point of TBDMSGe$H_3$ (**21**) was estimated to be between 20–80 mbar at room temperature. The removal of remaining $Et_2O$ was therefore conducted at 100 mbar. Despite being evacuated under these conditions, well below the vapor pressure of $Et_2O$, for several hours, it was impossible to fully remove the solvent. Analysis of the condensate already showed some loss of product, so the evacuation was stopped. The formation of a complex between $Et_2O$ and the germane could explain its persistence. In addition to about 9% w/w of $Et_2O$, 8% w/w of toluene from the previous step also remained in the final product (values calculated from $^1H$ NMR integrals, Figure 10). The remaining 83% w/w of the clear, colorless liquid are **21**, in a yield of 32% (based on **15**).

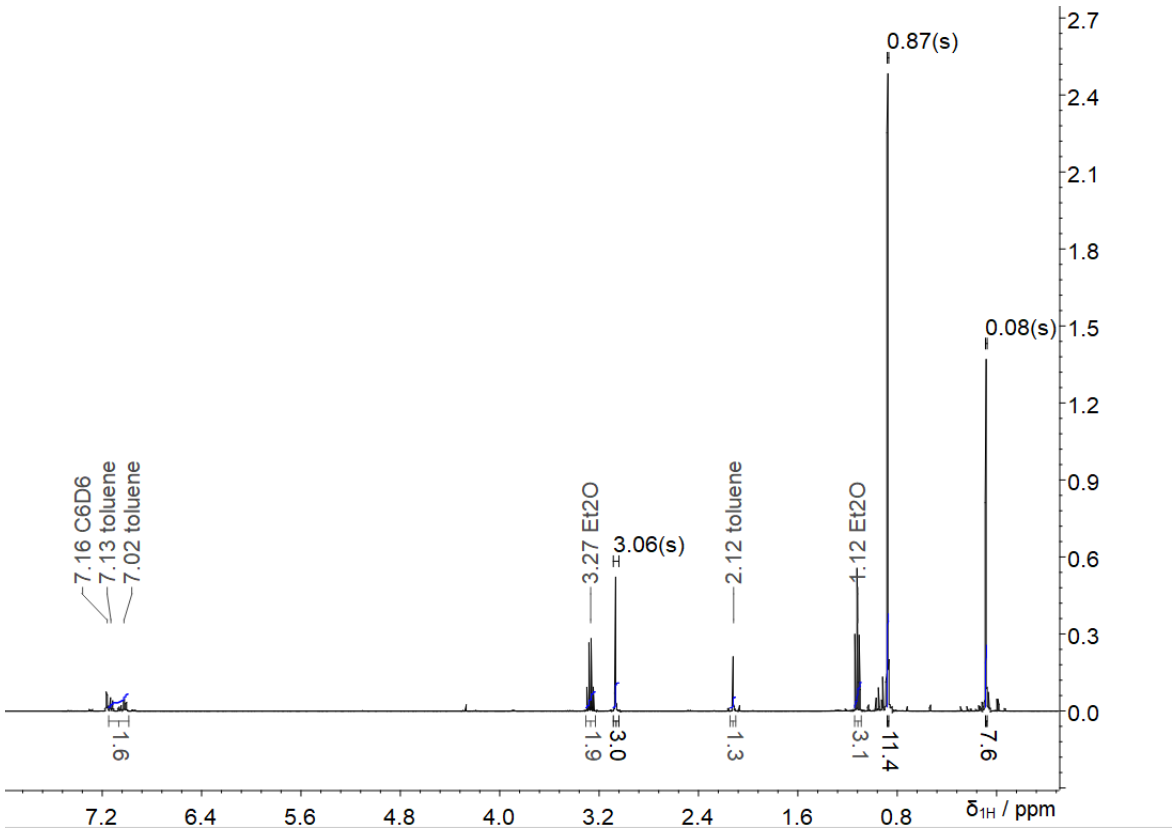


**Figure 10:** $^{1}H$ NMR (400 MHz, $C_6D_6$) of $TBDMSGeH_3$ (**21**) with residual $Et_2O$ and toluene

The room temperature boiling point of $DTBMSGeH_3$ (**22**) was estimated below 10 mbar. $Et_2O$ was fully removed from **22** after three hours at 100 mbar, despite this pressure being insufficient during the isolation of **21**. Thanks to the higher boiling point, no product was lost during evacuation either. **22** was obtained as clear, colorless liquid in 63% yield (based on **17**). The NMR spectra of the pure product are shown in Figure 11.

The trihydrides **21** and **22** are stable even at slightly elevated temperatures. They start degrading when heated above 100 °C (see Chapter 3.4.3). This provided an additional challenge when high resolution mass spectra were measured. At the standard injector temperature (280 °C), the trihydride product was not observed. The thermal degradation products TBDMSH and DTBMSH were found instead. Lowering the injector temperature to 250 °C was required to obtain mass spectra for **21** and **22**. The (trialkylsilyl)germanes need to be stored inertly, as exposure to the atmosphere causes slow oxidation.

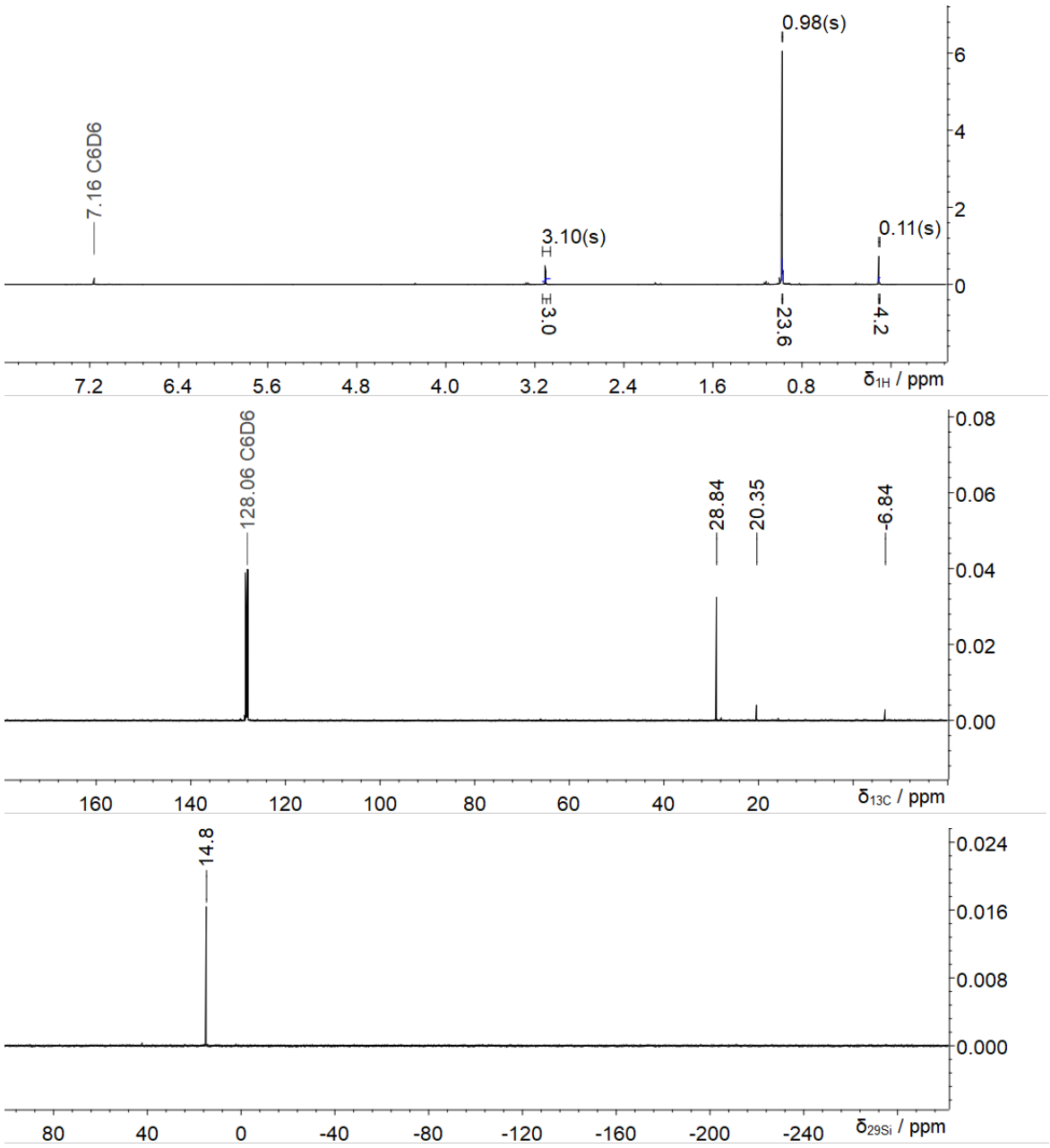


**Figure 11:** NMR spectra ($C_6D_6$) of DTBMSGeH$_3$ (**22**), top: $^{1}$H, middle: $^{13}$C, bottom: $^{29}$Si

## 3.3 Organolithium Reactivity with Arylgermanes

During the scale up of the lithiation of **4** (Chapter 3.2.1), an attempt using *n*-BuLi and $Et_2O$ failed to deliver the desired product. *n*-Bu(*p*-tolyl)$GeH_2$ (**23**) was formed instead and identified through $^1H$ NMR (Figure 12) and GC/MS. In general, there are two main pathways for the reaction of group 14 hydrides with organolithium bases: nucleophilic substitution and hydrogen metal exchange (Scheme 31).

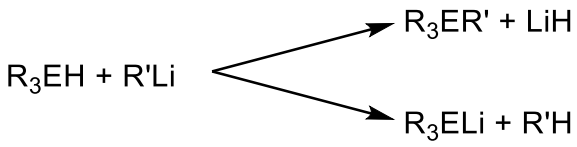


**Scheme 31:** Possible reactions of organic lithium bases with group 14 hydrides

Nucleophilic substitution is the expected mechanism when reacting silanes with organic lithium bases.[155] However, aryl germanes usually undergo hydrogen metal exchange due the higher electronegativity of germanium.[45] In the rare cases were nucleophilic exchange between germanium hydrides and organolithium reagents were observed, it was attributed to the relative concentration of the reagents or order of addition, which is not sufficient to explain the behavior observed for **4**.[54,153] Furthermore, nucleophilic substitution never occurred exclusively in these cases, some amount of starting material was always lithiated. Further investigations into the matter were those conducted.

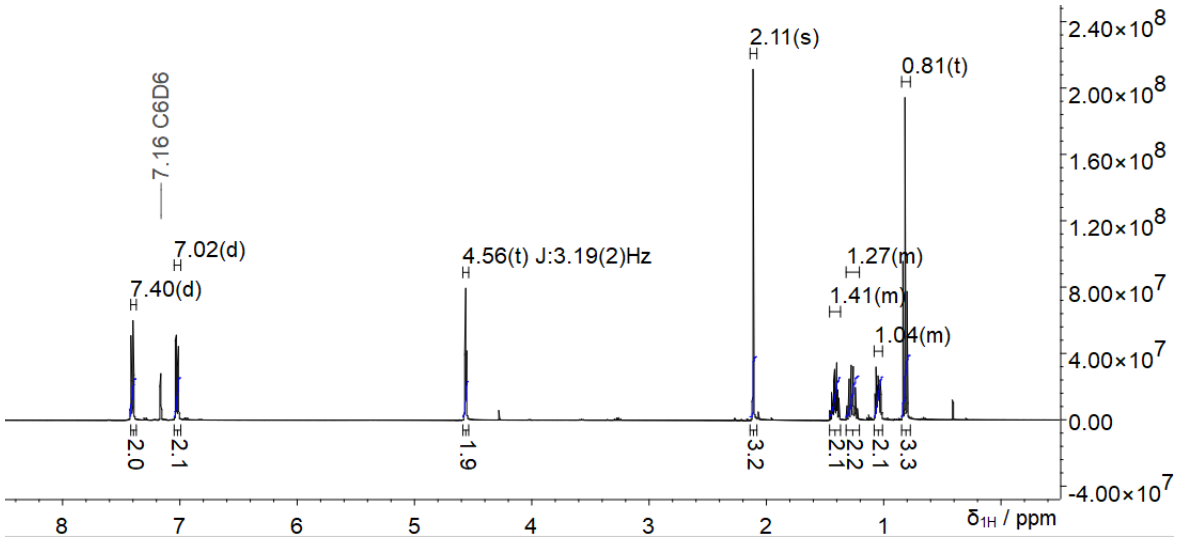


**Figure 12:** $^1H$ NMR (400 MHz, $C_6D_6$) of **23**

### 3.3.1 Solvent Dependency of Arylgermane Lithiation

First, the reproducibility of the experiment was verified through a second, intentional synthesis of **23**, which produced the same outcome after a much simpler workup. There were two obvious differences between the previously observed lithiation (*t*-BuLi, THF) and the butylation (*n*-BuLi, $Et_2O$) of **4**: the solvent, and the lithium base. In addition, the commercially obtained bases also introduce their own solvent (*t*-BuLi: *n*-pentane, *n*-BuLi: hexanes) in varying concentration into the mixture. Reacting **4** with *t*-BuLi in $Et_2O$ and with *n*-BuLi in THF were two obvious experiments to gather more information. In addition, both bases were reacted in *n*-pentane to provide data on nonpolar solvents. The result of this investigation (Table 4) clearly showed the solvent to be the most important factor. THF enforces the full lithiation of the germane, while *n*-pentane leads to butylation, resulting in the isolation of *t*-Bu(*p*-tolyl)$GeH_2$ (**24**), in addition to the previously obtained **23** (Figure 13).

**Table 4:** Reaction products of **4** with two BuLi bases in different solvents

| | **THF** | **$Et_2O$** | ***n*-pentane** |
|---|---|---|---|
| ***n*-BuLi** | *p*-tolylGe($H_2$)Li+*n*-Bu(*p*-tolyl)$GeH_2$ | *n*-Bu(*p*-tolyl)$GeH_2$ | *n*-Bu(*p*-tolyl)$GeH_2$ |
| ***t*-BuLi** | *p*-tolylGe($H_2$)Li | *p*-tolylGe($H_2$)Li+*t*-Bu(*p*-tolyl)$GeH_2$ | *t*-Bu(*p*-tolyl)$GeH_2$ |

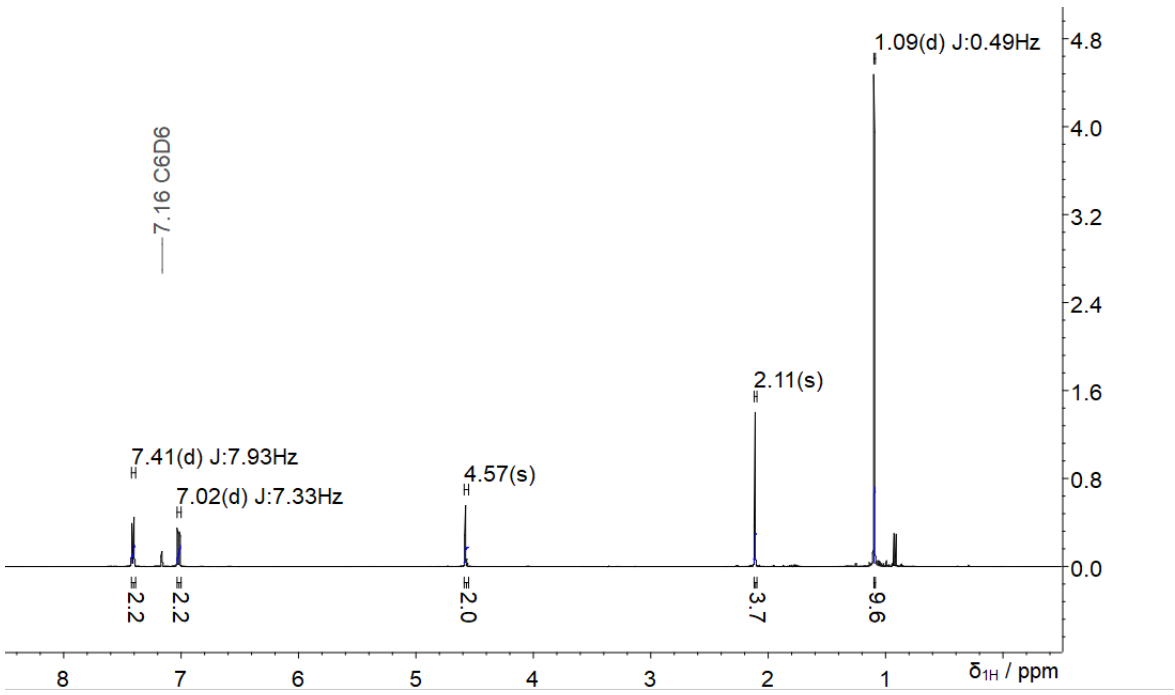


**Figure 13:** $^1H$ NMR (400 MHz, $C_6D_6$) of **24**

This pattern held through additional screenings with the two solvents. The use of THF always resulted in preferential lithiation, often without side products. Perhaps even more interesting, the outcomes of $Et_2O$ and *n*-pentane reactions were remarkably similar to each other, preferentially producing the nucleophilic substitution product in comparable amounts. It is surprising to see the polar, complexing $Et_2O$ align more closely with nonpolar *n*-pentane, rather than the similar etheric solvent THF. The screening reactions also demonstrated the relevance of steric factors on the outcome.

### 3.3.2 Steric factors

The outcome of the screenings is visualized in Table 5. It is important to note that these are only preliminary results. The small scale lowers stoichiometric accuracy, and the process was simplified to allow a higher throughput, the products were not isolated in most cases. The influence of steric factors is immediately obvious when comparing the behavior of the bulkier compounds **6** and **7** to the smaller **4** and **3**. Experiments with a mesityl or xylyl substituent always result primarily in the lithiated product. This can be explained by the different sizes of lithium and the organic part of the base. Even for MeLi, the smallest representative, the methyl group needs considerably more room to approach the germanium center than lithium. It is consequently not too surprising that steric shielding near the germanium center promotes the lithiation pathway.

Size differences are also the most likely explanation for the higher rates of nucleophilic substitution observed with MeLi, compared to the other investigated bases. MeLi also shows a tendency for double and even triple substitution at the same germane. Among the larger bases, *i*-BuLi and PhLi tend to favor nucleophilic substitution as well, whereas *n*-, *sec*- and *t*-BuLi promoted the hydrogen metal exchange. However, this cannot be attributed exclusively to sterics, as it seems very likely that the basicity also shapes the reaction. With multiple factors concurrently at play, a clear trend cannot be formulated yet.

Inhibiting the approach of RLi to the reaction site naturally also slows down the conversion. Slow reaction speeds interfere with experiments in etheric solvents, due to the limited stability of the organolithium reagents. This problem led to low conversions when investigating aryls with *o*-$CH_3$ groups in $Et_2O$. At the usual

concentration (~0.5 mol/L) side reactions dominated in the screening of **3** with *t*-BuLi, and of **5** with both *n*- and *t*-BuLi. Experiments with **5** at a higher concentration (0.8 mol/l) improved the conversions. With *n*-BuLi, most of the precursor reacted to the expected products. For *t*-BuLi, the improvements were not sufficient. Most of the reaction mixture consisted of starting material and degradation products. Because the increase in concentration limits the comparability to the other reactions, the adjusted experiments were not repeated for **3**. After theses issues with *o*-$CH_3$ aryl substituents, screening of the even bigger **7** was limited to reactions with MeLi. While the reaction in THF proceeded according to expectations, conversion amounts in $Et_2O$ were too low for sensible evaluations.

**Table 5:** Dominant product obtained from the reaction of specified aryl germane with specified organolithium base in specified solvent. Products of lithiation colored blue, products of nucleophilic substitution colored green. Field left blank if a combination was not screened.

| Solvent | Base | *p*-tolylGeH$_3$ | 2,6-xylylGeH$_3$ | *o*-tolylGeH$_3$ | mesitylGeH$_3$ |
|---|---|---|---|---|---|
| pentane | MeLi | | 2,6-xylylGe(H$_2$)Li | | |
| | *n*-BuLi | | 2,6-xylylGe(H$_2$)Li | | |
| | *i*-BuLi | *i*-Bu(*p*-tolyl)Ge(H)Li | | | |
| | *sec*-BuLi | *sec*-Bu(*p*-tolyl)GeH$_2$ | | | |
| | *t*-BuLi | | 2,6-xylylGe(H$_2$)Li | | |
| Et$_2$O | MeLi | Me(*p*-tolyl)GeH$_2$ | 2,6-xylylGe(H$_2$)Li + Me(2,6-xylyl)GeH$_2$ | | mesitylGeH$_3$ |
| | *n*-BuLi | *n*-Bu(*p*-tolyl)GeH$_2$ | 2,6-xylylGe(H$_2$)Li | *n*-Bu(*o*-tolyl)GeH$_2$ | |
| | *i*-BuLi | *i*-Bu(*p*-tolyl)GeH$_2$ | | | |
| | *sec*-BuLi | *sec*-Bu(*p*-tolyl)GeH$_2$ | | | |
| | *t*-BuLi | *t*-Bu(*p*-tolyl)GeH$_2$ | 2,6-xylylGeH$_3$ | *o*-tolylGeH$_3$ | |
| | PhLi | Ph(*p*-tolyl)GeH$_2$ | | | |
| THF | MeLi | Me(*p*-tolyl)GeH$_2$ | 2,6-xylylGe(H$_2$)Li | | mesitylGe(H$_2$)Li |
| | *n*-BuLi | *p*-tolylGe(H$_2$)Li | 2,6-xylylGe(H$_2$)Li | | |
| | *i*-BuLi | *i*-Bu(*p*-tolyl)GeH$_2$ | | | |
| | *sec*-BuLi | *p*-tolylGe(H$_2$)Li | | | |
| | *t*-BuLi | *p*-tolylGe(H$_2$)Li | 2,6-xylylGe(H$_2$)Li | | |
| | PhLi | *p*-tolylGe(H$_2$)Li | | | |

## 3.4 Decorated Germanium Nanoparticles Ge@R

### 3.4.1 Development of a Robust Coupling Process

Microwave Process

Traxler had previously reported a process for the microwave assisted dehydrogenative coupling of three germanium trihydrides: 1-naphthylGeH$_3$, benzylGeH$_3$ and 2,5-xylylGeH$_3$ (Scheme 32). The process had reliably produced partially dispersible orange, polymeric material, albeit in low yields.[141]

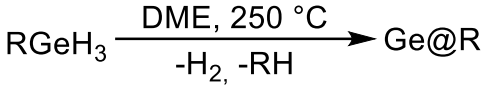


**Scheme 32:** Dehydrogenative coupling of germanium trihydrides as performed by Traxler[141]

For this thesis, Traxler's process was reproduced with *o*-tolylGeH$_3$ (**3**). Heating it for 10 min at 250 °C resulted in the previously reported orange solids. However, the yields were even lower than anticipated: 5.6% w/w from an uncatalyzed reaction (**25a**) and 10% w/w when the reaction was catalyzed with TMEDA (**25b**). Note that all nanoparticle yields are given as product weight divided by precursor weight. The varying amounts of cleaved aryl groups and the non-stoichiometric nature of the product render a conventional molar yield impractical. In the supernatant of **25a** and **25b**, large amounts of unreacted **3** were found. The next goal was thus to improve the yields by fully converting the starting material. Tripling the reaction time to 30 min (**25c**, 16% w/w) brought some improvements, but the majority of **3** remained unreacted. This also demonstrated diminishing returns for extended reaction times, as the threefold increase had only resulted in a small yield enhancement. Increasing the temperature further was not an option either, because the upper pressure limit of the microwave (30 bar) was almost surpassed even under the current conditions (Figure 14).

Consequently, a way to reduce the pressure inside the reaction vessel was required. There are two main components to the pressure buildup: Heating the reaction above the boiling point of the solvent ($bp_{DME}$ = 85 °C) sharply raises pressure during the initial temperature ramp. Cleavage of $H_2$ over the course of the reaction slowly increases it further, even after the terminal temperature is reached.

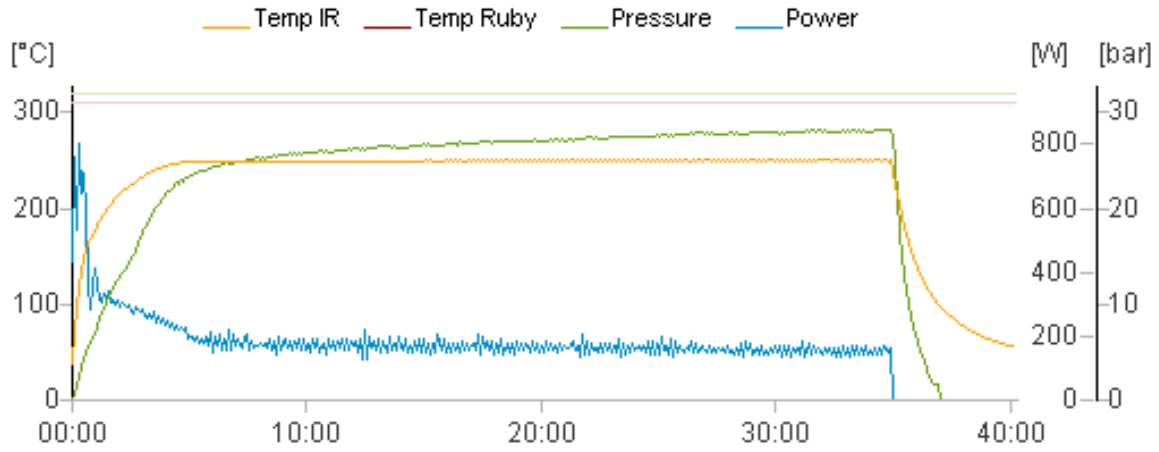


**Figure 14:** Temperature and pressure development during heating of **25c**

High pressures could potentially also be a contributing factor in the low conversion rates by progressively slowing the release of further $H_2$. Consistent with this idea, interrupting the reaction to cool it down and release the built-up $H_2$ before a second heating cycle improved the yield (**25d**, 22% w/w). The lower pressure facilitated by the venting method also enabled an increased reaction temperature of 260 °C (**25e,** 36% w/w). Unfortunately, the pressure was running up against the 30 bar limit again (Figure 15) and it seemed likely that with a further temperature increase, solvent pressure alone would be enough to initiate an emergency shutdown.

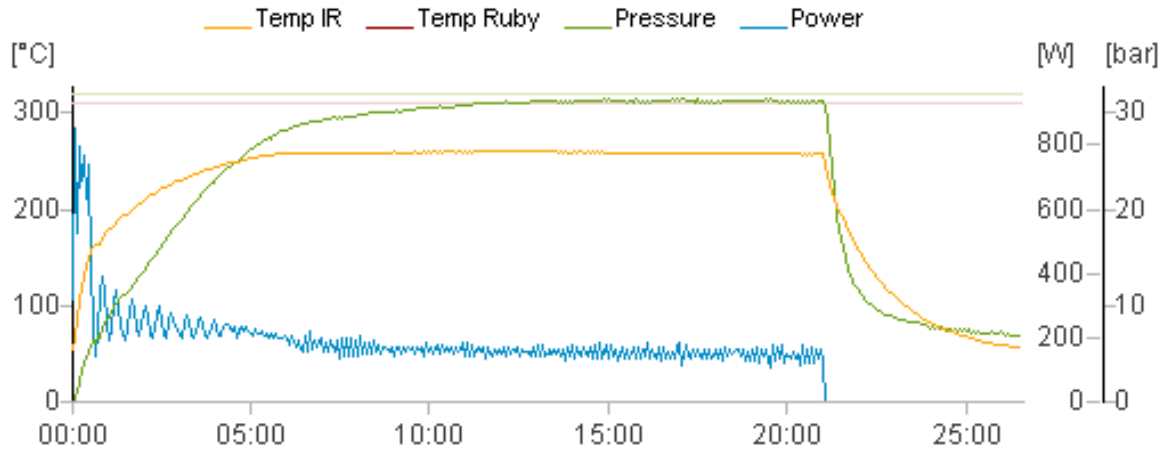


**Figure 15:** Temperature and pressure development during heating of **25d,** cycle 2.

The most straightforward solution was replacement of DME with a higher boiling solvent. First, toluene was investigated. The improvement in reaction pressure was immediately notable and, thanks to the even higher temperature, the yield was improved once again (**25f**, 56% w/w). However, a different issue occurred. Toluene

itself is nonpolar and cannot efficiently absorb the microwave radiation. This slowed heating rates considerably. As a consequence, the microwave programming initiated the hold time before reaching the target temperature (265 °C). The effect was particularly pronounced during later cycles where lower amounts of **3** remained available. The target temperature was never reached throughout these cycles (Figure 16). Reaction time and temperature thus become impossible to control, and the reactions are not reproducible. Consequently, toluene was discarded as potential solvent after only one experiment.

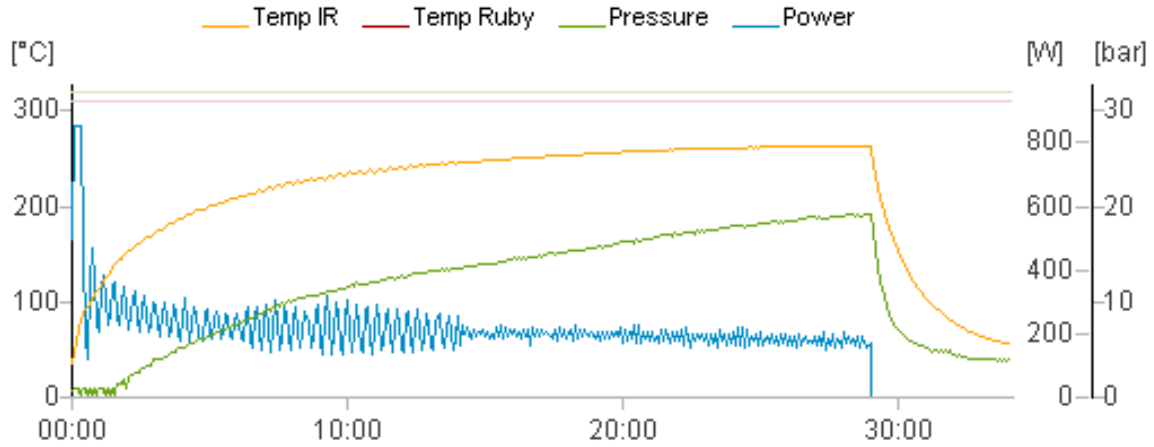


**Figure 16:** Temperature and pressure development during heating of **25f,** cycle 4.

It was evident that the solvent needed to be both polar and high boiling. These criteria lead to bis(2-methoxyethyl)ether (diglyme, Scheme 33), an ether similar to DME. Its boiling point is also far higher than even that of toluene ($bp_{diglyme}$ = 162 °C), enabling even higher reaction temperatures. The use of diglyme finally facilitated the coveted full conversion of **3** at 270 °C (**25g**, 76% w/w). The absence of starting material in the reaction mixture was verified by GC/MS. The difference in yield to 100% is due to the cleavage and subsequent removal of toluene. Heating to 270 °C in diglyme was also used for the full conversion of **7** to the Ge@mesityl nanomaterial **26a** (46% w/w).

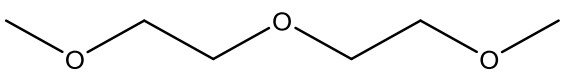


**Scheme 33:** Structure of diglyme

Unfortunately, some limitations of the microwave reaction emerged over time. Because no internal thermometer was available, temperatures were only measured

externally with an infrared sensor. The microwave keeps applying heat until this sensor detects the target temperature set by the user. The inhomogeneous reaction mixtures can cause two reactions nominally conducted at the same temperature to receive different amounts of thermal energy, limiting reproducibility. Additionally, because the utilized microwave model was not compatible with inert working techniques, atmospheric contamination was introduced to varying degrees during preparation, venting and product transfer.

Reflux Process

The limitations of the microwave provided motivation to investigate reactions under reflux conditions. $ArGeH_3$, diglyme and, optionally, TMEDA were mixed inside a Schlenk tube. After refluxing under stirring, the volatiles were removed *in vacuo*. Refluxing with TMEDA for one day resulted in incomplete conversion (**27a**, 48% w/w), but extending the reaction to three days (**27b**, 75% w/w) remedied this.

Expanding the process to mesitylgermanium trihydride (**7**) went less smoothly than during microwave reactions. An attempt to couple **7** with TMEDA in 24 h of reflux only lead to a brown liquid (**29c**). Full conversion required four days of reflux (**29a**, 54% w/w). Without TMEDA, the yield after four days was still minuscule (**29b**). Even with a doubled reaction time of eight days, considerable amounts of starting material remained (**29d**, 22% w/w). Due to these results, no 24 h reflux coupling of 2,6-xylyl$GeH_3$ (**5**) was attempted. **5** was refluxed for 4 days to generate **28a** (59% w/w).

Unfortunately, all attempts to produce nanoparticles from *n*-Bu$GeH_3$ (**8**) failed. Overnight reflux in diglyme with TMEDA did not result in an observable color change, and no product was found after vacuum workup. Even extended reaction times of three days or one week did not change this result. The problem is the low boiling point of **8** (74 °C). This prevents the starting material from reaching the high temperatures required to facilitate dehydrogenative coupling of germanes. An attempt to circumvent the issue through a pressurized reaction inside a Carius tube (180 °C) also failed. While this produced small amounts of orange solids, the reaction mixture also destroyed the seal of the tube. The product was contaminated with syringe plastic and additives as a result. Alkyl decorated germanium nanoparticles were not the main focus of this work, hence no further experiments to

produce them were conducted. If they become of interest, additional research into a suitable coupling process will be necessary.

Due to the novelty of the (trialkylsilyl)germanes and their expected differences in reactivity, several additional experiments were undertaken to establish a suitable dehydrogenative coupling process. Stirring **21** with TMEDA at room temperature did not result in any visible reaction. Similarly, refluxing the sample with TMEDA in $C_6D_6$ did not produce any evidence of dehydrogenative coupling. However, when diglyme was used as a solvent instead and the reaction temperature increased to 110 °C, a color change to yellow occurred within 1 h. The color deepened further with increasing reaction time. The reaction was terminated after 3 hours because orange/brown precipitate had begun forming. After removal of volatile components under reduced pressure, a GC/MS of the residue demonstrated the formation of a dimer formation (Figure 17).

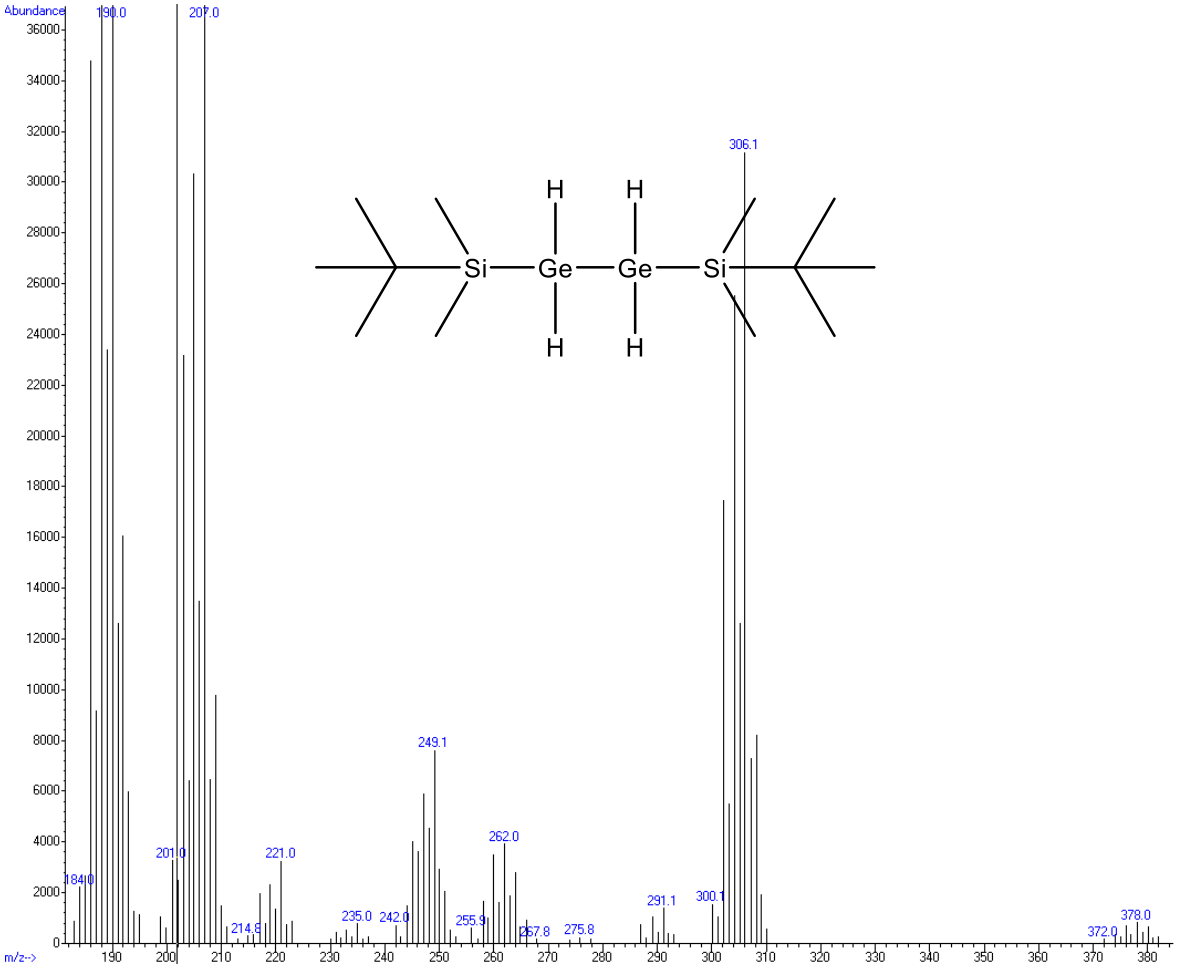


**Figure 17:** Mass spectrum of $(TBDMSGeH_2)_2$

This proves the occurrence of dehydrogenative coupling. Subjecting **22** to the same conditions produced a similar result, with a color change to orange and the formation of precipitate as evidence of a reaction taking place. The yields of coupling products **31** and **32** were insufficient for any further characterization. The development of a facile, reproducible coupling process for (trialkylsilyl)germanes and the characterization of the resulting materials go beyond the scope of this work.

### 3.4.2 Mechanism of Nanoparticle Formation[156]

Arylgermanium trihydrides, diglyme and TMEDA are all colorless liquids. Consequently, at the beginning of the dehydrogenative coupling process the solution only absorbs in the UV range (Figure 18). The observed peaks are primarily due to the trihydride (reference spectrum in appendix).

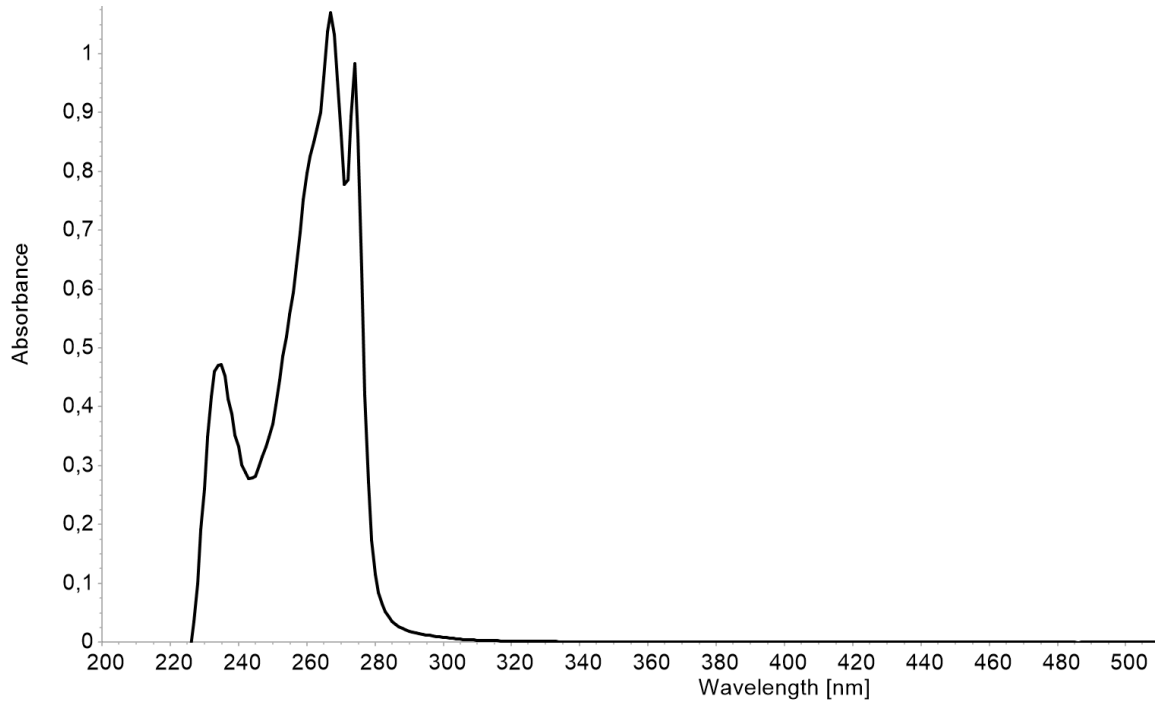


**Figure 18:** UV/Vis spectrum of reaction mixture **27e** in THF, prior to heating. c = 10 mL/L.

Over time, the solution turns yellow, orange, red and even brown, if it is concentrated enough (Figure 19). The reason for the change in absorptivity is quantum confinement of the valence electrons, a size dependent phenomenon discussed in chapter 2.3.1. The red shifting absorption thus showcases the growing nanoparticles. After 72 hours at 162 °C, no starting material is left (Chapter 3.4.1, **27b**) and the growth slows down notably.

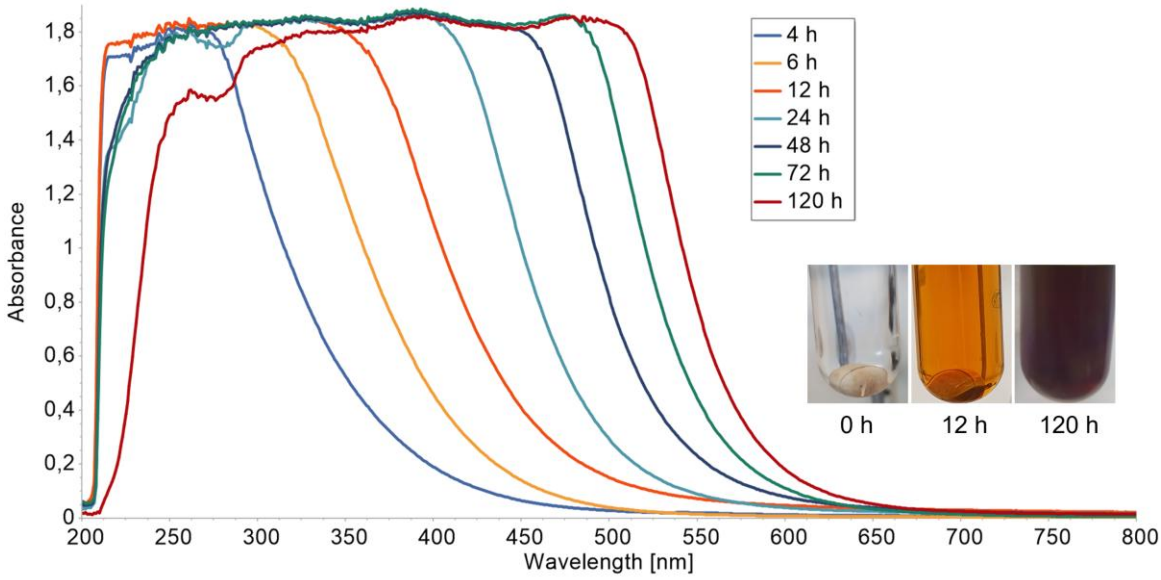


**Figure 19:** UV/Vis spectra of **27e** after various reaction times. c~10 mg/mL. Intentionally recorded at concentrations with absorbance>1 to better showcase the blue shifting onset of absorption.[156]

In the dehydrogenative coupling of tin trihydrides $ArSnH_3$ the polymerization proceeds *via* a dimeric intermediate $Ar(H_2)Sn\text{-}Sn(H_2)Ar$. This intermediate was isolated in a sterically stabilized compound (Ar = bis-2,6-(2,4,6-triisopropylphenyl)-phenyl)[132] and also shown *in situ* for a smaller species (Ar = *o*-tolyl).[10] To elucidate the mechanism of germanium couplings $^1H$ NMR spectra of **27e** were taken. Soon after the reaction start, signals appear at 5.18 ppm and 4.50 ppm which get more pronounced over time (Figure 20, top). They were assigned as germanium hydrides based on their characteristic shifts. The assignment was confirmed by the $^1H$ NMR of **27f** produced from deuteride **12** under identical conditions. The spectra are identical, except for the signals at 5.18 ppm and 4.50 ppm (Figure 20, bottom). Because the GeH signals do not exhibit the polymer broadening visible both in the aromatic and the aliphatic region of the spectrum, it can be concluded that they stem from discreet oligomers. The intensity of the GeH peaks reaches a maximum after about 24 h and then starts decreasing again, until they eventually disappear (Figure 21).

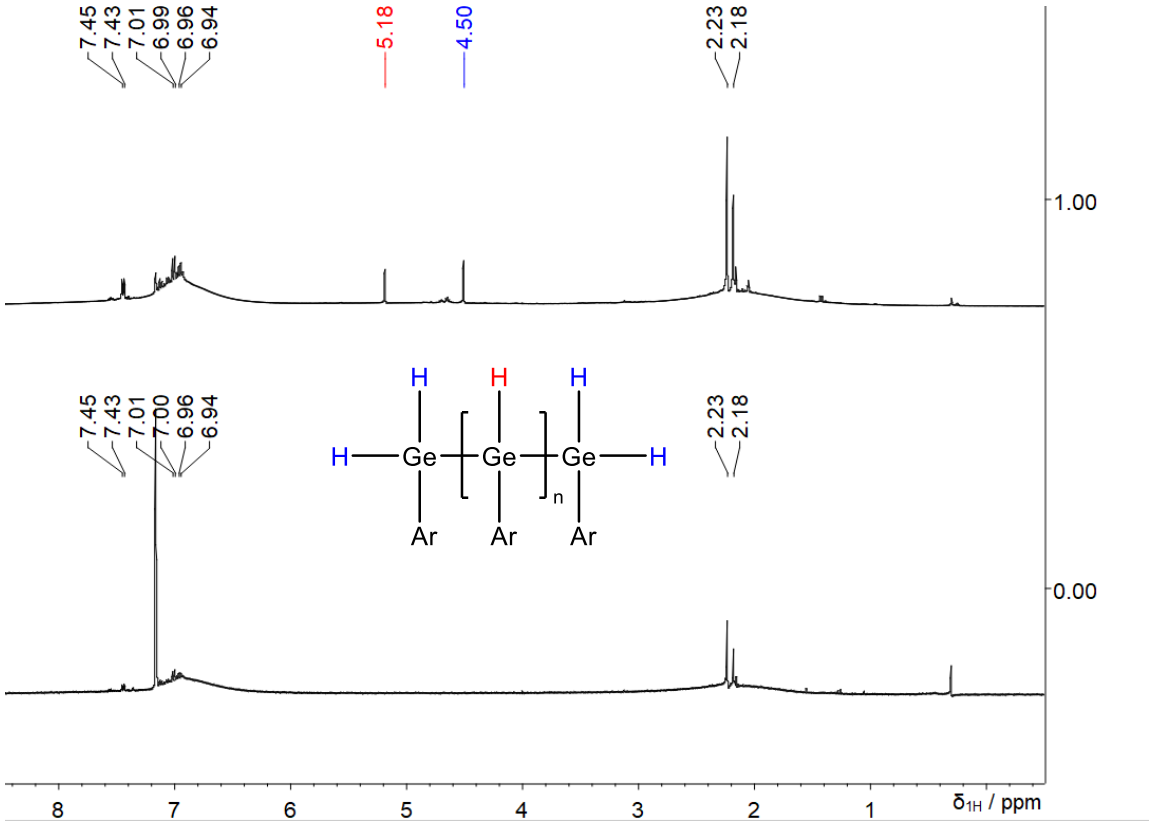


**Figure 20:** $^{1}$H NMR (400 MHz, $C_6D_6$) of **27e$_{24}$** (top) and **27f** (bottom)

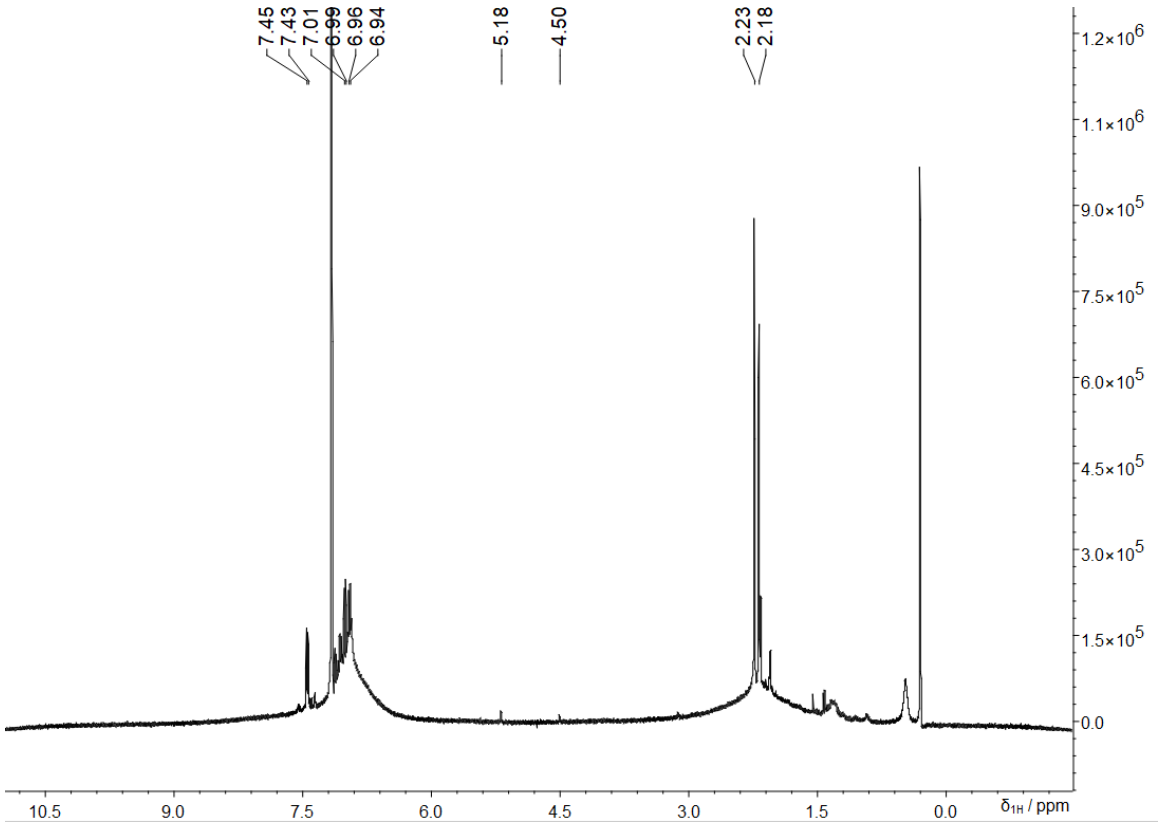


**Figure 21:** $^{1}$H NMR (400 MHz, $C_6D_6$) of **27e$_{72}$**

Comparison of the observed shifts to literature values for other oligogermanes (Table 6) led to assignment of the signal at 5.18 ppm as a bridging group inside an oligomer, while the signal at 4.51 ppm was assigned as an oligomeric end group (Scheme 34). Isolation of the oligomers was attempted *via* recondensation at 95 °C, $9.6*10^{-3}$ mbar. Only one species was both stable and volatile enough to be isolated by this process.

**Table 6:** $^{1}$H NMR shifts reported for various arylgermanes[156]

| **Substance** | **δ($GeH_2$)** | **δ(GeH) [ppm]** |
|---|---|---|
| $R_3GeH$ | - | 5.5-6.8[142] |
| $R_2GeH_2$ | 4.9-5.8[142] | - |
| $H_2PhGeGePhH_2$ | 4.40[157] | - |
| $H_2MesGeGeMesH_2$ | 4.50[60] | - |
| $H_2PhGeGeH_3$ | 4.60[159] | - |
| $H_2(2,6Trip_2C_6H_3)GeSn(2,6\text{-}Mes_2C_6H_3)$ | 5.87[160] | - |
| $(Ar^{NiPr2}Ge(H))_3$ | 4.70, 4.88[161] | 4.99[161] |
| $H_2PhGe(GeHPh)GePhH_2$ | 4.50[158] | 5.25[158] |
| $Ph_3Ge(GeHPh)GePh_3$ | - | 5.27[162] |
| $[(PhGeH)_{1/3}(PhGe)_{2/3}]_n$ | | 4.5-5.5[128] |
| This work | 4.50 | 5.18 |

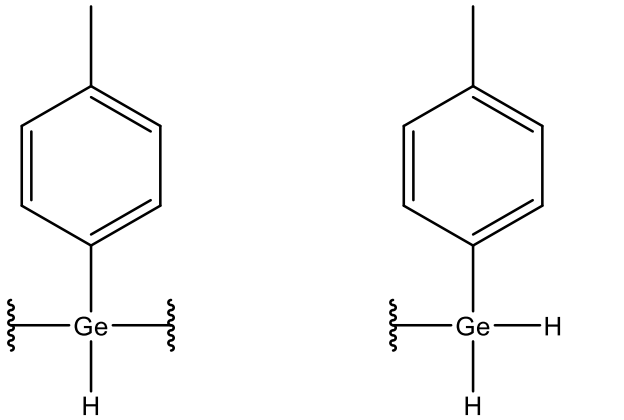


δ(GeH) = 5.18 ppm  δ($GeH_2$) = 4.51 ppm

**Scheme 34:** Assignment of observed GeH shifts to two different oligomer moieties

The $^{1}$H NMR (Figure 22) of this compound lacks the previously observed signals at 4.51 ppm. The integral ratios (ArH:GeH:$ArCH_3$=4:1:3) also demonstrate the lack of an end group. The isolated compound is consequently a cyclic oligomer, either the trimer or the tetramer, the most volatile representatives of the group. Calculations showed that cyclic structures are energetically favorable for germanium tri- and

tetramers.[163] The boiling point of the dimer can be expected to be considerably lower than that of cyclic oligomers. If present in the mixture, it should have appeared in the condensate. Its absence suggests that the dimer is an unstable intermediate that quickly reacts onward to higher oligomers.

In the dehydrogenative coupling of arylgermanium trihydrides, new Ge-Ge bonds are not only formed at the expense of Ge-H bonds. Elemental analysis of the nanoparticles (**27a**: C: 36.92%, H: 3.73%) shows that Ge-C bonds are also cleaved ([*o*-tolylGe]$_n$ calcd: C: 51.34%, H: 4.31%). Analogous behavior was previously reported for the dehydrogenative coupling of aryltin trihydrides. While multiple different removal mechanisms could conceivably occur, the presence of toluene in the reaction solution indicated that the tolyl group is primarily split off *via* α-elimination. No other cleavage products were found.

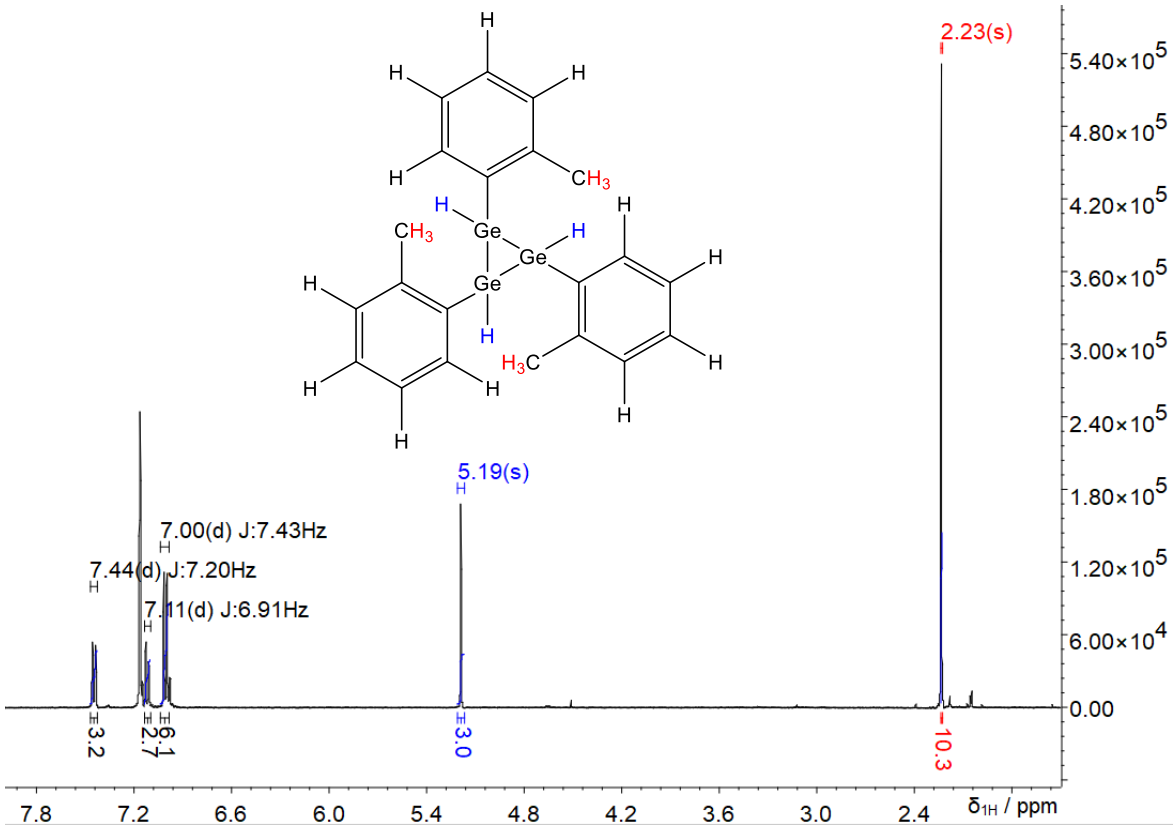


**Figure 22:** $^1$H NMR (400 MHz, $C_6D_6$) of a cyclic oligomer isolated from **27a** *via* recondensation

Comparing a pair of otherwise identical samples with and without TMEDA clearly demonstrated the catalytic effect of the amine base. The pairs **25a** *vs* **25b** and **27a** *vs* **27c** both show more yield for catalyzed reactions, due to higher conversion of

starting material in the same time. The catalytic mechanism can be expected to work along lines similar to those proposed for the analogous stannanes (Chapter 2.4.1). Either the nitrogen lone pairs of TMEDA coordinate to the metal center and weaken the Ge-H bonds, or the base abstracts $H^+$, which subsequently reacts with another hydrogen atom to form $H_2$. Catalysis of germanes appears to speed up reactions by a factor of less than two. This is far weaker than the catalytic effect on stannanes, where reactions that would ordinarily require days or weeks occur in less than an hour in the presence of TMEDA.

### 3.4.3 Characterization of Aryl Decorated Germanium Nanoparticles[156]

Appearance

**Figure 23:** Appearance of **27a**

All nanoparticles Ge@aryl were obtained as orange, red or brown powder (Figure 23). Under an optical microscope, the powder was revealed to be made up by agglomerated pieces. The size and color of the agglomerates depends on the treatment of the powder prior to analysis. In the standard isolation procedure, the nanoparticles were obtained from their diglyme solution through solvent evaporation and then dumped from the reaction flask into a weighing boat and transferred to a small vial. When stuck to the flask or the plastic of the weighing boat, the powder was liberated through scraping with a spatula. This procedure led to transparent agglomerates with a size of 50–100 µm and a deep red coloration (Figure 24). Some amount of smaller agglomerates, caused by unintentional crushing of bigger pieces while transferring them, can also be seen. A similar appearance was reported for germanium nanoparticles obtained *via* disproportionation of GeBr.[120]

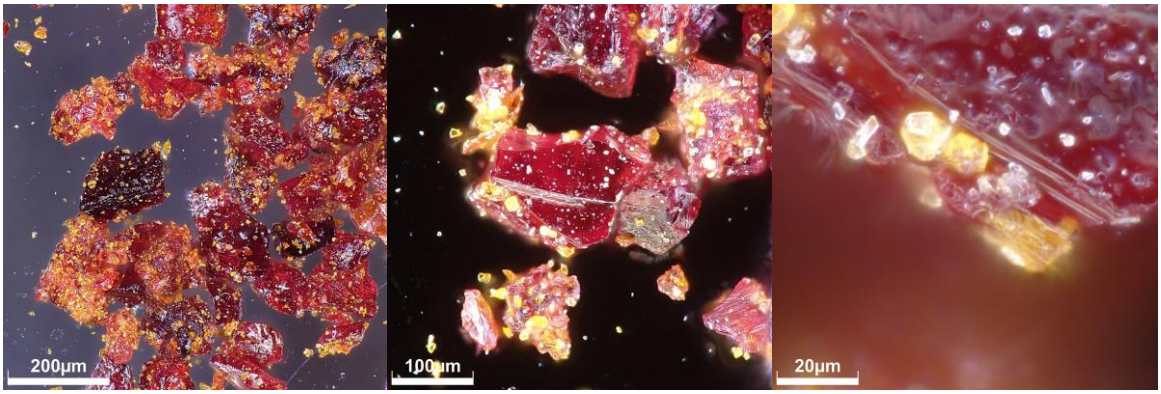


**Figure 24:** Optical microscopy image of **27a** as obtained, taken in dark field mode at various magnifications

Through application of mechanical force, these agglomerates can be ground to a fine powder (Figure 25). When powdered, the nanoparticles appear yellow or in some cases even white in color. This is caused by the shorter optical path length, as the absorptivity of the powder continuously falls with increasing wave lengths. Thinner (or more dilute) samples are barely absorbent in the visible range (Figure 26).

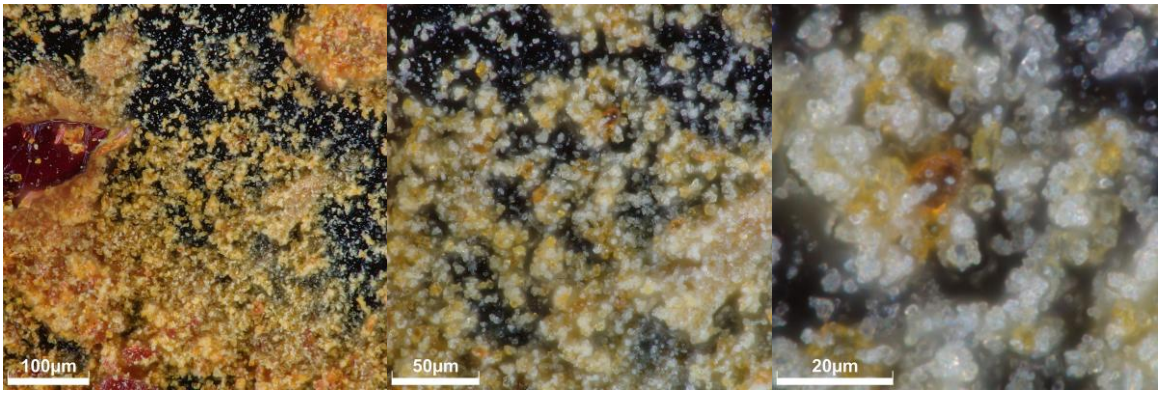


**Figure 25:** Optical microscopy of ground **27a**, taken in dark field mode at various magnifications

The same structures found with optical microscopy are also visible under SEM (Figure 27). The highest magnification (x 50k) reveals the individual nanoparticles making up the rough agglomerate surface. However, they are not big and differentiated enough to determine their size from these images. Nanoparticles synthesized with very short reaction times (*via* microwave) agglomerate to regular spherical structures (Figure 28). A similar observation was previously reported for Sn@*o*-tolyl. When the material was prepared with short reaction times (through the addition of TMEDA), spherical agglomerates were the result, whereas long reaction times led to more irregular structures.[123,156]

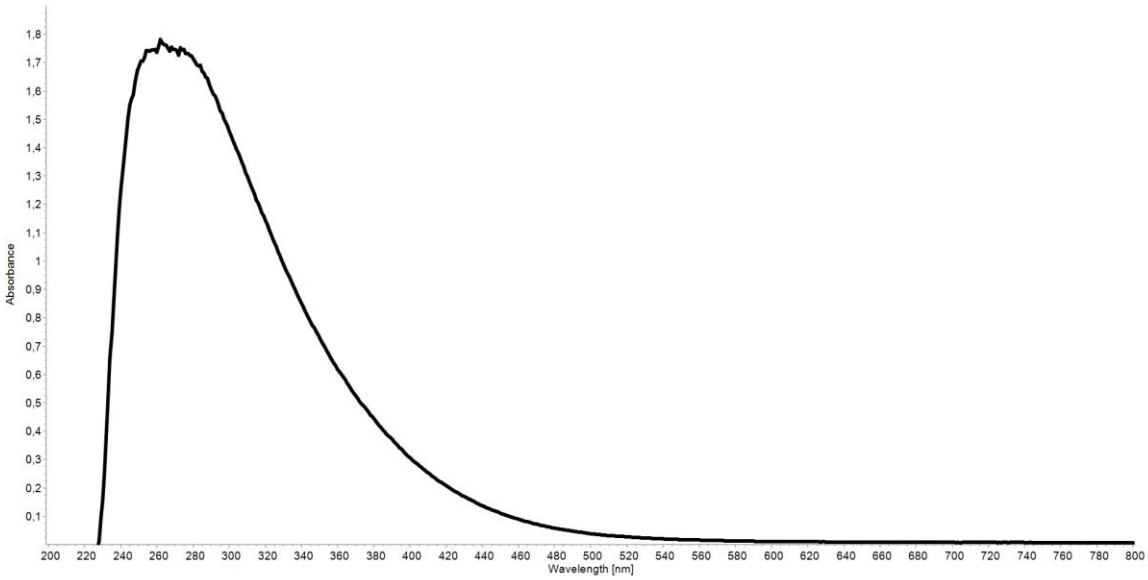


**Figure 26:** UV/Vis spectrum of **27a** in THF, c~1 mg/mL

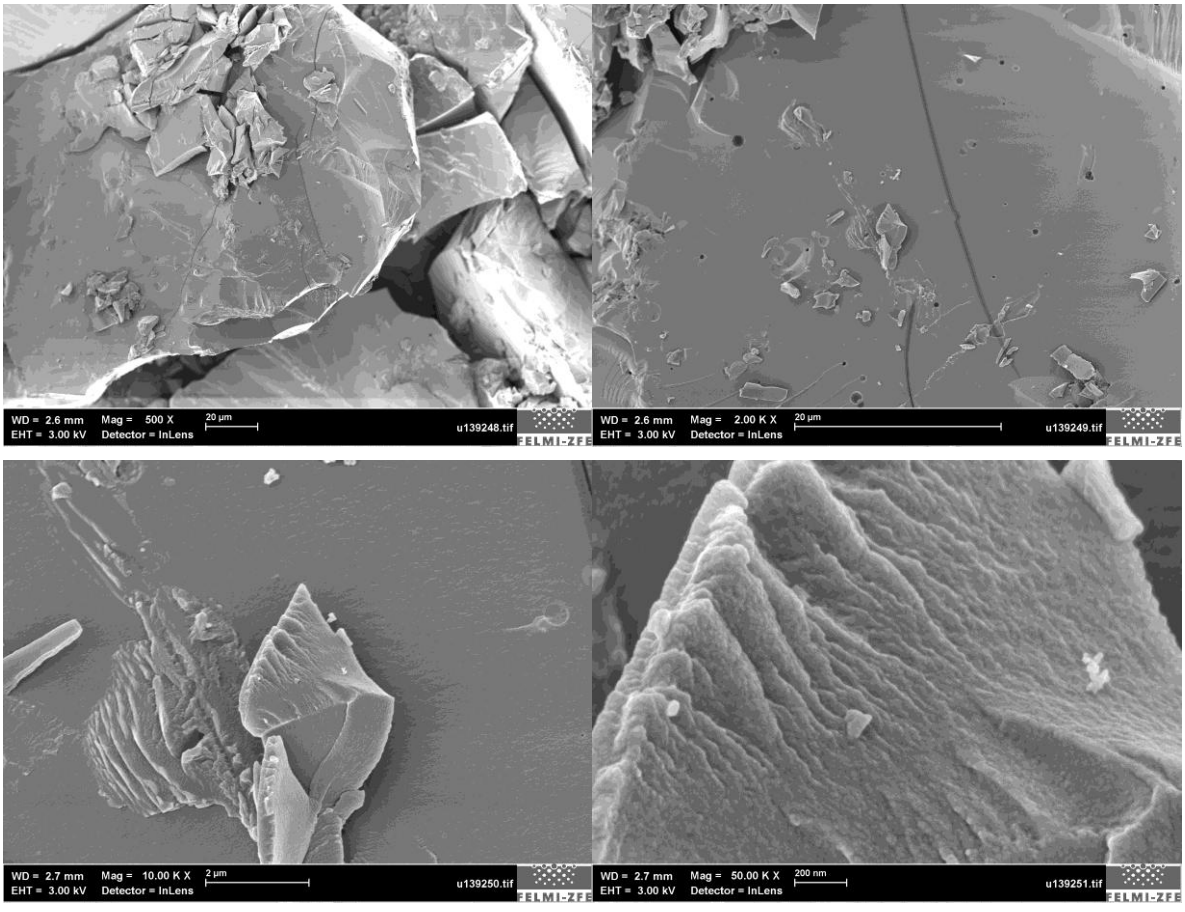


**Figure 27:** SEM images of **27a** at various magnifications

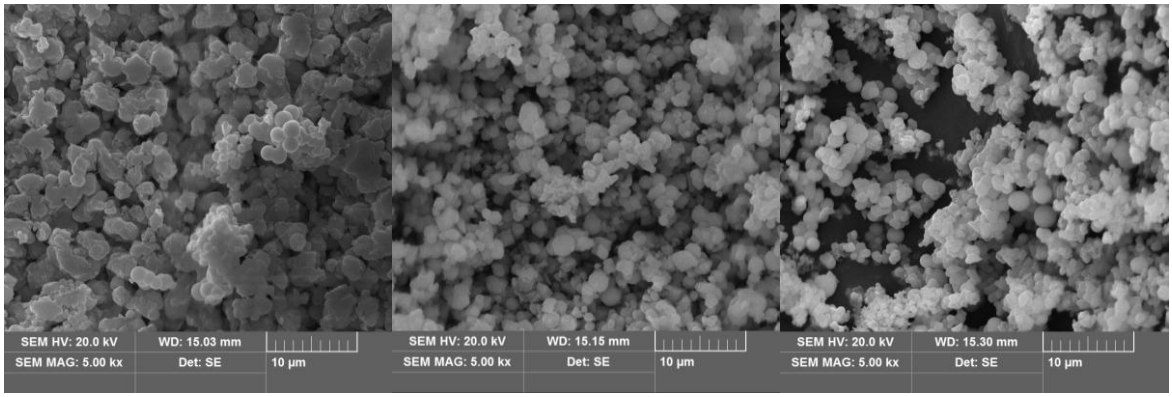


**Figure 28:** SEM images of **25g** (left), **25i** (middle) and **26a** (right).

## Particle Size

Multiple methods were used to determine the particle size of several Ge@aryl samples in both the solid and liquid state. Unfortunately, attempts to use TEM for solid state determinations fell through (Figure 29). A potential reason is the non-inert sample preparation. While the particles are somewhat resistant to oxidation and degrade only slowly (see below), TEM necessitates measuring the very edge of an agglomerate in order to observe only a single layer. It is possible that the vulnerable agglomerate surface is oxidized much quicker than the rest of the material. A different explanation is damage caused by the beam itself. A previously reported failure to resolve Sn@aryl nanoparticles using TEM was attributed to beam damage and a resulting degradation of the organic hull.[10]

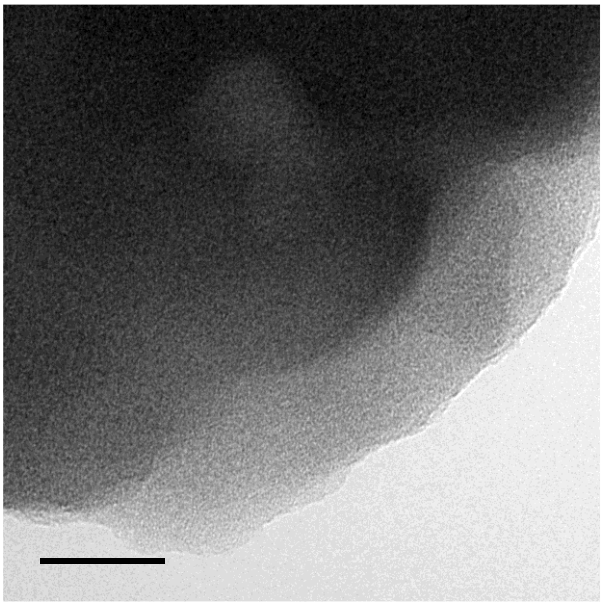

**Figure 29:** TEM image of the edge of an agglomerate of **27a**, jutting out beyond the support grid

AFM was likewise unusable. When the sample film was prepared from a concentrated solution, only agglomerates were found. If a more dilute solution was used, no signals were detected at all.

In lieu of usable TEM data, the solid-state particle size was elucidated *via* SAXS. A repeating length in the single nanometer range (correlation length) causes a scattering peak at small Bragg angles (Figure 30). In small nanoparticles, the interparticle distance (closely related to the particle diameter) is such a repeating length. The size of the nanoparticles can therefore be approximated with Equation 1.

$$Equation\ 1: d = \frac{2\pi}{q}$$

*q ... scattering vector, d...particle diameter*

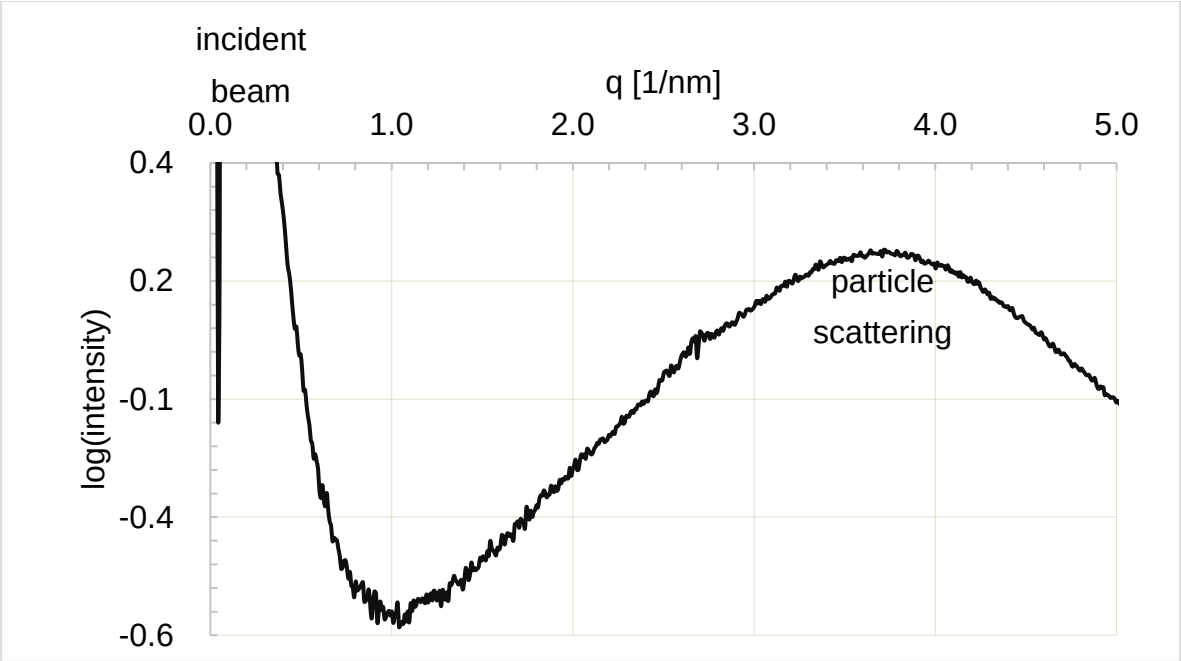


**Figure 30:** Powder SAXS curve of **27a**

With this method, a particle size of 1.7 nm was calculated for **27a.** This value (and all size values given hereafter) represents the peak of the distribution, as the particles have a broad range of different diameters.

The size of the final material can be directed through both the chosen aryl substituent and the reaction conditions. Extending the reaction time to achieve full conversion unsurprisingly results in an increased size, with **27b** having a diameter of 1.8 nm.

Foregoing the use of TMEDA will also increase the size of the obtained particles. While **27c** gave no scattering signal (Figure 31), most likely due to a broad size distribution caused by the premature reaction termination, **27d** shows a major increase in size to 2.6 nm. Increased sizes for nanomaterials obtained from uncatalyzed reactions was also reported for Sn@aryl particles.[134]

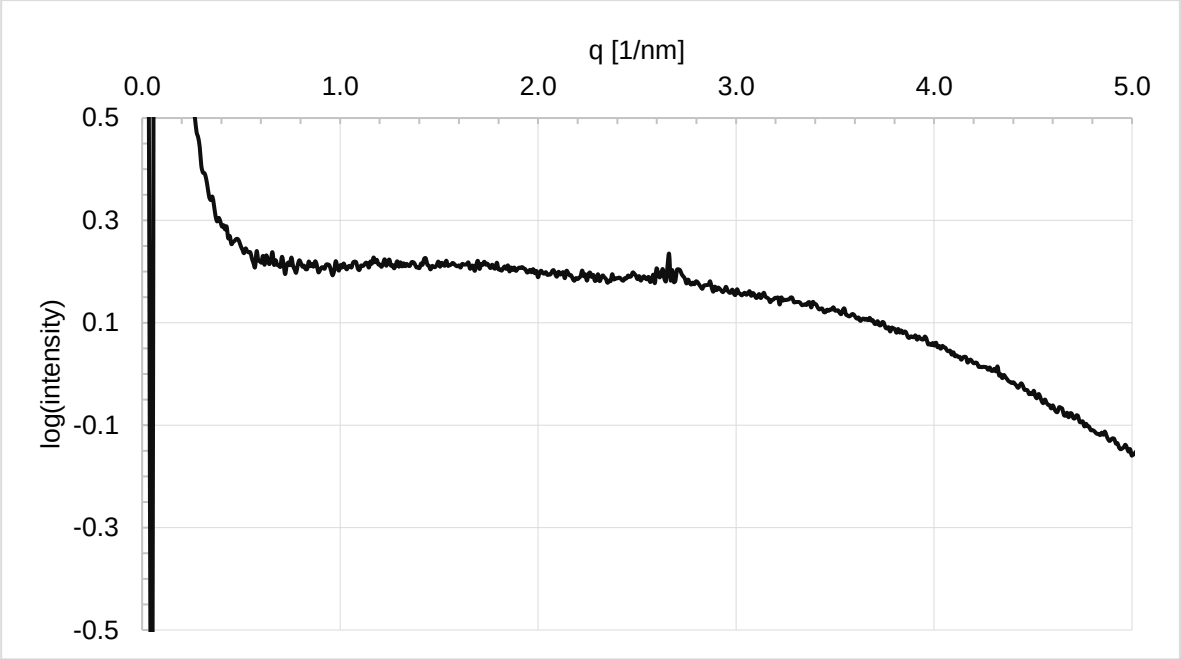


**Figure 31:** Powder SAXS curve of **27c**

The reason for this lies in the characteristics of the catalysis: Because it primarily speeds up hydrogen abstraction, more aryl substituents remain attached. This is evidenced by elemental analysis (Table 7). With more Ge-C bonds remaining, less Ge-Ge binding sites are available and the growth is stymied.

**Table 7:** Elemental analysis of three Ge@aryl pairs synthesized with (left) and without (right) TMEDA

| Compound | 27b | 27d | 28a | 28b | 29a | 29b |
|---|---|---|---|---|---|---|
| **C [%]** | 35.70 | 32.95 | 34.03 | 28.96 | 37.18 | 28.70 |
| **H [%]** | 3.70 | 3.22 | 3.39 | 2.89 | 4.51 | 3.83 |

Increasing the reaction temperature through use of a microwave offers another way to increase the products' particle size. The comparison of the microwave reactions carried out at 240 °C (**25h**, 2.4 nm), 270 °C (**25g**, 2.6 nm) and 300 °C (**25i**, 2.7 nm) also reveals a general temperature dependence of the diameter. The reason is once

again the amount of available catenation sites. In this case, additional *o*-tolyl ligands are cleaved by the heating of the material beyond its decomposition temperature (~250 °C, see below).

Finally, the choice of aryl substituent can also drastically influence the size. Here, bigger groups lead to bigger particles. There are two different effects simultaneously promoting this result. First, a bigger group of course increases the space requirements of the organic particle hull. Secondly, the amount of potential Ge-Ge bindings sites is once again crucial. The bigger substituents are better leaving groups. They are more easily cleaved from germanium (see below). This also explains why the size differences are more pronounced in samples synthesized in the microwave or without TMEDA, where dearylation plays a larger overall role. The increased removal rate for larger substituents is once again supported by elemental analysis. It is interesting to note that, counter to this observation, a 24 h reflux reaction did not produce any isolable solids for mesityl (**29c**), despite resulting in decent yields for *o*-tolyl (**27a**: 48% w/w). A possible explanation is, that the initial oligomerization is more dependent on $H_2$ abstraction, which is sterically hindered by larger aryl groups and does not benefit from having a better leaving group. Ge@mesityl formation would then only become faster than Ge@*o*-tolyl formation in the later particle growth stages, hence resulting in a lower degree of polymerization after 24 hours, but a higher one after 72 hours. The general trends established for Ge@*o*-tolyl (temperature and catalyst dependency of nanoparticle diameter) were reproduced in both Ge@2,6-xylyl and Ge@mesityl. All determined solid state sizes for the produced nanomaterials are listed in Table 8.

**Table 8:** SAXS correlation lengths' (in nm) of the Ge@aryl compounds prepared in this work

| Compound | a | b | c | d | e | f | g | h | i |
|---|---|---|---|---|---|---|---|---|---|
| **25** | nd | nd | nd | 2.3 | 2.2 | 2.9 | 2.6 | 2.4 | 2.7 |
| **26** | 4.2 | nd | - | - | - | - | - | - | - |
| **27** | 1.7 | 1.8 | nd | 2.6 | 1.8 (120 h) | 1.7 | - | - | - |
| **28** | 2.2 | 4.5 | - | - | - | - | - | - | - |
| **29** | 2.5 | 6.3 | nd | 5.2 | - | - | - | - | - |

"nd"…not determinable; "-"…number/letter combination not used

The hydrodynamic radius $R_h$ of the particles was determined with GPC. The peak for the $R_h$ distribution of **27a** is at 1.4 nm, giving a of 2.8 nm (Figure 32). While this value is bigger than the particle size found with powder SAXS (1.7 nm), the

discrepancy is easily explained by the solvation sphere. Additional solvent molecules are attached to the nanoparticles in their dispersed state, increasing their overall size. In **27g**, produced with only 8 h of reflux, the entire distribution is of course shifted to smaller sizes, with the peak at 1.2 nm.

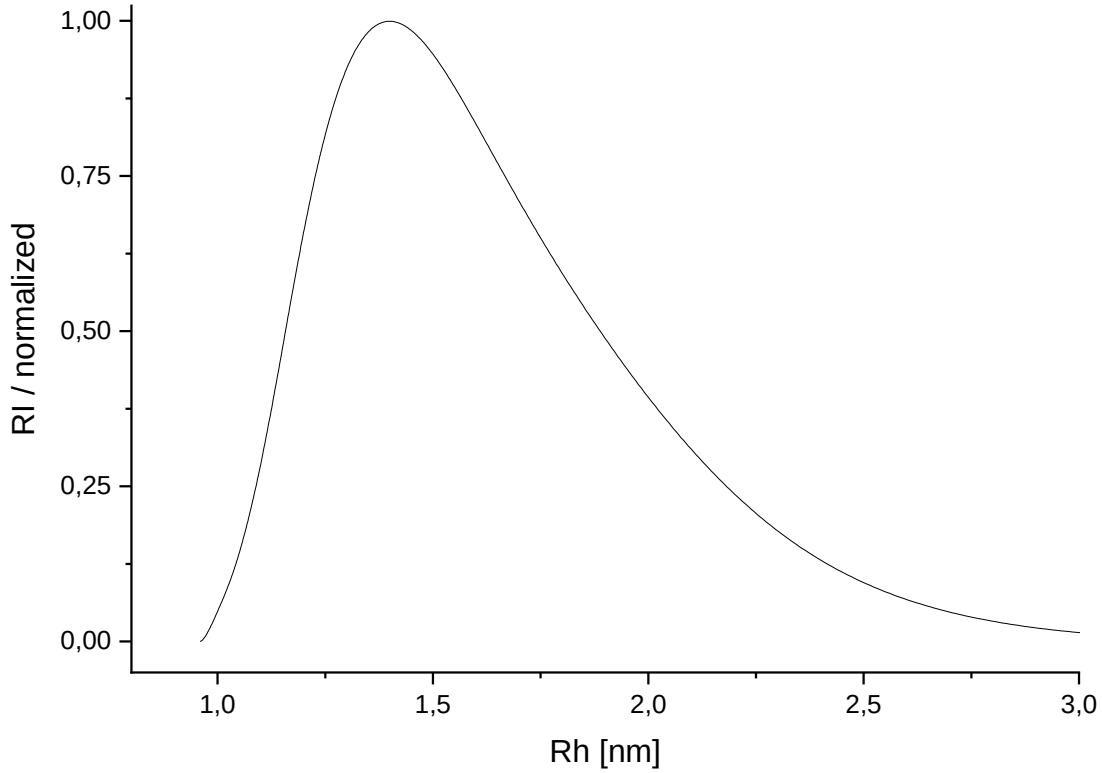


**Figure 32:** GPC elution curve for **27a** dispersed in THF[156]

Attempts to calculate $R_h$ were also made *via* DLS. The shorter preparation and measurement times would have allowed for the screening of more samples. Unfortunately, the calculated distributions were much broader than those obtained from other methods (Figure 33). Additionally, results for the same sample fluctuated significantly, both within multiple runs under the same conditions (σ=39%) and when comparing the averaged results of measurements under varying conditions (σ=6.0%). The main reason for the unsatisfactory outcome is the small size of Ge@aryl particles. They are at the lower edge of the range measurable with DLS (0.3 nm–10 µm). Because scattering intensity depends on the particle size by a power of ~6, the measured intensities are very low. Tiny contaminations with larger particles caused strong interferences. Several attempts were made to remove all larger particles: use of glass syringes for both nanomaterial synthesis and sample preparation to avoid leech-out of syringe materials, filtration (20 nm and 200 nm) and

surfactant addition (*n*-$Bu_3P$). However, the interferences persisted. It is possible that they are a modelling artifact. The absorption of visible light by the particles poses a further problem. The resultant energy uptake can cause local temperature hotspots, resulting in faster convection and smaller calculated sizes.

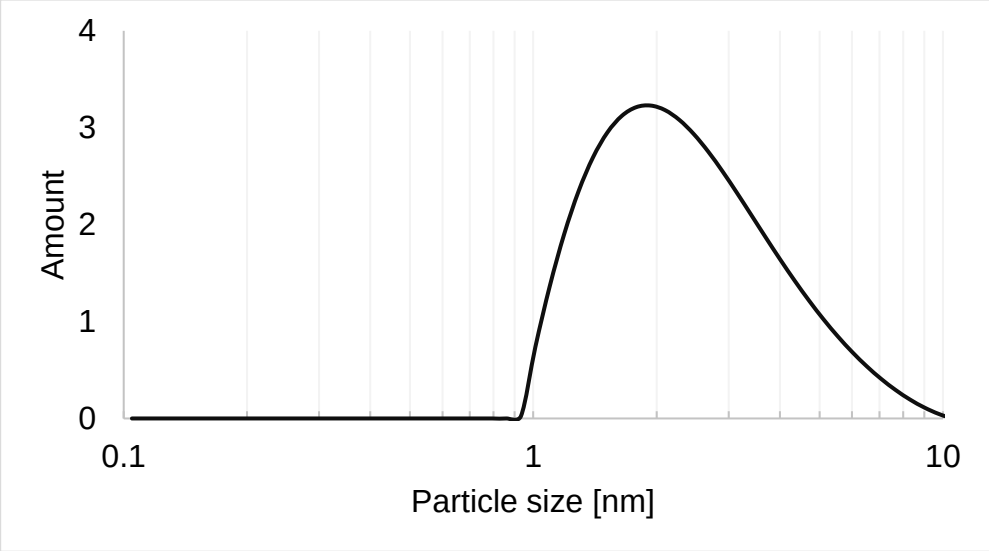


**Figure 33:** DLS of **27a**, prepared with glass syringe, filtrated (200 nm), 25 °C, backscatter mode

Plans to monitor the increasing particle sizes during reaction **27e** with DLS had to be discarded because the standard deviation was vastly higher than the expected size changes between samples. A significant size difference was only observed between samples from the very beginning and the very end of the reaction (Figure 34). Despite all the issues, the sizes obtained *via* GPC and DLS provided a surprisingly reasonable match (**27a**: DLS=2.7±1.3 nm, GPC=2.8 nm).

In addition to the methods described, the Scherrer equation was used to estimate a low single digit nanometer size from the powder XRD spectrum of **27a** (Figure 38). While there are some uncertainties attached to each of the applied techniques, the good overall agreement between them provides high confidence in the obtained results. The Ge@aryl materials prepared in this work are among the smallest germanium nanoparticles from solution syntheses. Reported sizes typically begin at 2 nm, but can also be considerably larger.[5,96,117] The small size is crucial for the exhibition of quantum confinement effects (2.3.1). The relatively broad range within which Ge@aryl sizes can be tuned (1.7–6.3 nm powder size obtained in this work) is an additional benefit, due to the strong size dependency of quantum effects.

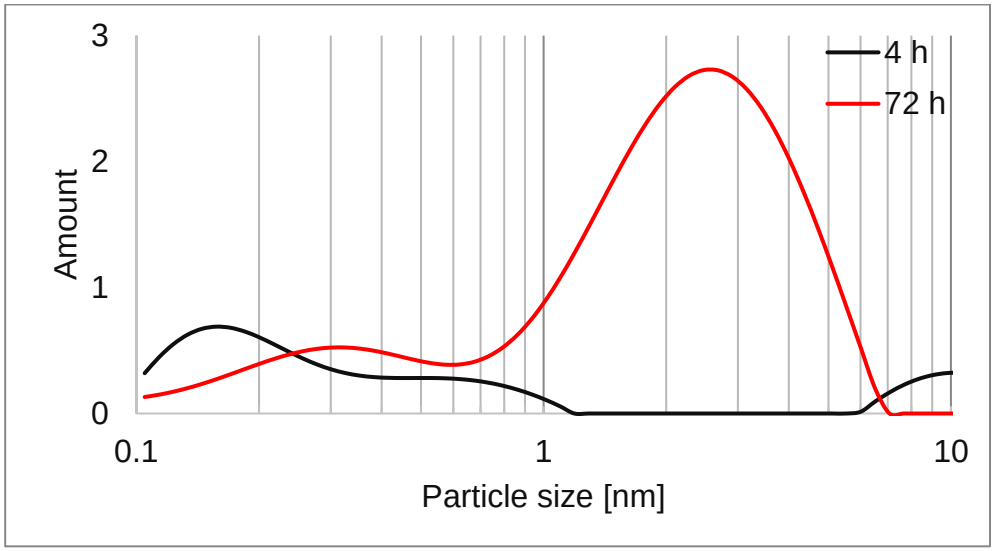


**Figure 34:** DLS of **27e** after 4 h and 120 h, prepared with glass syringe, filtrated (200 nm), added *n*-$Bu_3P$ surfactant, 25 °C, backscatter mode

Chemical Composition

TOF-MS was employed to gain more specific insights into the chemical makeup than those provided by elemental analysis. Unfortunately, the standard sample **27a** proved too big and heavy to ionize without fragmentation. No useful data was gathered in linear mode. While the size range in reflectron mode is not big enough to capture particles, several smaller $tolyl_mGe_n$ clusters were recorded (Figure 35). These clusters could originate either in fragmentation of larger nanoparticles, or in the photoionization of smaller oligomers. As the presence of *o*-$tolyl_3Ge$ shows, the tolyl groups wander during ionization.

A previously reported mass spectrum for Ge@benzyl nanoparticles from partially converted $benzylGeH_3$[141] inspired the idea to synthesize smaller nanoparticles through premature termination of the coupling reaction after 8 hours (**27g**). Unfortunately, the low yield and unfavorable consistency (sticky, viscous slime) prevented the gathering of SAXS and EA data. GPC was used to confirm the smaller size of this material (see above). The idea proved its merit when complete **27g** particles were successfully measured with linear mode TOF-MS (Figure 36).

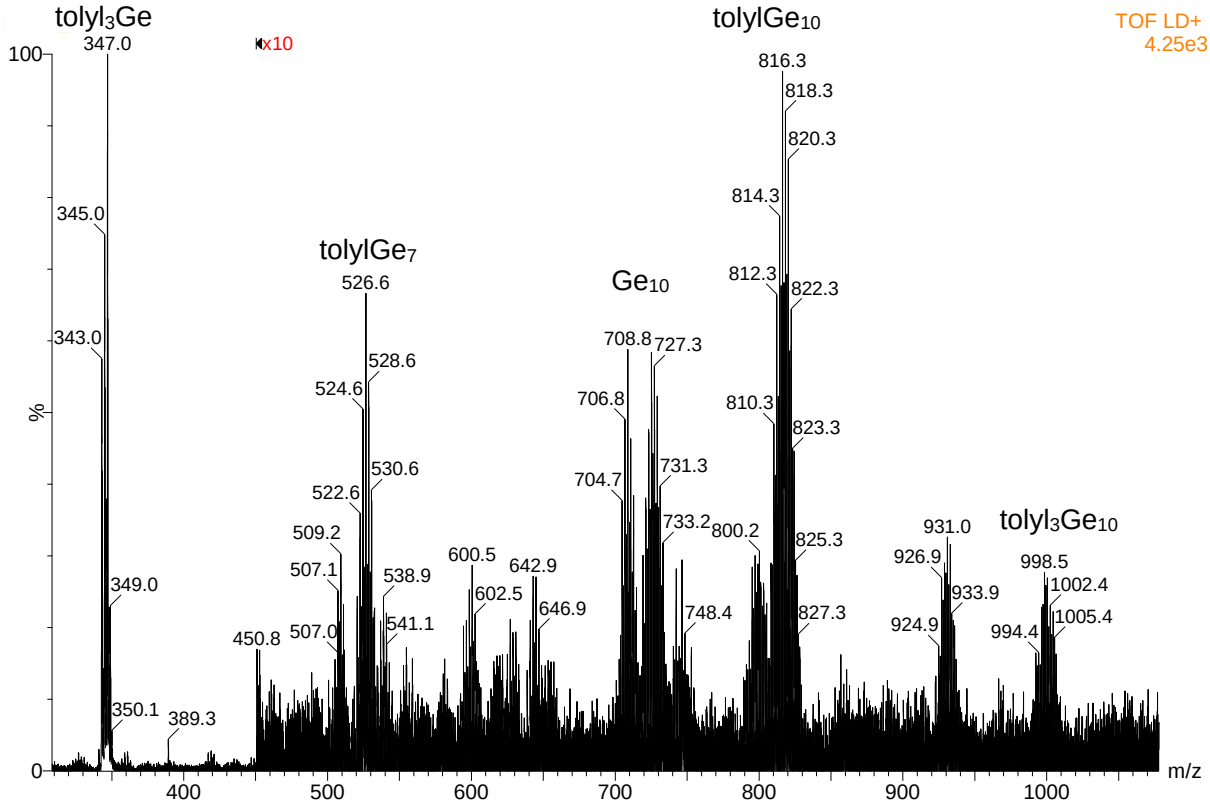


**Figure 35:** Reflectron mode TOF-MS of **27a**

At lower *m*/*z* ranges, the previously described clusters are found. *o*-tolyl$_3$Ge$_{10}$ is once again the largest cluster, beyond which the ion count enters a continuous decline until about *m*/*z* = 3400. At this point, a sharp rise in the curve shows the presence of nanoparticles. The peak of the distribution lies at *m*/*z* = 4506.4. Based on this weight, the most common compounds in the sample are of the type *o*-tolyl$_{21-n}$Ge$_{35+n}$H$_{7+17n}$. While no elemental analysis is available for this sample, the best fit for the elemental analyses of other Ge@*o*-tolyl compounds is found with n=0–3 (Table 9).

**Table 9:** Found elemental distribution of **27a** and **27c** alongside calculated values for *o*-tolyl$_{21-n}$Ge$_{35+n}$H$_{7+17n}$ compounds with n=0–3.

| | **27a** | **27c** | ***o*-tolyl$_{21}$Ge$_{35}$H$_7$** | ***o*-tolyl$_{20}$Ge$_{36}$H$_{24}$** | ***o*-tolyl$_{19}$Ge$_{37}$H$_{41}$** | ***o*-tolyl$_{18}$Ge$_{38}$H$_{58}$** |
|---|---|---|---|---|---|---|
| **C [%]** | 36.92 | 39.27 | 39.56 | 37.69 | 35.82 | 33.94 |
| **H [%]** | 3.73 | 4.08 | 3.48 | 3.71 | 3.93 | 4.16 |

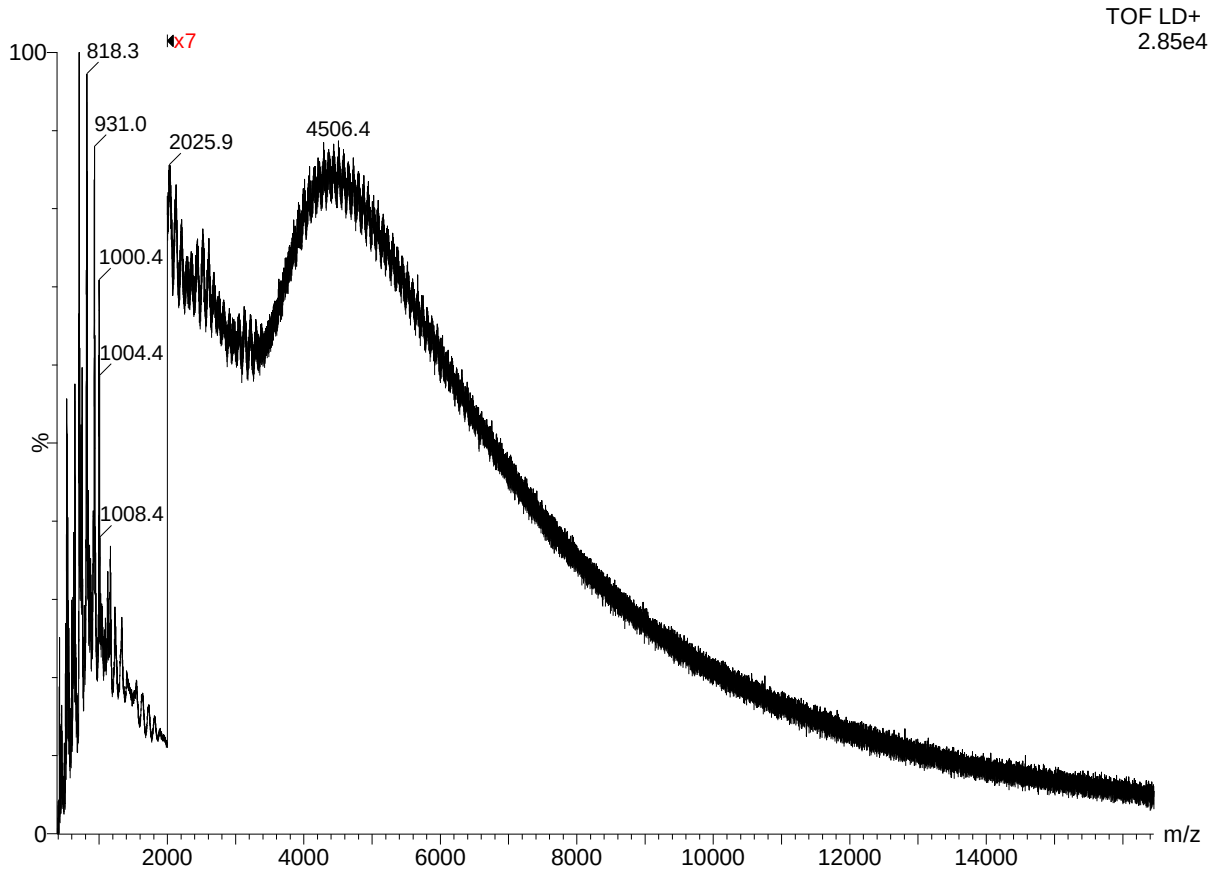


**Figure 36:** Linear mode TOF-MS of **27g**[156]

The metallic character of the nanoparticles was confirmed by XPS (Figure 37). The main peak in the 3d spectrum is at an energy of 30 eV, consistent with a Ge(0) and Ge(I) oxidation state.[164,165] The Ge(II) 3d peak has been reported at 32.6 and 32.8 eV. The absence of a corresponding peak precludes the presence of Ge(II) in the samples.[164,166] The presence of Ge(0) was confirmed by the energy of the Ge $2p_{3/2}$ peak.[166] A low-intensity shoulder on the high binding energy side of the Ge $2p_{3/2}$ peaks originates from Ge(I).[134]

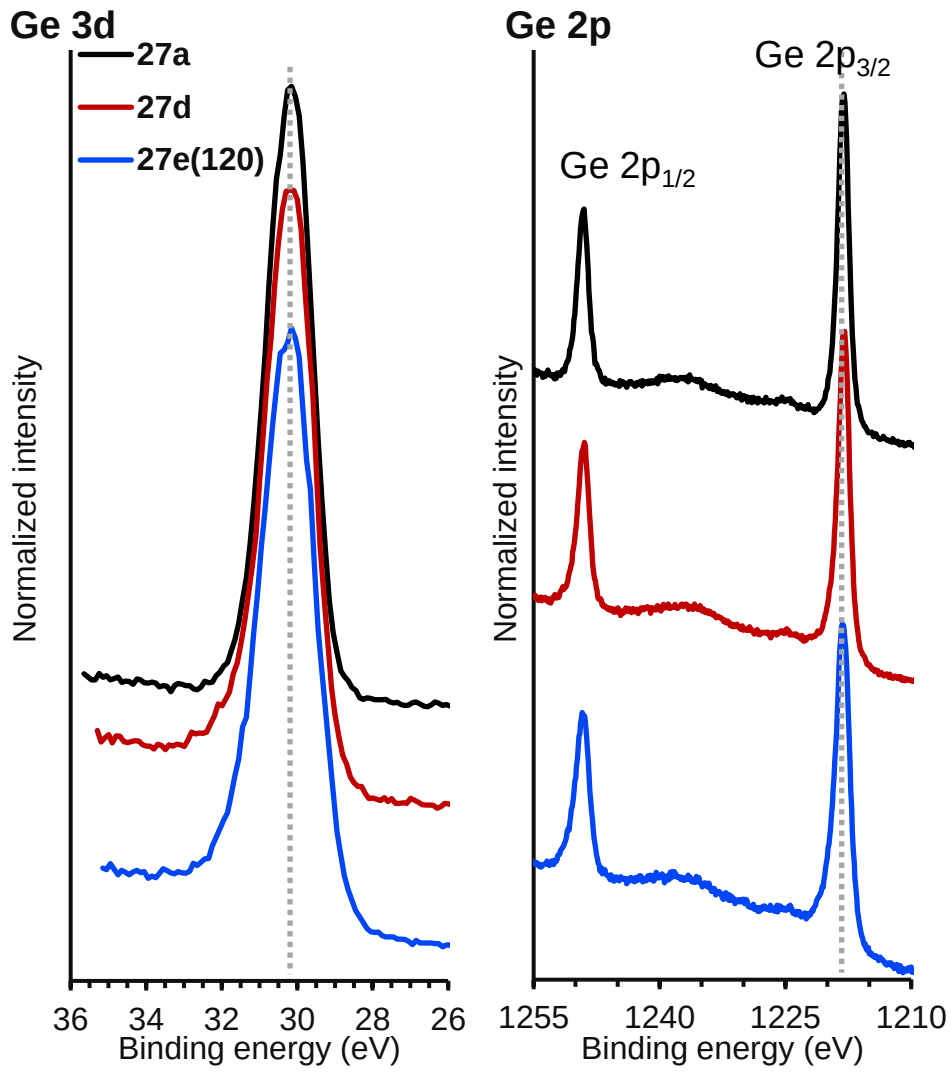


**Figure 37:** High resolution Ge 3d (left) and Ge 2p (right) XPS spectra for various Ge@*o*-tolyl materials

The metallic character, as well as the presence of nanocrystalline domains, was also confirmed with powder XRD (Figure 38). While it would initially appear that the sample does not match the α-Ge reference, this is due to the small size of the crystalline domains. The resulting broad peaks cause an overlap between the scattering signals of the 0|2|2, 1|1|3 and 2|2|2 planes. Similar spectra with overlapping signals have been previously reported for small α-Ge domains.[96,117]

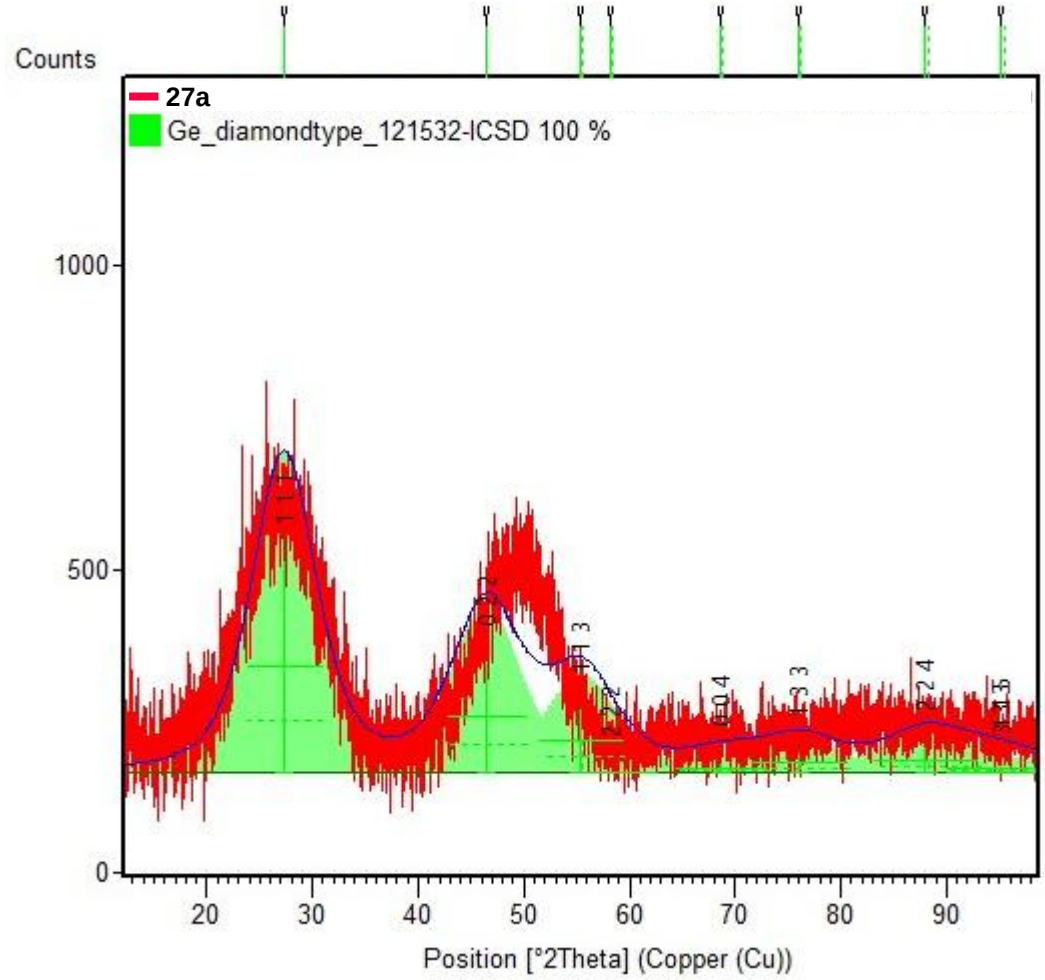


**Figure 38:** Powder XRD spectrum of **27a**, overlaid with a reference spectrum for α-Ge[167]

The small size of the crystalline domains provided motivation for high temperature annealing experiments, in the hopes of expanding them. Base on the thermal data for Ge@*o*-tolyl (Figure 43), three annealing temperatures were selected: Slightly below the decomposition temperature (220 °C), the onset of decomposition (240 °C) and the endpoint of thermal decomposition (500 °C). The sample of **27a** treated with 220 °C underwent a small size increase (SAXS: 1.7 nm → 1.8 nm). This is expected for Ge@*o*-tolyl produced with 24 h of reflux, as the presence of smaller oligomers provides additional growth potential. The annealed sample has the same size as Ge@*o*-tolyl after 72 h of reflux (**27b**). Other changes in material characteristics were not observed. The sample treated with 240 °C exhibited the same size increase to 1.8 nm. In addition, a weight loss of about 25% was recorded, and the resulting material had become indispersible in all investigated solvents. Treatment at 500 °C similarly caused weight reduction and loss of dispersibility. The annealing at 500 °C resulted in sharper XRD peaks (Figure 39). It appears that the anticipated expansion

of crystalline α-Ge domains did indeed occur. However, the improvement was small and the resulting XRD spectrum still exhibits overlapping peaks. Due to the only marginal improvements in crystallinity and the concurrent loss of dispersibility, annealing was not pursued any further.

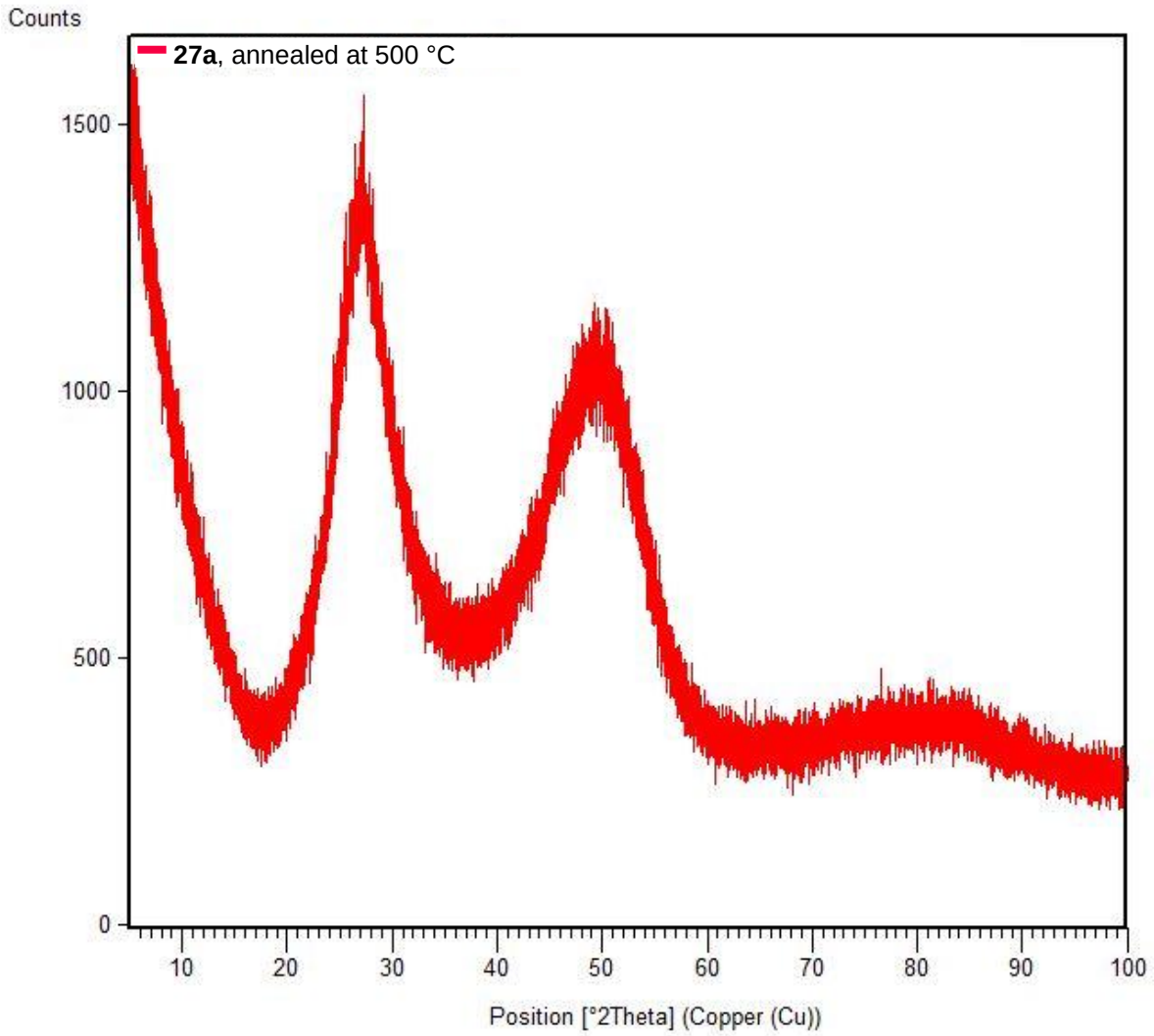


**Figure 39:** Powder XRD spectrum of **27a**, annealed for 4 h at 500 °C

WAXS spectra show the same α-Ge diffractions found with powder XRD, even though they are less pronounced (Figure 40). The measured 2θ values can be converted to q values with Equation 2, giving q=17 $nm^{-1}$ and 34 $nm^{-1}$ for the two relevant peaks. Powder WAXS was used to confirm the presence of α-Ge domains in all nanoparticulate samples, as it is cheaper and faster than powder XRD.

$$Equation\ 2: |q| = \frac{4\pi}{\lambda} * sin(\frac{2\theta}{2})$$

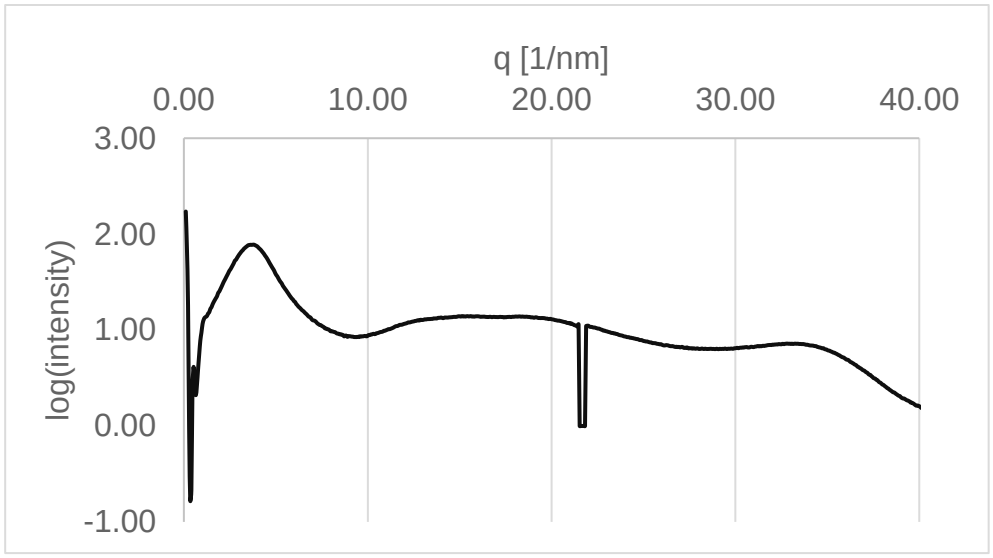


**Figure 40:** Powder WAXS curve of **27a**

An attempt was also made to investigate the bonding situation using FT-IR. First, spectra of both trihydride and trideuteride starting material were gathered to establish a baseline (Figure 41). The Ge-D vibration (1482 $cm^{-1}$) is shifted to lower wavenumbers from Ge-H (2062 $cm^{-1}$), as expected for heavier isotopes. The spectra for different nanomaterials are largely identical (Figure 42). Neither differences in substituent, nor in synthetic method cause any major changes. More subtle differences are hard to determine due to the strong background across the entire spectrum. Difference in the fingerprint area between Ge@mesityl and the various Ge@*o*-tolyl materials are due to the additional $CH_3$ groups in the former. Apart from that, the bonding situation in the various Ge@aryl nanomaterials is very similar.

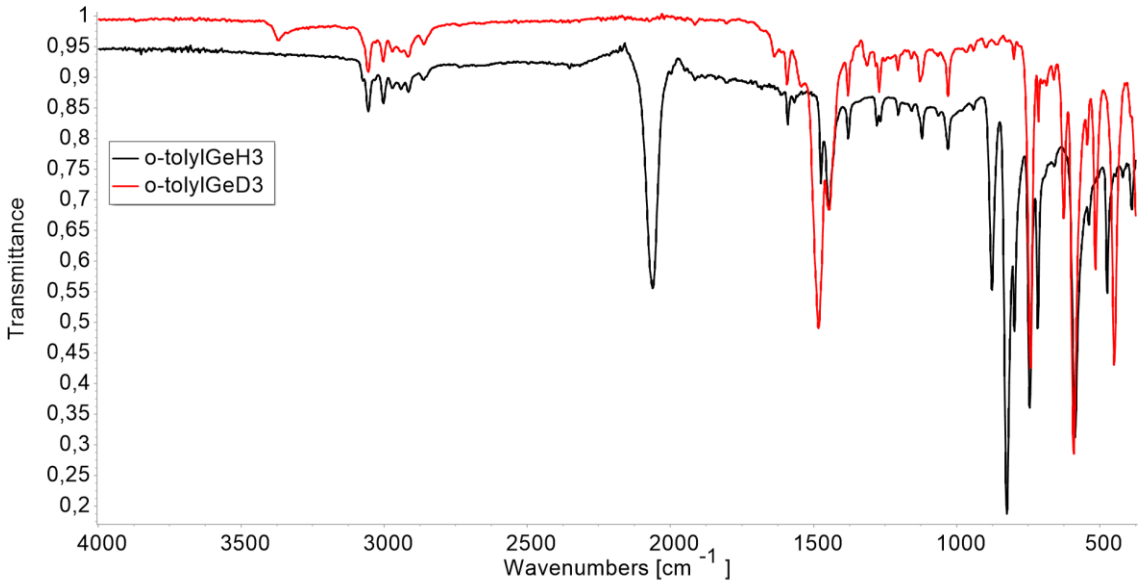


**Figure 41:** FT-IR spectra of **3** and **12**

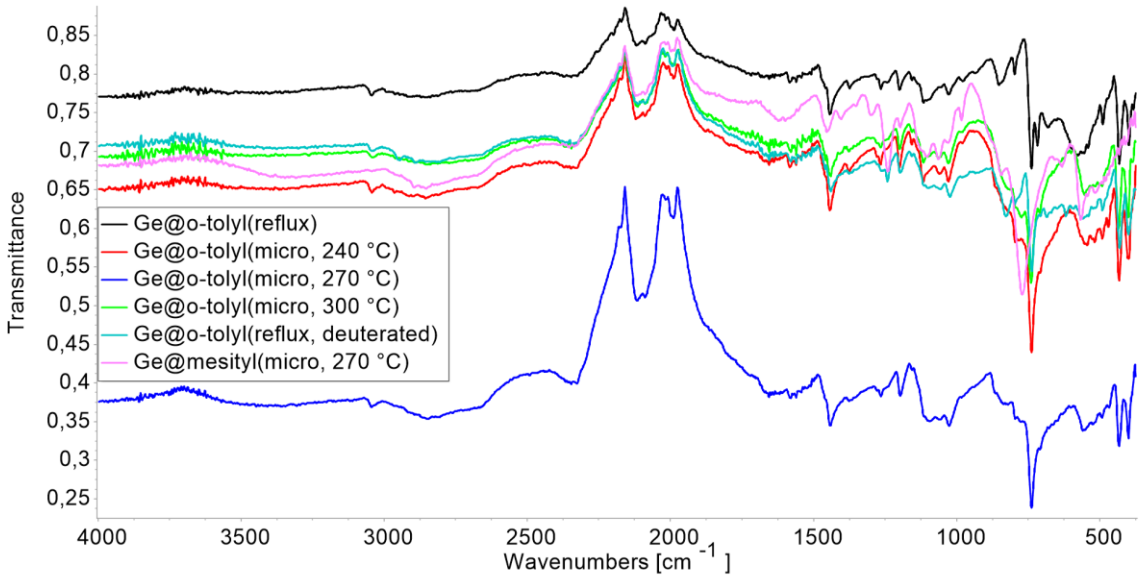


**Figure 42:** FT-IR spectra of several Ge@aryl samples

## Stability and Reactivity

The nanoparticles' behavior under elevated temperatures was investigated with STA-MS. The curve produced for **27a** is shown in Figure 43. Several characteristic fragments were tracked alongside $CO_2$, $H_2O$ and OH streams: *m*/*z*=91 $[C_7H_7]^+$, 77 $[C_6H_4]^+$ and 65 $[C_5H_5]^+$. An initial increase in mass occurs due to oxidation and hydrolysis with residual $H_2O$ and $CO_2$, as well as a loss of lift. The thermal degradation starts at about 250 °C, indicated by both mass loss and an increase in ion streams for all tracked masses. Accordingly, the particles are largely safe from

thermal degradation at reflux temperatures. The same thing is not true for microwave reactions. All temperatures used to couple **3** in the microwave are close to or above the decomposition temperature. This explains the observed differences in size and carbon content (see above). The terminal mass after STA-MS is about 70%. The germanium content of **27a** is slightly lower at about 60% according to its elemental analysis (C: 36.92%, H: 3.73%), but the lack of a reliable 100% mass baseline and the different temperatures of STA-MS and EA can account for this discrepancy.

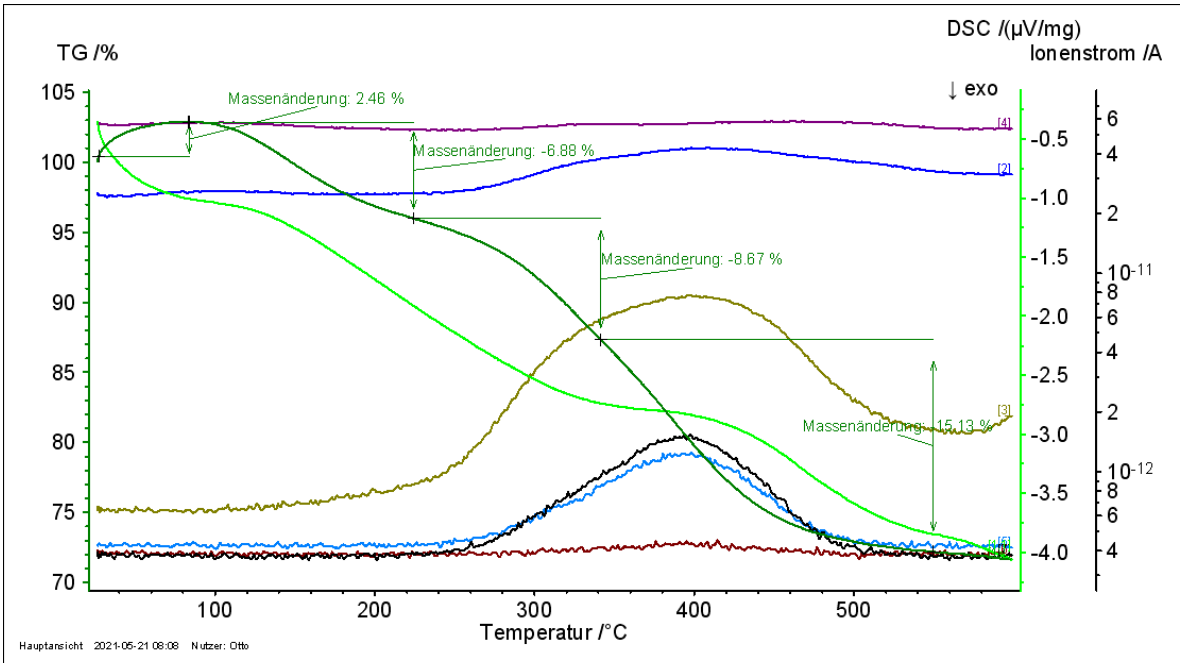


| [#] Gerät | Datei | Datum | Versuchs-ID | Probe | Masse/mg | Segment | Bereich | Atmosphäre | Korr. |
|---|---|---|---|---|---|---|---|---|---|
| [1.1] STA 449F1 | ACT_GeAryl_210520.ngb-ss1 | 2021-05-20 | ACT_GeAryl_210520 | ACT_GeAryl_210520 | 7.086 | 1/2 | 30°C/5.0(K/min)/600°C | N2, 50.0ml/min / N2, 50.0ml/min | TG:A00 |
| [2] QMS 403 | act_gearyl_210520_m18.00_s1.imp | 2021-05-20 | act_gearyl_210520 | Masse 18.00 | | 1/1 | 27°C/5.0(K/min)/599°C | | --- |
| [3] QMS 403 | act_gearyl_210520_m44.00_s1.imp | 2021-05-20 | act_gearyl_210520 | Masse 44.00 | | 1/1 | 27°C/5.0(K/min)/599°C | | --- |
| [4] QMS 403 | act_gearyl_210520_m17.00_s1.imp | 2021-05-20 | act_gearyl_210520 | Masse 17.00 | | 1/1 | 27°C/5.0(K/min)/599°C | | --- |
| [5] QMS 403 | act_gearyl_210520_m65.00_s1.imp | 2021-05-20 | act_gearyl_210520 | Masse 65.00 | | 1/1 | 27°C/5.0(K/min)/599°C | | --- |
| [6] QMS 403 | act_gearyl_210520_m77.00_s1.imp | 2021-05-20 | act_gearyl_210520 | Masse 77.00 | | 1/1 | 27°C/5.0(K/min)/599°C | | --- |
| [7] QMS 403 | act_gearyl_210520_m91.00_s1.imp | 2021-05-20 | act_gearyl_210520 | Masse 91.00 | | 1/1 | 27°C/5.0(K/min)/599°C | | --- |

Erzeugt mit NETZSCH Proteus Software

**Figure 43:** STA-MS for **27a**

Very similar decomposition behavior was reported for a crosslinked phenylgermane polymer obtained from the dehydrogenative coupling of $PhGeH_3$ under zirconocene catalysis. Using TGA, Choi and Tanaka observed an onset of decomposition at 250 °C, and full loss of all organic content at 580 °C. They also observed extrusion of fragments $Ph_2Ge$ and $Ph_3Ge$, in line with the *o*-$tolyl_3Ge$ fragment observed during mass spectroscopy.[128]

The STA-MS diagram for **29a** (Figure 44) depicts thermal degradation beginning at a lower temperature of ~220 °C. The maximum mass loss is also recorded at a considerably lower temperature. This explains the much lower organic content of

**26a** (C: 14.56%, H: 2.53%) compared to **25g** (C: 28.96%, H: 2.89%) despite the use of identical reaction conditions. It is also supports the above proposed theory that larger aryl substituents lead to bigger nanoparticles because they are more easily removed and thus provide higher growth potential.

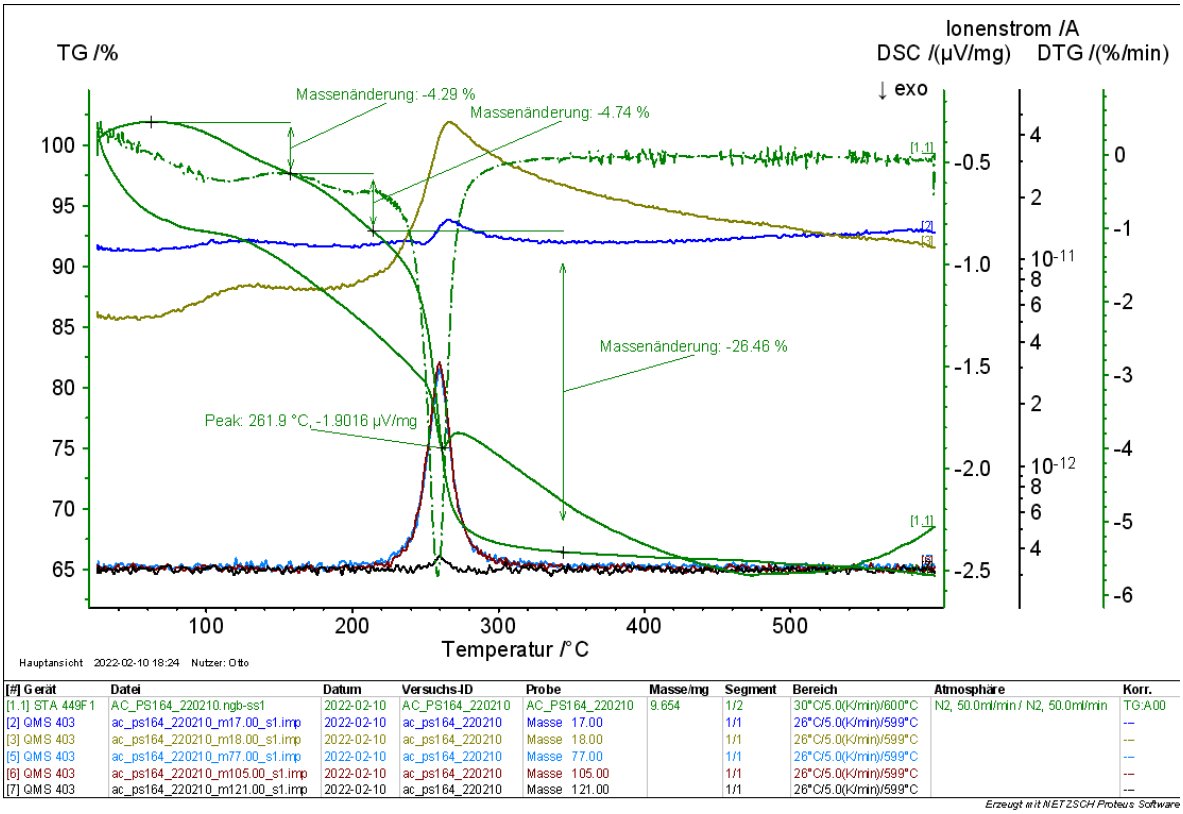


| [#] Gerät | Datei | Datum | Versuchs-ID | Probe | Masse/mg | Segment | Bereich | Atmosphäre | Korr. |
|---|---|---|---|---|---|---|---|---|---|
| [1.1] STA 449F1 | AC_PS164_220210.ngb-ss1 | 2022-02-10 | AC_PS164_220210 | AC_PS164_220210 | 9.654 | 1/2 | 30°C/5.0(K/min)/600°C | N2, 50.0ml/min / N2, 50.0ml/min | TG:A00 |
| [2] QMS 403 | ac_ps164_220210_m17.00_s1.imp | 2022-02-10 | ac_ps164_220210 | Masse 17.00 | | 1/1 | 26°C/5.0(K/min)/599°C | | --- |
| [3] QMS 403 | ac_ps164_220210_m18.00_s1.imp | 2022-02-10 | ac_ps164_220210 | Masse 18.00 | | 1/1 | 26°C/5.0(K/min)/599°C | | --- |
| [5] QMS 403 | ac_ps164_220210_m77.00_s1.imp | 2022-02-10 | ac_ps164_220210 | Masse 77.00 | | 1/1 | 26°C/5.0(K/min)/599°C | | --- |
| [6] QMS 403 | ac_ps164_220210_m105.00_s1.imp | 2022-02-10 | ac_ps164_220210 | Masse 105.00 | | 1/1 | 26°C/5.0(K/min)/599°C | | --- |
| [7] QMS 403 | ac_ps164_220210_m121.00_s1.imp | 2022-02-10 | ac_ps164_220210 | Masse 121.00 | | 1/1 | 26°C/5.0(K/min)/599°C | | --- |

Erzeugt mit NETZSCH Proteus Software

**Figure 44:** STA-MS for **29a**

In order to test the atmospheric stability of the particles, a sample of **25g** was removed from the glovebox and exposed to air. The UV/Vis spectrum (Figure 45) shows the progressive oxidation of the sample over the course of three days. This causes an expected decrease in absorption at higher wavelengths, as Ge(0) domains become smaller due to being partially oxidized to Ge(IV), and the size dependent absorption shifts to smaller wave lengths. Below wavelengths of 250 nm, the absorption increases. This is consistent with the reported UV/Vis spectrum for $GeO_2$, which displays almost no absorption above 300 nm, but very strong optical absorption at about 220 nm. After longer air exposure, the particles lost their full dispersibility, preventing further UV/Vis monitoring. Because oxidation causes the uptake of additional weight in the form of oxygen, an observed decrease in the relative carbon content (28.96%→27.28%) was to be expected. The powder size

(SAXS) remained essentially unchanged at 2.6 nm. While no $GeO_2$ refractions were found with either WAXS or IR (Figure 46), this is likely due to insufficient size of the oxidized domains.

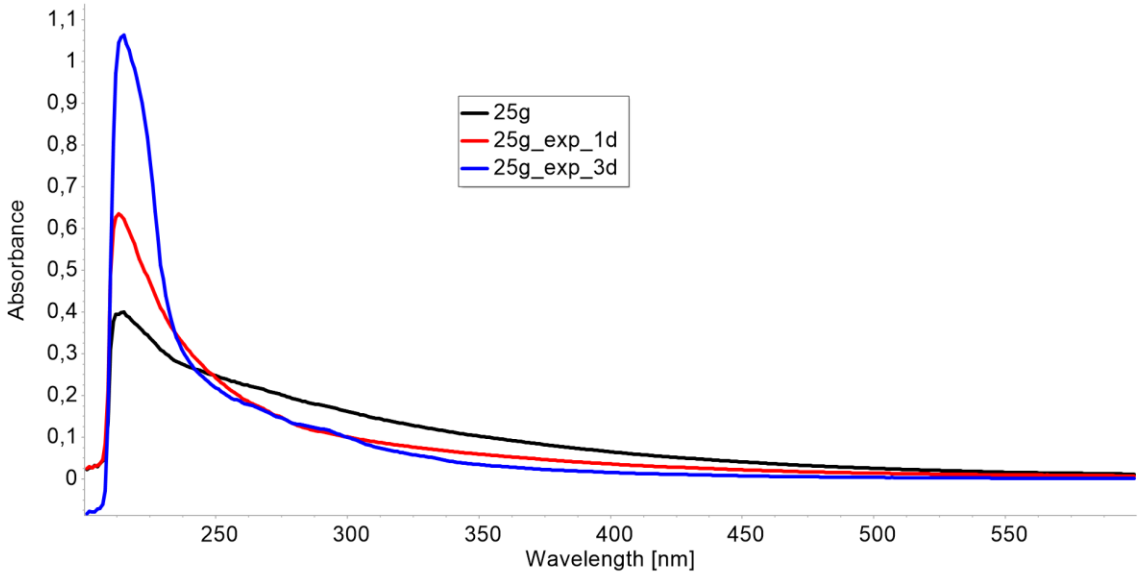


**Figure 45:** UV/Vis of **25g** after different air exposure durations, at a concentration of ~100 mg/L

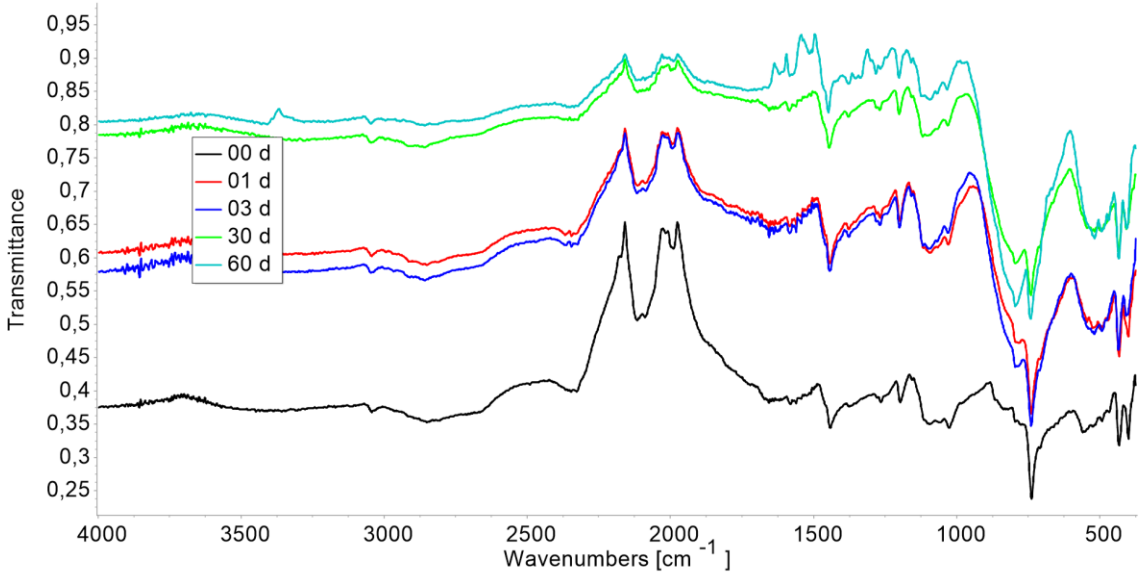


**Figure 46:** IR spectrum of **25g** after different air exposure durations

A separate sample (**27b**) was brought into contact with degassed $H_2O$. Due to the hydrophobic nature of the particles (Figure 47) vigorous stirring had to be employed to ensure sufficient contact. Despite that, no change was observable after three days.

**Figure 47:** Hydrophobic nanoparticles **27b** in contact with $H_2O$

The particles were therefore kept in contact with the water for a full month, before $H_2O$ was removed under reduced pressure. Despite the long contact time, the observed changes were minimal. The particles remained fully dispersible in THF. Only a small decrease in carbon content (35.70%→34.11%) and size (SAXS: 1.8 nm→1.7 nm) was detected. It is safe to conclude that the particles are quite resistant towards $H_2O$ exposure.

Oxidation of Ge(0) to $GeO_2$ and subsequent dissolution in $H_2O$ can be utilized for post synthetic size control of germanium nanoparticles. Such a process was reported by Kim *et al*..[168] Their method was successfully applied to Ge@*o*-tolyl nanoparticles, despite the differences in size and composition. Oxidation with $H_2O_2$ followed by dissolution of the $GeO_2$ with $H_2O$ led to a decrease in size (SAXS: 1.9 nm→1.3 nm) which corresponds to 62% volume reduction (Figure 48). Of course, the lower overall sample volumes, smaller particle sizes and presence of organic substituents complicate the procedure compared to the literature reported one. Precise size control through the use of calculated $H_2O_2$ amounts is not feasible here.

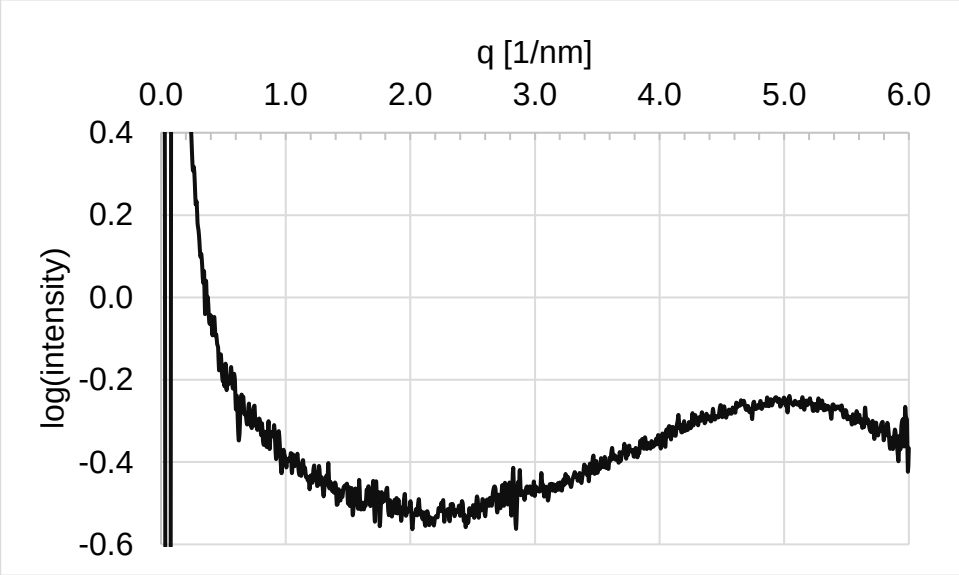


**Figure 48:** Powder SAXS curve of **27e$_{120}$** after $H_2O_2/H_2O$ etching.

During the earliest stages of research into Ge@aryl particles, the residual Ge-H bonds found in some samples (*i.e.* **27a**, **27e$_{24}$,** also see Figure 20) were thought to be part of the actual nanomaterial, rather than discreet oligomers. This led to an attempt to leverage them for functionalization of the particles *via* a hydrogermylation reaction. 3-chloro-1-propene was used in excess as reagent, and azobisisobutyronitrile (AIBN) as initiator. After refluxing the reaction overnight and removing all volatile components under vacuum, no visual changes were observed. However, a $^1$H NMR (Figure 49) revealed that in addition to the Ge-H bonds, almost all *o*-tolyl groups had been removed. New signals had appeared in their stead. The shifts of these new signals are in the expected range for a chloropropylene germane. They exhibit strong polymer broadening, indicating that the chloropropylene is indeed attached to the nanoparticles. The substituent exchange can also be seen in the IR spectrum (Figure 50). The newly appeared peak at 2923 cm$^{-1}$ is consistent with C-H stretching vibrations while the signal at 1450 cm$^{-1}$ is the corresponding C-H bending vibration.

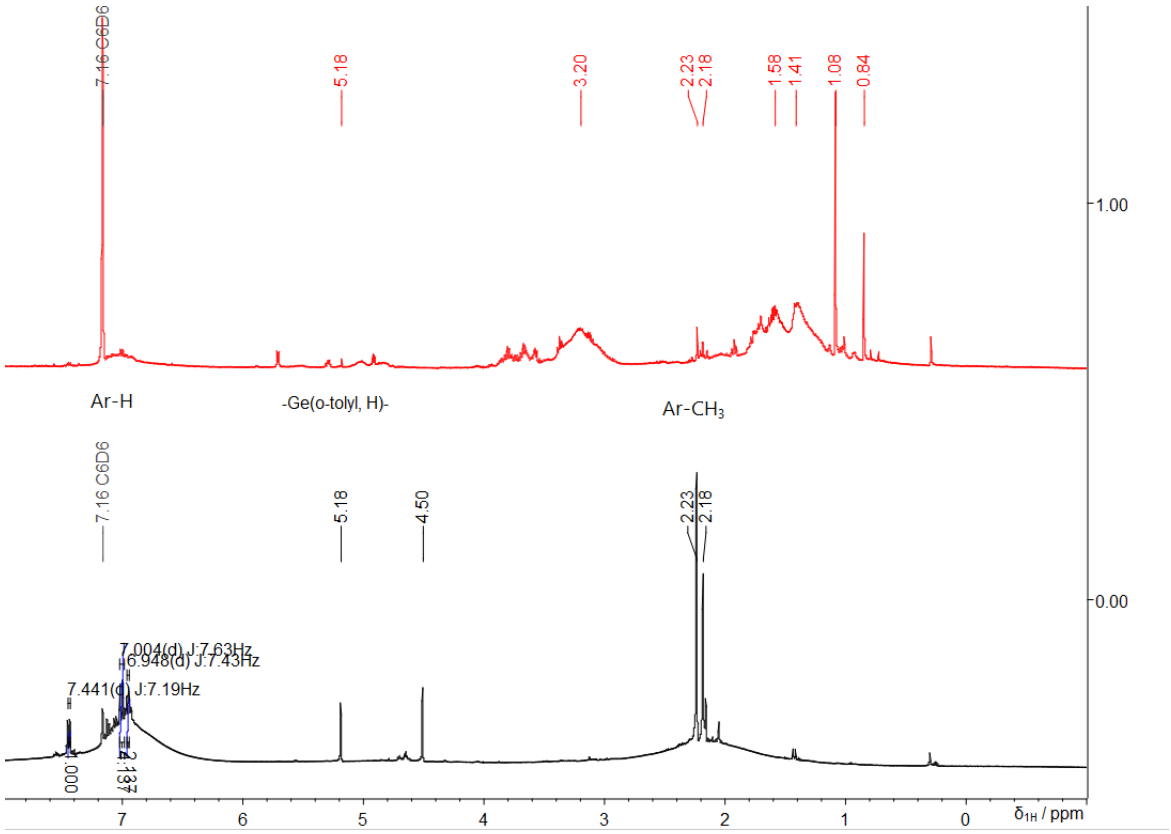


**Figure 49:** $^{1}$H NMR spectra ($C_6D_6$, 400 MHz) for **27a** (bottom) and **33** (top)


**Figure 50:** Overlay of AT-IR spectra for **27a** (black) and **33** (red)

It appears that instead of the intended hydrogermylation, the nanoparticles were subjected to a radical substitution reaction (Scheme 35). This discovery is actually superior to the intended outcome. Replacing the numerous *o*-tolyl groups allows for a far more extensive functionalization of the particles compared to the relatively few remaining Ge-H bonds. Additionally, as is now understood, the Ge-H signals stem from oligomers. Consequently, the nanoparticles would not have been functionalized by a hydrogermylation reaction. The possibility to replace almost all aryl groups without compromising the particle structure shows great promise for future functionalization attempts.

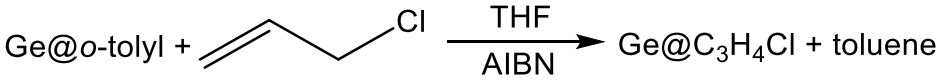


**Scheme 35:** Surface derivatization of Ge@*o*-tolyl *via* radical substitution

# IV. Conclusion and Outlook

In this work, a reliable and reproducible dehydrogenative coupling process for the preparation of aryl decorated germanium nanoparticles Ge@Ar from arylgermanium trihydrides $ArGeH_3$ was developed. A cyclic oligomer intermediate $[ArGeH]_n$ (n=3, 4) was isolated from the reaction mixture and characterized with $^1H$ NMR. Upon further growth, some aromatic groups are removed in addition to dehydrogenation. This results in “naked” Ge atoms, connected exclusively to other Ge atoms. Remaining aryl groups decorate the formed nanoparticles (Scheme 36).

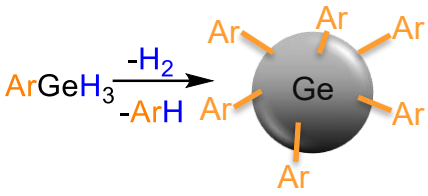


**Scheme 36:** Dehydrogenative coupling of arylgermanium trihydrides to aryl decorated germanium nanoparticles

The presence of metallic Ge(0) in these particles was demonstrated with XPS, and even the formation of nanocrystalline α-Ge domains could be proven with XPS and WAXS. Particle sizes obtained in this work range from 1.4 nm to 6.3 nm. Varying the aryl group of the starting material showed that larger aryls are more easily cleaved, leading to bigger sizes. The size can be further shaped through the choice of reaction conditions or $H_2O_2$ etching. All Ge@Ar materials exhibit strong, size dependent absorption in the visible spectrum, due to quantum confinement of their electrons. Their full dispersibility in common solvents is crucial for many characterization techniques. It also enables the use of material processing techniques, such as spin coating, that would not be possible otherwise. Preliminary functionalization experiments with the nanoparticles showed great promise. The decorating *o*-tolyl groups were successfully replaced with propylene chloride, facilitated by AIBN. However, the resulting material still needs to be characterized more thoroughly. Also of interest would be the replacement of *o*-tolyl groups with a halogen *via* a dearylation reagent such as TfOH or $HCl/AlCl_3$. Investigating the behavior of more exotic arylgermane precursors is another potential research avenue. For example, by having two germane moieties attached to the same aromatic ring, it could serve

as a spacer, presumably causing a subsequently prepared polymer to have a very different structure. Finally, characterizing the electronic properties of the Ge@Ar particles would be a worthwhile endeavor.

In addition to experiments with the well-established arylgermanes, (*t*-BuMe$_2$Si)GeH$_3$ (**21**) and (*t*-Bu$_2$MeSi)GeH$_3$ (**22**) were synthesized as novel precursors for dehydrogenative coupling. A synthetic strategy was developed to circumvent the inherent instability of the required (trialkylsilyl)halogermane precursors. The promising prospects of (trialkylsilyl)germanes for dehydrogenative coupling were demonstrated through thermal degradation experiments. The next steps in this field require the development of a robust coupling process for the (trialkylsilyl)germanes and the comprehensive characterization of the resulting material. The preparation of the silylgermane starting materials could also be further optimized to improve yields and increase availability of the starting material for coupling experiments.

The reactivity of organolithium bases towards arylgermanium trihydride was discovered to strongly depend on the used solvents. Reactions carried out in THF or with very bulky substituents preferentially lead to a metal/hydrogen exchange, producing the lithiated germane. Reactions in Et$_2$O or *n*-pentane, on the other hand, result in a nucleophilic substitution, causing the alkylation or arylation of the germane (Scheme 37). Steric factors also play a role in this system, with larger substituents pushing the reaction more towards metal/hydrogen exchange. All reactions were performed with commercially obtained solutions of organolithium reagents, so result interpretation is complicated by concentration differences and introduction of a second solvent into the system. Further research into organolithium reactivity should thus begin by reproducing the results in clean reactions with a single solvent and consistent reagent concentrations.

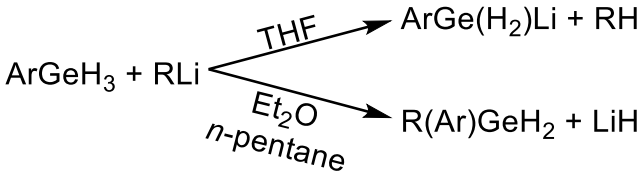


**Scheme 37:** Solvent dependency in reactions of arylgermanium trihydrides with organolithium bases

# V. Experimental

## 5.1 General Aspects

Most air and moisture sensitive reactions were carried out using standard Schlenk technique under an argon atmosphere. Cases where a glovebox was used instead are specified. The argon was pre-dried with a catalytic tower from Air Liquide. $Et_2O$, THF, DCM, toluene, benzene and *n*-pentane were dried using a ready-made system from "Innovative Technology Inc.". THF was additionally distilled over $LiAlH_4$ for further drying and removal of the stabilizer. 1,4-Dioxane was dried over a potassium mirror and deoxygenated with three freeze-pump cycles. $CCl_4$, dimethoxy ethane (DME) and diglyme were dried over a molecular sieve (3 Å), the latter two were additionally deoxygenated overnight with an $N_2$ stream. Crystalline *t*-BuLi was obtained through slow solvent evaporation from commercial *t*-BuLi solution inside a glovebox. All solvents and chemicals not specified either here or in the synthetic section (Chapter 5.3) were obtained from commercial sources and used as received.

## 5.2 Analytics

NMR Spectroscopy

NMR spectra were obtained on either a Varian INOVA 300 MHz with RS2D Pulse console ($^1$H, $^{13}$C), or a Bruker AV-400FT ($^1$H, $^{13}$C, $^{29}$Si) or a Jeol ECZ 400 with Royalprobe$^{TM}$ HFX ($^1$H, $^{13}$C, $^{29}$Si) or a Bruker Avance Neo 700 SB with 5 mm BBO probe ($^{73}$Ge). The spectra were referenced using residual undeuterated solvent. The shifts are given relative to $Me_4Si$ ($^1$H, $^{13}$C, $^{29}$Si) or $Me_4Ge$ ($^{73}$Ge). The abbreviations d, t, q, and m are used to indicate duplets, triplets, quartets and multiplets, respectively. Spectra were processed and analyzed using JEOL Analytical Software Network (Jason) for $^1$H, $^{13}$C and $^{29}$Si, and MestreNova for $^{73}$Ge.

Gas Chromatography – Mass Spectrometry (GC/MS)

Gas chromatographies were run with helium as carrier gas (0.92726 mL/min) on an Agilent Technologies 7890A system with a HP5 column (30 m x 0.25 mm x 0.025 µm). Samples were injected manually with a syringe at an injector temperature of 250 °C, and chromatographed starting at 40 °C (hold 2 min), ramped up to 300 °C

(20 °C/min), then held another 10 min. Mass spectra were measured with an Agilent Technologies 5975C mass detector in full scan mode (50–500 *m*/*z*).

High Resolution Mass Spectrometry (HRMS)

Direct analysis in Real Time (DART) MS were measured on a JEOL AccuTOF CS (JMS-T100CS). GC/HRMS were measured on a JMS-T2000GC (AccuTOFTM GC-Alpha) with an 8890 GC system (column: DB-5MS, 30 m x 0.25 mm x 0.25 µm) and a 7693A autosampler from Agilent. GC conditions: inlet at 250 °C; He at a constant flow rate of 1.0 mL/min, split ratio 10; temperature program: 40 °C for 3 min, heating to 250 °C at a rate of 20 °C/min, isothermal at 250 °C for 4 min. Data was analysed on MassLynx 4.1.

Time of Flight – Mass Spectrometry (TOFMS)

Matrix assisted laser desorption ionization (MALDI) and laser desorption ionization (LDI) TOFMS were carried out on a Waters micro MX. Ions were generated by irradiation just above the threshold laser power (laser: wavelength 337 nm, operated at a frequency of 5 Hz). Approximately 100–150 spectra were averaged. For MALDI-TOF-MS samples were prepared by mixing a solution of DCTB (2-[(2E)-3-(4-tertbutylphenyl)-2-methylprop-2-enylidene]malononitrile; c=10 mg/mL in THF) and a solution of the sample (c=0.05 mg/mL in THF) in a ratio of 10:5 (v/v). 0.5 µL of the resulting mixture were deposited on the sample plate (stainless steel) and allowed to dry under ambient conditions. For LDI-TOF-MS 0.5 µL of product solution were deposited directly on the MALDI target. The data was analyzed with MassLynx 4.1.

Simultaneous Thermal Analysis – Mass Spectrometer Coupling (STA-MS)

The thermal behavior was investigated with a STA449F1A coupled to a QMS 403c mass spectrometer. Brief air exposure was unavoidable during sample preparation, but the heating itself was performed under an inert $N_2$ atmosphere. The samples were analyzed at temperatures from 30 °C to 600 °C, with a heating rate of 5 °C/min. Characteristic mass fragments were selected for tracking based on their intensities in a GC/MS of the corresponding monomer.

Small- and Wide-Angle X-ray Scattering (SAXS and WAXS)

Samples were filled into a VarioStage (Anton Paar) inside a glovebox and secured with an adhesive tape (Scotch® Magic™ Tape). The sample holder was carried from

the glovebox to the instrument inside an argon filled bucket. The measurements were carried out at room temperature in transmission mode on a SAXS-Point 2.0 (Anton Paar, Graz). Radiation was generated by a micro-X-ray source (Primux 100, Anton Paar, Graz) producing Cu-Kα radiation (154.2 nm) at 50 W. Detection was performed by a 2D X-ray detector (EIGER R 1M, Dectris, Switzerland). SAXS was recorded at 542 mm sample-detector distance, WAXS at 77 mm. Measurement data was processed with Microsoft Excel.

Powder X-ray Diffraction (XRD)

Powder XRD experiments were carried out on XRDynamic 500 diffractometer from Anton Paar with a Cu-Kα X-ray source. 2θ angles were collected from 12° to 100°.

X-ray Crystallography

Single crystal X-ray data was collected at 100 K on a Bruker Kappa Apex II CCD diffractometer[169] using Mo-Kα radiation (λ=0.71073 Å). The unit-cell constants and the orientation matrices were determined by the program CELL_NOW.[170] Data integration was carried out using SAINT.[169] Empirical absorption corrections were applied using SADABS.[171] The structures were solved with use of the intrinsic phasing option in SHELXT[172] and refined by the full-matrix least-squares procedures in SHELXL[172,173] as implemented in the program SHELXLE.[174] The space group assignments and structural solutions were evaluated using PLATON.[175] Non-hydrogen atoms were refined anisotropically. Hydrogen atoms were located in a difference map for **7** and located in calculated positions for **9**. Centroids and planes were determined by features of the programs Mercury[176] and Diamond.[177] All crystal structure representations were made with the program Diamond[177] with all non-carbon atoms displayed as 30% ellipsoids. CIF files were edited, validated and formatted either with the programs encifer,[178] publCIF,[179] or Olex2.[180]

X-ray Photoelectron Spectroscopy (XPS)

XPS measurements were performed using a Supra+ device (Kratos, Manchester, UK) using an Al-Kα excitation source. The spectra were calibrated based on the C-C/C-H peak at 284.8 eV in the C 1s spectra. The powder samples were attached to the carbon tape and placed on a Si wafer. The Si wafer was attached to the sample holder. Measurements were performed at a takeoff angle of 90° on a spot size of

300 by 700 microns and a pass energy of 20 eV. Data acquisition and processing were performed using ESCApe 1.5 software (Kratos).

Optical Microscopy

Digital optical microscopy was done on an Olympus DSX1000 equipped with DSX10-XLOB objectives and various illumination techniques.

Scanning Electron Microscopy (SEM)

Prior to scanning electron microscopy, the samples were sputtered with a 10 nm thick iridium layer to guarantee good electrical conductivity. For this kind of sample preparation, a high vacuum magnetron sputter coater from Leica ACE600 was used. The samples were analyzed in the Zeiss Ultra 55 SEM with field emission gun using 3 keV electron energy. For acquiring the surface sensitive high-resolution images, the In-lens secondary electron detector at small working distances (about 3 mm) was used.

Transmission Electron Microscopy (TEM)

Nano-structural details of selected particles were analyzed by transmission electron microscopy (TEM) using a FEI Tecnai F20 operated at an acceleration voltage of 200 kV. The microscope was fitted with a Schottky field emission gun and an ultra-Scan CCD camera for high-resolution imaging. The images were processed with Digital Micrograph software. The TEM grids were prepared by the standard preparation procedure for powder samples. The sample particles were suspended in alcohol and dropped onto a copper TEM grid which was covered with a holey carbon support film.

Dynamic Light Scattering (DLS)

DLS plots were measured on a Litesizer 500 from Anton Paar in a glass cuvette at 25 °C in side scatter mode. The obtained data was evaluated with the program Kalliope and plotted using Microsoft Excel.

Gel Permeation Chromatography (GPC)

Gel permeation chromatography (GPC) was done on equipment provided by WGE Dr. Bures. The system was operated with THF (separating columns were from

MZ-Gel SD plus, linear 5 µ; RI detector SEC 3010). Poly(styrene) standards purchased from Polymer Standard Service were used for calibration.

Infrared Spectroscopy

All samples were measured as powder in substance on a Bruker ALPHA FT-IR spectrometer in attenuated total reflection mode and a diamond sample stage. The measurements were set up using OPUS and evaluated using Spectragryph.[181]

Ultraviolet-visible spectroscopy (UV/Vis)

The UV/Vis absorption spectra were measured in THF at the specified concentration. A background measurement was taken first using pure THF, and automatically subtracted from all subsequent measurements. Samples and blanks were mounted with 1 cm thickness under an inert atmosphere in quartz glass cuvettes. The spectra were acquired on an Agilent Technologies Cary 60 UV/Vis spectrophotometer. The gathered data was processed using Spectragryph.[181]

Elemental Analysis (EA)

Samples for elemental analysis were prepared and weighed inside a glovebox. The CHN contents were then measured on a VARIO Micro Cube from Heraeus.

## 5.3 Synthetic Procedures

### 5.3.1 Organogermanes

$ArGeX_3$ *via* Grignard Reaction

The aryl bromide was dissolved in dry $Et_2O$ or THF. About 10% of this solution were immediately added to a suspension of Mg in dry $Et_2O$ or THF. After the reaction had started, the rest of the solution was slowly added over the course of 30 min. The mixture was subsequently refluxed for another 2 h. Excess Mg was filtrated off through a Schlenk frit with Celite® and the obtained brown solution was transferred into a dropping funnel atop a flask with $GeCl_4$ in dry $Et_2O$. While cooling the flask to -70 °C, the Grignard solution was dripped into it over the course of 2 h and the reaction was stirred overnight. The next day, the solution was quenched with HCl. The layers were separated, the aqueous layer extracted with $Et_2O$, the combined organic layers dried over $Na_2SO_4$ and filtrated. Solvents were removed at the rotovap. Residual aryl bromide was removed through evacuation. The formation of

$ArGeX_3$ was verified by GC/MS. No further purification was undertaken, consequently neither yield nor NMR spectra were recorded.

phenyl$GeX_3$: Reaction of Mg (12.01 g, 494 mmol) in dry THF (50 mL), bromobenzene (67.1 g, 427 mmol) in dry THF (100 mL) and $GeCl_4$ (93.5 g, 436 mmol) in dry $Et_2O$ (100 mL). Quenched with 4 M HCl (200 mL). Extracted with $Et_2O$ (2x50 mL). Bromobenzene removed at 40 °C, 1 mbar. MS (EI, 70 eV): *m*/*z*(%) 255.9(31) $[M]^+$, 220.9(54) $[M - Cl]^+$, 112.0(100) $[C_6H_5Cl]^+$, 77.1(51) $[C_6H_5]^+$.

*o*-tolyl$GeX_3$: Reaction of Mg (10 g, 411 mmol) in dry $Et_2O$ (50 mL), 2-bromotoluene (58.3 g, 341 mmol) in dry $Et_2O$ (200 mL) and $GeCl_4$ (75.2 g, 351 mmol) in dry $Et_2O$ (100 mL). Quenched with 4 M HCl (200 mL). Extracted with $Et_2O$ (3x100 mL). 2-bromotoluene removed at room temperature, 0.1 mbar. MS (EI, 70 eV): *m*/*z*(%) = 269.9(14) $[M]^+$, 233.9(49) $[M - HCl]^+$, 90.0(100) $[C_7H_6]^+$.

*p*-tolyl$GeX_3$: Reaction of Mg (21.0 g, 864 mmol) in dry THF (50 mL), 4-bromotoluene (125 g, 731 mmol) in dry THF (200 mL) and $GeCl_4$ (165 g, 768 mmol) in dry $Et_2O$ (500 mL). Quenched with 4 M HCl (500 mL). Extracted with $Et_2O$ (2x250 mL). 4-bromotoluene removed at 40 °C, 0.5 mbar. MS (EI, 70 eV): *m*/*z*(%) = 269.9(34) $[M]^+$, 234.9(32) $[M - Cl]^+$, 91.1(100) $[C_7H_7]^+$.

2,5-xylyl$GeX_3$: Reaction of Mg (2.80 g, 115 mmol) in dry THF (25 mL), 2-bromo-*p*-xylene (18.2 g, 98.3 mmol) in dry THF (100 mL) and $GeCl_4$ (22.4 g, 104 mmol) in dry $Et_2O$ (70 mL). Quenched with 4 M HCl (150 mL), extracted with $Et_2O$ (2x50 mL). 2-bromo-*p*-xylene removed at room temperature, $9.2*10^{-3}$ mbar. MS (EI, 70 eV): *m*/*z*(%) = 283.9(27) $[M]^+$, 248.9(10) $[M - Cl]^+$, 105.1(100) $[C_8H_9]^+$.

2,6-xylyl$GeX_3$: Reaction of Mg (5.07 g, 209 mmol) in dry THF (50 mL), 2-bromo-*m*-xylene (26.3 g, 142 mmol) in dry THF (150 mL) and $GeCl_4$ (32.0 g, 149 mmol) in dry $Et_2O$ (100 mL). Quenched with 2.5 M HCl (250 mL), extracted with $Et_2O$ (2x100 mL). 2-bromo-*m*-xylene removed at romm temperature, $5.3*10^{-3}$ mbar. MS (EI, 70 eV): *m*/*z*(%) = 283.9(14) $[M]^+$, 247.9(37) $[M - HCl]^+$, 104.1(100) $[C_8H_8]^+$

<u>Mesityl$GeCl_3$, crude</u>

Magnesium (2.62 g, 108 mmol) was suspended in dry THF (25 mL). 20% of a solution of bromo-mesitylene (18.1 g, 90.9 mmol) in dry THF (100 mL) were immediately added to the magnesium. The mixture was brought to reflux with a heat

gun to start the reaction, after which the rest of the bromo-mesitylene solution was added dropwise over 30 min. After complete addition, a heating mantle was added to keep the reaction at reflux for another 2 hours, then dry 1,4-dioxane (25 mL) was added at room temperature. The reaction was brought to reflux again for 30 min, then the heating mantle was removed and the suspension allowed to cool to room temperature. The supernatant was filtrated off through a cannula, the precipitated $MgBr_2$ was washed once with THF (20 mL). The solution with the Grignard reagent was dripped into a solution of $GeCl_4$ (20.6 g, 95.9 mmol) in dry THF (100 mL) over the course of 2 hours while cooling to -75 °C. After warming to room temperature, the solution was briefly brought to reflux using a heating mantle, then immediately allowed to cool to room temperature again. The solvents were removed *in vacuo* and replaced with *n*-pentane (40 mL), which was filtrated *via* cannula. The residue was washed twice more with pentane (2x10 mL), then the solvent was evaporated to produce a yellow powder. Residual bromo-mesitylene was removed through evacuation at 80 °C, 0.01 mbar. Yield was not determined due to the crude nature of the product.

MS (EI, 70 eV): *m*/*z*(%) = 297.9(22) $[M]^+$, 261.9(48) $[M - HCl]^+$, 118.1(100) $[C_9H_{10}]^+$.

<u>*p*-tolylGeX$_3$ *via* GeCl$_2$ insertion</u>

$GeCl_4$ (13.46 g, 62.8 mmol), $Et_3SiH$ (10.79 g, 93.8 mmol), 1,4-dioxane (13.8 mL, 14.3 g, 162 mmol) and dry toluene (31 mL) were mixed in a flask. They were refluxed for 44 hours under stirring. After cooling to room temperature, the resulting suspension was filtrated and the collected colorless crystals dried to yield 10.23 g (70%) of $GeCl_2$*1,4-dioxane. The $GeCl_2$*1,4-dioxane (10.23 g, 44.2 mmol) was mixed with $AlCl_3$ (0.348 g, 2.61 mmol) and suspended in 4-bromotoluene (180 mL) at 30 °C. Then the mixture was heated to 120 °C overnight. After being allowed to cool to about 50 °C, $AlCl_3$ was removed through filtration. 4-Bromotoluene was subsequently condensed off at 43 °C, 0.5 mbar to yield 11.67 g (84%) of yellow solution. The product mixture consists of various mixed trihalides, therefore no NMR spectra were taken.

MS (EI, 70 eV): *m*/*z*(%) = 269.9(34) $[M]^+$, 234.9(32) $[M - Cl]^+$, 91.1(100) $[C_7H_7]^+$.

*n*-$BuGeCl_3$ (**1**)

About 20% of 1-bromobutane (127 g, 927 mmol) dissolved in dry $Et_2O$ (150 mL) were added to Mg (24.75 g, 1.02 mol) suspended in dry $Et_2O$ (50 mL),. After the reaction had started, the rest of the bromobutane solution was added over 20 min. Additional dry $Et_2O$ (250 mL) was added and the reaction stirred overnight. It was subsequently filtrated through Celite® directly into a flask containing $SnCl_4$ (46.75 g, 179 mmol) in dry $Et_2O$ (250 mL) while cooling to 0 °C. After removing the ice bath, the solution was stirred once more overnight, then quenched with $H_2O$ (400 mL). The phases were separated, the aqueous phase extracted twice more with $Et_2O$ (2x200 mL) and the combined organic phases dried over $Na_2SO_4$. The solvents were removed at the rotovap to yield 54.2 g (87%) *n*-$Bu_4Sn$ as clear, colorless liquid. The *n*-$Bu_4Sn$ (54.2 g, 156 mmol) was mixed with $GeCl_4$ (33.7 g, 157 mmol) inside a Carius tube and heated to 215 °C for six hours. After cooling back down, residual $GeC_4$ was removed under vacuum (room temperature, 10 mbar). Then 22.46 g (61%) of **2** were isolated as clear colorless liquid through recondensation (70 °C, 17 mbar).

$^1$H NMR ($C_6D_6$, 400 MHz): δ = 1.35–1.20 (m, 4 H, $CH_2$), 0.99 (m, 2 H, $CH_2$), 0.63 (t, 3 H, $^3J_{H\text{-}H}$ = 7. Hz, $CH_3$) ppm. MS (EI, 70 eV): *m*/*z*(%) = 199.9(14) $[M - HCl]^+$, 178.8(55) $[M - C_4H_9]^+$, 163.9(50) $[M - 2\ HCl]^+$, 108.9(35) $[GeCl]^+$, 57.1(100) $[C_4H_9]^+$.

$ArGeH_3$

Mixed halides $ArGeX_3$ (X=Cl, Br) were dissolved in dry $Et_2O$. Freshly ground $LiAlH_4$ was added portion wise while cooling with an ice bath. After complete addition, the ice bath was removed and the mixture stirred for two more hours. The flask was then put into an ice bath again and the excess of $LiAlH_4$ was quenched with dilute aqueous $H_2SO_4$. The organic phase was transferred into a separate flask containing $CaCl_2$ *via* cannula and the aqueous phase was extracted with $Et_2O$. The combined organic phases were then filtrated into a third flask *via* cannula and the solvents were removed under vacuum. The product was isolated as colorless liquid through recondensation.

phenyl$GeH_3$ (**2**): Crude phenyl$GeX_3$ obtained *via* Grignard reaction of bromobenzene (67.1 g, 427 mmol) and $GeCl_4$ (93.5, 436 mmol), dissolved in dry $Et_2O$ (125 mL), reacted with $LiAlH_4$ (15.17 g, 400 mmol), quenched with $H_2SO_4$ (5%,

105 mL), extracted with $Et_2O$ (2x50 mL). Recondensed at room temperature, 9.8*10$^{-3}$ mbar. Yield: 6.24 g (9.4% based on $GeCl_4$). $^1$H NMR ($C_6D_6$, 400 MHz): δ = 7.33 (d, 1 H, $^3J_{H-H}$ = 1.8 Hz, Ar-H), 7.31 (d, 1 H, $^3J_{H-H}$ = 2.2 Hz, Ar-H), 7.14–7.05 (m, 4 H, Ar-H), 4.24 (s, 3 H, $GeH_3$) ppm. $^{13}$C{H} NMR ($C_6D_6$, 101 MHz): δ = 135.7, 131.3, 129.2, 128.6 ppm. *m*/*z*(%) = 152.0(100) $[M]^+$, 79.1(79) $[C_6H_7]^+$.

*o*-tolylGeH$_3$ (**3**): Crude *o*-tolylGeX$_3$ obtained *via* Grignard reaction of 2-bromotoluene (58.3 g, 341 mmol) and $GeCl_4$ (75.2 g, 351 mmol), dissolved in dry $Et_2O$ (100 mL), reacted with $LiAlH_4$ (14.0 g, 369 mmol), quenched with $H_2SO_4$ (1%, 100 mL), extracted with dry $Et_2O$ (3x50 mL). Recondensed at room temperature, 0.03 mbar. Yield: 12.8 g (22.5% based on $GeCl_4$). $^1$H NMR ($C_6D_6$, 300 MHz): δ = 7.38 (d, 1 H, $^3J_{H-H}$ = 6.9 Hz, Ar-H), 7.11 (dd, 1 H, $^3J_{H-H}$ =7.5 Hz, 7.00–6.94 (m, 2 H, Ar-H), 4.22 (s, 3 H, $GeH_3$), 2.16 (s, 3 H, Ar-$CH_3$) ppm. $^{13}$C{H} NMR ($C_6D_6$, 75.5 MHz): δ = 143.5, 136.8, 131.7, 130.0, 129.6, 125.9, 23.1 ppm. MS (EI, 70 eV): *m*/*z*(%) = 166(58) $[M]^+$, 150.9(9) $[M - CH_3]^+$, 91.1(100) $[C_7H_7]^+$. EA calcd. for $C_7H_{10}Ge$: C: 50.41%, H: 6.04%. Found: C: 51.53%; H: 5.66%. UV-Vis (THF): $\lambda_{max}$ (ϵ)=274 (400), 267 (450).

*p*-tolylGeH$_3$ (**4**): a) Crude *p*-tolylGeX$_3$ obtained *via* Grignard reaction of 4-bromotoluene (125 g, 731 mmol) and $GeCl_4$ (165 g, 768 mmol), dissolved in dry $Et_2O$ (200 mL), reacted with $LiAlH_4$ (27.2 g, 717 mmol), quenched with $H_2SO_4$ (1%, 250 mL), extracted with $Et_2O$ (3x100 mL). Isolated at room temperature, 5*10$^{-3}$ mbar. Yield: 15.8 g (12.3% based on $GeCl_4$). b) Crude *p*-tolylGeX$_3$ (11.67 g, 37.1 mmol) obtained *via* $GeCl_2$ insertion, dissolved in dry $Et_2O$ (90 mL), reacted with $LiAlH_4$ (2.67 g, 70 mmol), quenched with $H_2SO_4$ (1%, 80 mL), extracted with $Et_2O$ (3x20 mL). Recondensed at 40 °C, 1 mbar. Yield: 5.03 g (81% based on *p*-tolylGeX$_3$, 47.6% based on $GeCl_4$). $^1$H NMR ($C_6D_6$, 400 MHz): δ = 7.28 (d, 2 H, $^3J_{H-H}$ = 7.7 Hz, Ar-H), 6.94 (d, 2 H, $^3J_{H-H}$ = 7.6 Hz, Ar-H), 4.28 (s, 3 H, $GeH_3$), 2.06 (s, 3 H, Ar-$CH_3$) ppm; $^{13}$C{H} NMR ($C_6D_6$, 101 MHz): δ = 138.9, 135.7, 129.5, 127.5, 21.4 ppm. MS (EI, 70 eV): *m*/*z*(%) = 166.0(68) $[M]^+$, 151.0(10) $[M - CH_3]^+$, 91.1(100) $[C_7H_7]^+$.

2,5-xylylGeH$_3$ (**5**): Crude 2,5-xylylGeX$_3$ obtained *via* Grignard reaction of 2-bromo-*p*-xylene (18.2 g, 98.3 mmol) and $GeCl_4$ (22.4 g, 104 mmol), dissolved in dry $Et_2O$ (150 mL), reacted with $LiAlH_4$ (3.83 g, 101 mmol), quenched with $H_2SO_4$ (1%, 150 mL), extracted with $Et_2O$ (2x50 mL). Isolated at room temperature, 8.9*10$^{-3}$ mbar. Yield: 14.8 g (66.2% based on $GeCl_4$). $^1$H NMR ($C_6D_6$, 300 MHz): δ = 7.25 (s, 1 H, Ar-H), 6.94 (d, 2 H, $^3J_{H-H}$ = 7.7 Hz, Ar-H), 4.26 (s, 3 H, $GeH_3$), 2.27 (s,

3 H, Ar-$CH_3$), 2.21 (s, 3 H, Ar-$CH_3$) ppm; $^{13}C\{H\}$ NMR ($C_6D_6$, 75.5 MHz): δ = 140.0, 137.2, 134.6, 131.0, 130.3, 129.1, 22.3, 20.4 ppm. MS (EI, 70 eV): *m*/*z*(%) = 180.0(64) $[M]^+$, 105.1(100) $[C_8H_9]^+$, 91.1(96) $[C_7H_7]^+$.

2,6-xylylGe$H_3$ (**6**): Crude 2,6-xylylGe$X_3$ obtained *via* Grignard reaction of 2-bromo-*m*-xylene (26.3 g, 142 mmol) and $GeCl_4$ (32.0 g, 149 mmol), dissolved in dry $Et_2O$ (100 mL), reacted with $LiAlH_4$ (5.24 g, 138 mmol), quenched with $H_2SO_4$ (1%, 150 mL), extracted with $Et_2O$ (2x50 mL). Isolated at room temperature, $9.8*10^{-3}$ mbar. Yield: 10.12 g (37.6% based on $GeCl_4$). $^1H$ NMR ($C_6D_6$, 400 MHz): δ = 7.04 (t, 1 H, $^3J_{H-H}$ = 7.6 Hz, Ar-H), 6.88 (d, 2 H, $^3J_{H-H}$ = 7.6 Hz, Ar-H), 4.17 (s, 3 H, $GeH_3$), 2.24 (s, 6 H, Ar-$CH_3$) ppm. MS (EI, 70 eV): *m*/*z*(%) = 180.0(34) $[M]^+$, 165.0(9) $[M - CH_3]^+$, 107.1(100) $[C_8H_{11}]^+$

mesitylGe$H_3$ (**7**): Crude mesitylGe$Cl_3$ obtained *via* Grignard reaction of bromo-mesitylene (18.1 g, 90.9 mmol) and $GeCl_4$ (20.6 g, 95.9 mmol), dissolved in dry $Et_2O$ (125 mL), quenched with $H_2SO_4$ (4%, 125 mL), extracted with $Et_2O$ (2x30 mL). Isolated at room temperature, $9.1*10^{-3}$ mbar. Yield: 7.18 g (38.4% based on $GeCl_4$). $^1H$ NMR ($C_6D_6$, 300 MHz): δ = 6.71 (s, 2 H, Ar-H), 4.20 (s, 3 H, Ge-H), 2.26 (s, 6 H, Ar-$CH_3$), 2.11 (s, 3 H, Ar-H) ppm; $^{13}C\{H\}$ NMR ($C_6D_6$, 75.5 MHz): δ = 143.6, 138.6, 128.4, 128.2, 24.0, 21.0 ppm. MS (EI, 70 eV): *m*/*z*(%) = 194.1(23) $[M]^+$, 179.0(7) $[M - CH_3]^+$, 121.1(100) $[C_9H_{13}]^+$.

<u>*n*-butylGe$H_3$ (**8**)</u>

**1** (11.5 g, 48.7 mmol) was dissolved in dry diglyme (50 mL). $LiAlH_4$ (3.4 g, 89.6 mmol) was added while cooling to -25 °C. The resulting suspension was stirred overnight. The product was isolated as colorless liquid (5.17 g, 80%) by condensing it directly out of the reaction mixture at 80 °C, 200 mbar.

$^1H$ NMR ($C_6D_6$, 400 MHz): δ = 3.57 (t, 3 H, $^3J_{H-H}$ = 3.40 Hz, $GeH_3$), 1.32–1.17 (m, 4 H, $CH_2$), 0.82–0.78 (m, 5 H, $CH_2$&$CH_3$) ppm; MS (EI, 70 eV) *m*/*z*(%) = 102.9(63) $[C_2H_5GeH]^+$, 74.9(100) $[GeH]^+$, 57.1(79) $[C_4H_9]^+$.

<u>MesitylGe$Cl_3$ (**9**)</u>

**7** (6.11 g, 31.4 mmol) was dissolved in $CCl_4$ (15 mL), then a spatula tip of palladium (~10 mg) was added. The reaction was refluxed overnight. After cooling back to room temperature, palladium was filtrated off *via* cannula and the solvent removed *in*

*vacuo* to yield **9** (4.12 g, 44%) as colorless powder. To grow an X-ray crystal, some product (1 g) was dissolved in toluene (5 mL) at 80 °C. The solution was allowed to slowly cool to room temperature, then placed inside a fridge. After one week, colorless crystals were observed.

$^{1}$H NMR ($C_6D_6$, 300 MHz): δ = 6.40 (s, 2 H, Ar-H), 2.40 (s, 6 H, Ar-$CH_3$), 1.86 (s, 3 H, Ar-$CH_3$) ppm; $^{13}$C{H} NMR ($CDCl_3$, 75.5 MHz): δ = 143.3, 143.6, 130.7, 129.1, 23.9, 21.2 ppm. MS (EI, 70 eV): *m*/*z*(%) = 297.9(22) $[M]^+$, 261.9(48) $[M – HCl]^+$, 118.1(100) $[C_9H_{10}]^+$.

<u>*o*-tolylGeCl$_3$ (**10**)</u>

**3** (3.60 g, 21.5 mmol) was dissolved in dry THF (50 mL) and cooled to 0 °C. TCCA (6.00 g, 25.8 mmol) was added portion-wise over 30 min. After an additional 30 min at 0 °C, the cooling bath was removed and the reaction stirred overnight. The solvent was removed *in vacuo* and replaced with *n*-pentane (20 mL), then the mixture was filtrated through a cannula. The residue was washed twice with *n*-pentane (2x10 mL). The solvents were removed again to yield 4.10 g (71%) of **10** as clear colorless liquid.

$^{1}$H NMR ($C_6D_6$, 300 MHz): δ = 7.54 (d, 1 H, $^{3}J_{H-H}$ = 7.6 Hz, Ar-H), 6.96 (dd, 1 H, $^{3}J_{H-H}$ = 7.4 Hz, Ar-H), 6.85–6.70 (m, 2 H, Ar-H), 2.32 ppm; $^{13}$C{H} NMR ($C_6D_6$, 75.5 MHz): δ = 142.1, 133.8, 133.3, 132.5, 131.8, 126.5, 22.0 ppm. MS (EI, 70 eV): *m*/*z*(%) = 269.8(20) $[M]^+$, 233.9(67) $[M – HCl]^+$, 90.0(100) $[C_7H_6]^+$. EA calcd. for $C_7H_7GeCl_3$: C: 31.13%, H: 2.61%. Found: C: 33.04%; H: 2.86%.

<u>*o*-tolylGe(Cl)H$_2$ (**11**)</u>

**3** (1.22 g, 7.29 mmol) was dissolved in dry THF (30 mL). The solution was cooled to -80 °C and TCCA (0.57 g, 2.43 mmol) was added in small portions, with each portion delayed until the previous one had fully dissolved. After complete addition, the reaction vessel was kept inside the cooling bath overnight, and the two of them were allowed to slowly warm to room temperature together. The solvent was removed *in vacuo* and replaced with *n*-pentane (20 mL). The mixture was filtrated through a cannula and the solvent removed through evacuation once again to yield 1.41 g (96%) of **11** as clear, colorless liquid.

$^{1}$H NMR ($C_6D_6$, 400 MHz): δ = 7.32 (d, 1 H, $^{3}J_{H-H}$ = 7.4 Hz, Ar-H), 7.06 (dd, 1 H, $^{3}J_{H-H}$ = 7.5 Hz, Ar-H), 6.94 (t, 1 H, $^{3}J_{H-H}$ = 7.4 Hz, Ar-H), 6.88 (d, 1H, $^{3}J_{H-H}$ = 7.6 Hz, Ar-H), 5.62 (s, 2 H, Ge-H), 2.15 (s, 3 H, Ar-$CH_3$) ppm; $^{13}$C{H} NMR ($C_6D_6$, 101 MHz): δ = 142.6, 134.6, 132.5, 131.1, 129.9, 125.8, 21.7 ppm. MS (DI, 70 eV): *m*/*z*(%) = 202.0(25) $[M]^+$, 165(24) $[C_7H_7Ge]^+$, 93.1(100) $[C_7H_9]^+$.

<u>*o*-tolylGe$D_3$ (**12**)</u>

**10** (3.96 g, 14.7 mmol) was dissolved in dry $Et_2O$ (15 mL) and cooled to 0 °C. $LiAlD_4$ (1.51 g, 36.0 mmol) was added and the resulting suspension stirred for 2 h at room temperature. Then the reaction was cooled to 0 °C again and quenched with aqueous $H_2SO_4$ (1%, 20 mL). The phases were separated, the aqueous phase extracted twice more with $Et_2O$ (2x10 mL), the combined organic phases dried over $CaCl_2$ and the solvent removed *in vacuo*. The product was isolated by recondensation (room temperature, 9.5*10$^{-3}$ mbar) to yield 1.73 g (69.6%) of clear colorless liquid.

$^{1}$H NMR ($C_6D_6$, 400 MHz): δ = 7.37 (d, 1 H, $^{3}J_{H-H}$ = 7.2 Hz, Ar-H), 7.11 (dd, 1 H, $^{3}J_{H-H}$ = 7.5 Hz, Ar-H), 7.00–6.95 (m, 2 H, Ar-H), 2.16 (s, 3 H, Ar-$CH_3$) ppm; $^{13}$C{H} NMR ($C_6D_6$, 101 MHz): δ = 143.5, 136.8, 131.7, 129.9, 129.5, 125.8, 23.1 ppm. IR: $\tilde{\nu}$=3100–2800 (br), 1590 (w), 1482 (vs), 1447 (m) cm$^{-1}$. *m*/*z*(%) = 167.0(80) $[M]^+$, 152.0(11) $[M - CH_3]^+$, 95.1(100) $[C_7H_5D_3]^+$. EA calcd. for $C_7H_7GeD_3$: C: 50.41%, H: 6.04%. Found: C: 49.45%; H: 5.29%.

<u>Attempted preparation of (*o*-tolylGe$H_2$)$_2$</u>

Magnesium (0.71 g, 29.1 mmol) was heated under vacuum inside a Schlenk flask. After cooling to room temperature, **11** (1.47 g, 7.29 mmol) was added, then the mix was heated to 60 °C. First dry THF (1 mL), then 1,2-dibromoethane (0.1 mL, 0.22 g, 1.2 mmol) were added. The reaction was cooled to 40 °C, and more THF (3 mL) was added. The reaction was stirred overnight, then cooled to room temperature and filtrated through a cannula. The residue was washed twice with $Et_2O$ (2x5 mL) and the obtained solution extracted with HCl (5 M, 10 mL). The aqueous phase was extracted three times with $Et_2O$ (3x5 mL), the combined organic phases were dried over $Na_2SO_4$ and the solvents removed under reduced pressure to yield small amounts of clear, colorless liquid. Analytics (GC/MS, NMR) showed that a mixture of various coupling and rearrangement products had been obtained.

### 5.3.2 Silylgermanes

Me(*p*-tolyl)$GeH_2$ *via* *p*-tolyl$Ge(H_2)Li$

A C. Young NMR tube was charged with crystalline *t*-BuLi (9.0 mg, 0.14 mmol) inside a glovebox. After removal from the box, the bottom of the tube was cooled with $N_2$(l), evacuated, and THF[$d_8$] (0.6 mL) condensed inside. Then the tube was submerged further in the $N_2$(l) and *p*-tolyl$GeH_3$ (22 mg, 0.13 mmol) condensed inside as well. The tube was closed while still evacuated and gradually thawed from top to bottom, allowing the *p*-tolyl$GeH_3$ and the majority of the THF[$d_8$] to liquefy and mix before coming into contact with the *t*-BuLi. After thawing fully, the tube was occasionally shaken to mix the components, until no more gas bubbles were forming. Then the tube was subjected to three freeze-pump cycles to remove the formed butane. After flushing the tube with nitrogen, a $^1$H NMR spectrum was measured.

*p*-tolyl$Ge(H_2)Li$: $^1$H NMR (THF[$d_8$], 400 MHz): δ = 6.81 (d, 2 H, $^3J_{H\text{-}H}$ = 7.6 MHz, Ar-H), 6.09 (d, 2 H, $^3J_{H\text{-}H}$ = 7.2 Hz), 2.65 (s, 2 H, $GeH_2$), 1.55 (s, 3 H, Ar-$CH_3$) ppm.

Next, the tube was frozen once more, MeI (0.23 g, 1.6 mmol) condensed inside and the tube shaken to mix the components. After 30 min, another $^1$H NMR spectrum was measured.

Me(*p*-tolyl)$GeH_2$: $^1$H NMR (THF[$d_8$], 400 MHz): δ = 7.35 (d, 2 H, $^3J_{H\text{-}H}$ = 7.9 Hz, Ar-H), 7.13 (d, 2 H, $^3J_{H\text{-}H}$ = 7.5 Hz, Ar-H), 4.29 (q, 2 H, $^3J_{H\text{-}H}$ = 3.8 Hz, $GeH_2$), 2.29 (s, 3 H, Ar-$CH_2$), 0.50 (t, 3 H, $^3J_{H\text{-}H}$ = 3.8 Hz, Ge-$CH_3$) ppm.

*t*-$Bu_2$MeSiBr (**13**)

**13** was prepared following a literature procedure.[182] $MeSiHCl_2$ (9.99 g, 87.6 mmol) was dissolved in dry *n*-pentane (25 mL) and cooled to 0 °C. *t*-BuLi in *n*-pentane (1.9 M, 94 mL, 179 mmol) was added over 30 min. The ice bath was removed and the reaction stirred for 40 h. Stirring was stopped and the suspension allowed to settle, then the supernatant was filtrated off *via* cannula. The solvent was removed *in vacuo* and *t*-$Bu_2$MeSiH was isolated by recondensation (room temperature, 0.01 mbar) as 8.975 g (56.6 mmol, 66%) of clear, colorless liquid.

This liquid was dissolved again in dry *n*-pentane (45 mL) and cooled to -40 °C. An exhaust tube was attached, then $Br_2$ (10.5 g, 66.0 mmol) added dropwise through a septum, until the orange coloration persisted. The clear, orange solution was stirred

for 3 h at room temperature. The volatiles were removed at room temperature, 10 mbar, and the product recondensed (85 °C, 10 mbar) to produce **13** as clear, colorless crystals in a yield of 10.35 g (77%).

$^{1}$H NMR ($C_6D_6$, 400 MHz): δ = 1.00 (s, 18 H, C-$CH_3$), 0.32 (s, 3 H, Si-$CH_3$) ppm; $^{29}$Si{H} NMR ($C_6D_6$, 39.5 MHz): δ = 42.0 ppm. MS (EI, 70 eV): *m*/*z*(%) = 236.1(5) $[M]^+$, 181.0(28) [M – *t*-Bu]$^+$ , 139.0(100) $[Me_2SiBr]^+$, 57.1(25) [*t*-Bu]$^+$.

<u>*t*-BuMeRSiGe(Ar)$H_2$</u>

$ArGeH_3$ was dissolved in THF in a Schlenk tube with a glass stir bar and cooled to -40 °C. *t*-BuLi in *n*-pentane was added dropwise with a syringe. The mixture was stirred for 30 min while cooling, then another 90 min at room temperature. In the meantime, a second flask was prepared containing either TBDMSCl or DTBMSBr in THF. This flask was cooled to -30 °C, then a syringe was used to slowly add the clear, yellow solution that had formed in the first flask. After stirring overnight, the volatiles (solvents, excess silicon halides) were removed at room temperature, 0.1 mbar. *n*-pentane was added to the residue and the obtained suspension was filtrated through a cannula into a separate flask. The solids were washed with more *n*-pentane. Then the solvents were evaporated under vacuum once again and the product was purified by recondensation. The obtained clear, colorless solution was evacuated one last time (30 °C, 0.1 mbar) to remove thermal degradation products.

TBDMSGe(phenyl)$H_2$ (**14**): Reaction of **2** (2.58 g, 16.9 mmol) in dry THF (15 mL), *t*-BuLi (1.9 M, 9.5 mL, 18.03 mmol) and TBDMSCl (2.56 g, 17.0 mmol) in dry THF (17 mL). Filtration with dry *n*-pentane (2x15 mL). Isolation at 60 °C, $5.0*10^{-3}$ mbar. Yield: 2.48 g (55%). $^{1}$H NMR ($C_6D_6$, 400): δ = 7.49 (m, 2 H, Ar-H), 7.14 (m, 3 H, Ar-H), 4.26 (s, 2 H, $GeH_2$), 0.91 (s, 9 H, C-$CH_3$), 0.11 (s, 3 H, Si-$CH_3$) ppm. $^{13}$C{H} NMR ($C_6D_6$, 101 MHz): δ = 136.1, 128.6, 128.3, 27.1, 18.0, 4.4 ppm. $^{29}$Si{H} NMR ($C_6D_6$, 39.5 MHz): δ = 3.6 ppm. MS (EI, 70 eV): *m*/*z*(%) = 268.1(3) $[M]^+$, 209.0(11) [M – *t*-Bu, – $H_2$]$^+$, 151.0(12) [phenylGe]$^+$; 115.1(21) [TBDMS]$^+$, 73.1(100) $[Me_3Si]^+$.

TBDMSGe(*p*-tolyl)$H_2$ (**15**): Reaction of **4** (8.9 g, 53.4 mmol) in dry THF (50 mL), *t*-BuLi (1.9 M, 30 mL, 57 mmol) and TBDMSCl (8.2 g, 54 mmol) in dry THF (30 mL). Filtration with dry *n*-pentane (50+2x30 mL). Isolation at 80 °C, $7.2*10^{-3}$ mbar. Yield: 7.11 g (47%). **15** was alternatively also synthesized under similar conditions with

*n*-BuLi at 0 °C, to a yield of 32%. $^{1}$H NMR ($C_6D_6$, 400): δ = 7.46 (d, 2 H, $^{3}J_{H-H}$ = 7.8 Hz, Ar-H), 7.00 (d, 2 H, $^{3}J_{H-H}$ = 7.4 Hz, Ar-H), 4.29 (s, 2 H, Ge-H), 2.10 (s, 3 H, Ar-$CH_3$), 0.92 (s, 9 H, C-$CH_3$), 0.13 (s, 6 H, Si-$CH_3$) ppm; $^{13}$C{H} NMR ($C_6D_6$, 101 MHz): δ = 137.8, 136.1, 131.1, 129.5, 27.1, 21.4, 18.0, -4.4 ppm; $^{29}$Si{H} NMR ($C_6D_6$, 39.5 MHz): δ = 3.4 ppm; $^{73}$Ge NMR ($C_6D_6$, 24.4 MHz): δ = -204.7 ppm. IR: $\tilde{\nu}$=3100–2800 (br), 2062 (vs), 1590 (w), 1475 (m), 1447 (m) $cm^{-1}$. HRMS (DART): *m*/*z* calcd. for $C_{13}H_{23}GeSi$ 281.0781 $[M - H]^+$, found 281.0791. EA calcd. for $C_{13}H_{23}GeSi$: C: 55.56%, H: 8.61%. Found: C: 53.00%; H: 8.64%.

TBDMSGe(2,6-xylyl)$H_2$ (**16**): Reaction of **5** (502 mg, 3.3 mmol) in dry THF (4 mL), *t*-BuLi (1.9 M, 2 mL, 3.8 mmol) and TBDMSCl (0.45 g, 3.0 mmol) in dry THF (4 mL). Filtration with dry *n*-pentane (5+2x2 mL). Isolation at 70 °C, 5.0*$10^{-3}$ mbar. Yield: 0.36 g (37%). $^{1}$H NMR ($C_6D_6$, 400): δ = 7.06 (dd, 1 H, $^{3}J_{H-H}$ = 8.1, 6.9 Hz, Ar-H), 6.96 (d, 2 H, $^{3}J_{H-H}$ = 7.5 Hz, Ar-H), 4.21 (s, 2 H, Ge-H), 2.37 (s, 6 H, Ar-$CH_3$), 0.92 (s, 9 H, C-$CH_3$), 0.09 (s, 6 H, Si-$CH_3$) ppm; $^{13}$C{H} NMR ($C_6D_6$, 101 MHz): δ = 143.5, 135.1, 128.4, 127.5, 26.9, 25.3, 18.0, -3.9 ppm; $^{29}$Si{H} NMR ($C_6D_6$, 39.5 MHz): δ = 4.2 ppm. MS (EI, 70 eV): *m*/*z*(%) = 296.1(4) $[M]^+$, 239.1(2) $[M - t\text{-Bu}]^+$, 179.0(20) $[xylylGe]^+$, 115.1(20) $[TBDMS]^+$, 105.1(13) $[xylyl]^+$, 73.1(100) $[Me_3Si]^+$.

DTBMSGe(*p*-tolyl)$H_2$ (**17**): Reaction of **4** (1.17 g, 7.02 mmol) in dry THF (10 mL), *t*-BuLi (1.9 M, 2 mL, 7.6 mmol) and DTBMSBr (1.8 g, 7.6 mmol) in dry THF (10 mL). Filtration with *n*-pentane (10+2x5 mL). Isolation at 160 °C, 5.6*$10^{-3}$ mbar. Yield: 1.06 g (47%). $^{1}$H NMR ($C_6D_6$, 400): δ = 7.49 (d, 2 H, $^{3}J_{H-H}$ = 7.6 Hz, Ar-H), 7.00 (d, 2 H, $^{3}J_{H-H}$ = 7.5 Hz, Ar-H), 4.35 (s, 2 H, Ge-H), 2.10 (s, 3 H, Ar-$CH_3$), 1.02 (s, 18 H, C-$CH_3$), 0.15 (s, 3 H, Si-$CH_3$) ppm; $^{13}$C{H} NMR ($C_6D_6$, 101 MHz): δ = 137.7, 136.2, 132.1, 129.5, 29.2, 21.4, 20.9, -7.2 ppm; $^{29}$Si{H} NMR ($C_6D_6$, 39.5 MHz): δ = 13.0 ppm; $^{73}$Ge NMR ($C_6D_6$, 24.4 MHz) δ = -207.3 ppm. HRMS (EI): *m*/*z* calcd. for $C_{16}H_{30}GeSi$ 324.1328 $[M]^+$, found 324.1308. EA calcd. for $C_{16}H_{30}GeSi$: C: 59.47%, H: 9.36%. Found: C: 58.99%, H: 9.05%.

TBDMSGe(mesityl)$H_2$ (**18**)

**7** (1.776 g, 9.12 mmol) was dissolved in dry THF (10 mL) in a Schlenk tube equipped with a glass stir bar. MeLi in $Et_2O$ (1.6 M, 6.5 mL, 10.4 mmol) was slowly added while stirring at 0 °C. The reaction was allowed to warm to room temperature and stirred for 2 d. TBDMSCl (1M in dry THF, 10.5 mL, 10.5 mmol) was added and the mixture

stirred for another day. Next, volatiles (solvents and excess TBDMSCl) were removed under vacuum (room temperature, 0.1 mbar). The residue was suspended in dry *n*-pentane (10 mL) and the suspension filtrated through Celite®. The filter cake was washed twice more with *n*-pentane (2x5 mL). The *n*-pentane was removed again under reduced pressure and the remaining clear, colorless liquid was recondensed (125 °C, 5.5*$10^{-3}$ mbar). The condensate was evacuated one last time (60 °C, 0.01 mbar) to remove traces of unreacted **7** and thermal degradation product TBDMSH. This left pure **18** as clear colorless liquid in a yield of 1.25 g (45%).

$^{1}$H NMR ($C_6D_6$, 400): δ = 6.80 (s, 2 H, Ar-H), 4.23 (s, 2 H, $GeH_2$), 2.39 (s, 6 H, Ar-$CH_3$), 2.14 (s, 3 H, Ar-$CH_3$), 0.94 (s, 9 H, C-$CH_3$), 0.11 (s, 6 H, Si-$CH_3$) ppm; $^{13}$C{H} NMR ($C_6D_6$, 101 MHz): δ = 143.3, 137.6, 131.1, 128.5, 27.0, 25.1, 21.2, 18.1, -3.9 ppm; $^{29}$Si{H} NMR ($C_6D_6$, 39.5 MHz): δ = 4.0 ppm; MS (EI, 70 eV): *m*/*z*(%) = 310.1(5) $[M]^+$, 253.1(2) [M – *t*-Bu]$^+$, 194.0(47) [mesitylGeH]$^+$, 119.1(21) [mesityl]$^+$, 115.1(10) [TBDMS]$^+$, 73.1(100) $[Me_3Si]^+$.

Attempts at Dearylation of TBDMSGe(*p*-tolyl)$H_2$ with TfOH

Attempt A: TfOH (18 µl, 0.20 mmol) was added to **9** (52 mg, 0.18 mmol) in dry $CH_2Cl_2$ (1 mL) at 0 °C. After stirring for 1 h, LiCl (79 mg, 1.9 mmol) was added and the mixture stirred over the weekend. Afterwards, the obtained suspension was pushed through a syringe filter and the solvents removed under vacuum to produce a mixture of yellow solid and colorless liquid (93 mg).

Attempt B: TfOH (32 µl, 0.362 mmol) was added dropwise to **9** (104 mg, 0.369 mmol) in dry $CH_2Cl_2$ (1 mL) at 0 °C. After stirring for 1 h, the solvent was removed under vacuum and replaced with $Et_2O$ (1 mL). Then $LiAlH_4$ (1 spatula tip, ~20 mg, ~0.5 mmol) was added and the mix stirred 1 h. $Et_2O$ was removed (room temperature, 200 mbar), then product isolation was attempted through recondensation (room temperature, 0.01 mbar). However, no condensate could be obtained.

Attempt C: TfOH(16 µl, 0.181 mmol) was added to **9** (57 mg, 0.20 mmol) in $CDCl_3$ (0.7 mL) at 0 °C. The reaction was monitored with regular $^{1}$H NMR spectra.

Attempt D: TfOH(18 µl, 0.20 mmol) was added to **9** (63 mg, 0.22 mmol) in dry toluene (1 mL) at -40 °C. After stirring for 1 h, MeLi (1.04 M in $Et_2O$, 0.25 mL, 0.251 mmol)

was added while still cooling to -40 °C. Next, the mixture was allowed to warm to room temperature. $Et_2O$ was removed (room temperature, 100 mbar) and $C_6D_6$ (1 ml) was added to facilitate NMR measurements.

Attempt E: TfOH(16 µl, 0.18 mmol) was added to **9** (60 mg, 0.21 mmol) in dry toluene at -60 °C. After stirring for 1 h, MeLi (1.04 M in $Et_2O$, 0.25 mL, 0.251 mmol) was added while still cooling to -60 °C. The cooling bath was removed and the mixture allowed to warm to room temperature. $Et_2O$ was evaporated (room temperature, 100 mbar) and replaced with $C_6D_6$ (1 ml) to facilitate NMR measurements.

Neither the triflate TBDMSGe(OTf)$H_2$ nor any of its derivatization products were found in any of the above attempts. Instead, the degradation product TBMDSOTf was identified: $^1$H NMR ($CDCl_3$, 400 MHz): δ = 1.01 (s, 9 H, C-$CH_3$), 0.46 (s, 6 H, Si-$CH_3$), consistent with reported values.[183]

TBDMSGe(Cl)$H_2$ (**19**), NMR scale monitoring

A C. Young NMR tube was charged with $C_6D_6$ (0.7 mL) and $AlCl_3$ (13.6 mg, 0.102 mmol) inside a glovebox. After addition of **15** (72 mg, 0.26 mmol) the tube was removed from the glovebox. Then HCl (1 M in $Et_2O$, 0.25 mL, 0.25 mmol) was injected to start the reaction. The compounds in the mixture were monitored *via* their characteristic $GeH_2$ resonance in $^1$H NMR ($C_6D_6$, 400 MHz): δ = 5.25 (s, 2 H, Ge(Cl)$H_2$), 4.25 (s, 2 H, Ge(tolyl)$H_2$) ppm.

*t*-BuMeRSiGe(Cl)$H_2$

A flask was charged with *t*-BuMeRSiGe(Ar)$H_2$ in $Et_2O$. HCl in $Et_2O$ was added, immediately followed by $AlCl_3$. The mixture was stirred overnight, then *n*-pentane was added and the precipitated $AlCl_3$ removed by filtration through Celite®. The filter cake was washed with more *n*-pentane and the combined filtrate solutions stored without further workup. The solvents were only removed directly before further use and replaced either with $C_6D_6$ (for NMR spectroscopy) or $Et_2O$ (for follow-up reactions).

TBDMSGe(Cl)$H_2$ (**19**): a) Reacted **14** (2.48 g, 9.36 mmoL) in dry $Et_2O$ (5 mL), HCl (2 M, 5.5 mL, 11 mmol) and $AlCl_3$ (0.250 g). Filtrated with *n*-pentane (10+10 mL). b) Reacted **15** (1.87 g, 6.64 mmol) in dry $Et_2O$ (5 mL), HCl (2 M, 3.8 mL, 7.6 mmol) and $AlCl_3$ (0.167). Filtrated with *n*-pentane (10+2x5 mL). Solvents removed at -20 °C,

1 mbar. c) Reacted **16** (1.12 g, 3.08 mmol) in dry $Et_2O$ (10 mL), HCl (2 M, 2 mL, 4 mmol) and $AlCl_3$ (0.110 g). Filtrated with dry *n*-pentane (10+10 mL). Solvents removed at -20 °C, 1 mbar. d) Reacted **18** (1.12 g, 3.66 mmol) in dry $Et_2O$ (4 mL), HCL (2 M, 2 mL, 4 mmol) and $AlCl_3$ (0.131 mg). Filtrated with dry *n*-pentane (10+10 mL). Solvents removed at -20 °C, 1 mbar. $^1$H NMR ($C_6D_6$, 400 MHz): δ = 5.25 (s, 2 H, Ge-H), 0.77 (s, 9 H, C-$CH_3$), 0.05 (s, 6 H, Si-$CH_3$) ppm; $^{13}$C{H} NMR ($C_6D_6$, 101 MHz): δ = 26.8, 18.2, -5.9 ppm; $^{29}$Si{H} NMR ($C_6D_6$, 39.5 MHz): δ = 8.8 ppm.

DTBMSGe(Cl)$H_2$ (**20**): Reacted **17** (1.0 g, 3.1 mmol) in dry $Et_2O$ (4 mL), HCl (2 M, 1.8 mL, 3.6 mmol) and $AlCl_3$ (136 mg). Filtrated with dry *n*-pentane (10+2x5 mL). Solvents removed at -25 °C, 0.1 mbar. $^1$H NMR ($C_6D_6$, 400 MHz): δ = 5.38 (s, 2 H, Ge-H), 0.92 (s, 18 H, C-$CH_3$), 0.10 (s, 3 H, Si-$CH_3$) ppm; $^{29}$Si{H} NMR ($C_6D_6$, 39.5 MHz): δ =16.4 ppm.

<u>*t*-BuMeRSiGe$H_3$</u>

$LiAlH_4$ was added to a solution of *t*-BuMeRSiGe(Cl)$H_2$ in $Et_2O$ at -20 °C. The reaction was stirred overnight at RT, then concentrated by evacuating it to 400 mbar for 1 h. Then the entire mixture was recondensed (30 °C, 0.1 mbar) and the remaining $Et_2O$ removed at 100 mbar to leave a clear, colorless liquid.

TBDMSGe$H_3$ (**21**): **19** [unknown amount obtained from **15** (1.87 g, 6.64 mmol)] in $Et_2O$ (20 mL), $LiAlH_4$ (740 mg, 14.3 mmol). Obtained 0.49 g of mixture: **21** (83% w/w), $Et_2O$ (9% w/w), toluene (8% w/w). Yield: 32% based on **15**.$^1$H NMR ($C_6D_6$, 400 MHz): δ = 3.06 (s, 3 H, Ge-H), 0.88 (s, 9 H, C-$CH_3$), 0.09 (s, 6 H, Si-$CH_3$) ppm; $^{13}$C{H} NMR ($C_6D_6$, 101 MHz): δ = 26.4, 17.2, -4.2 ppm; $^{29}$Si{H} NMR ($C_6D_6$, 39.5 MHz): δ = 4.4 ppm. HRMS (EI): *m*/*z* calcd. for $C_6H_{18}GeSi$ 192.0389 $[M]^+$, found 192.0382.

DTBMSGe$H_3$ (**22**): **20** [unknown amount obtained from **17** (1.0 g, 3.1 mmol)] in $Et_2O$ (10 mL), $LiAlH_4$ (470 mg, 12.4 mmol). Yield: 0.45 g (63% based on **17**). $^1$H NMR ($C_6D_6$, 400 MHz): δ = 3.10 (s, 3 H, Ge-H), 0.98 (s, 18 H, C-$CH_3$), 0.11 (s, 3 H, Si-$CH_3$) ppm; $^{13}$C{H} NMR ($C_6D_6$, 101 MHz) δ = 28.8, 20.3, -6.8 ppm; $^{29}$Si{H} NMR ($C_6D_6$, 39.5 MHz): δ = 14.8 ppm. HRMS (EI): *m*/*z* calcd. for $C_9H_{22}GeSi$ 232.0702 $[M - H_2]^+$, found 232.0708.

### 5.3.3 RLi reactivity studies

*n*-Bu(*p*-tolyl)$GeH_2$ (23)

a) Unintentional synthesis: **4** (384 mg, 2.3 mmol) was dissolved in dry $Et_2O$ (2.5 mL). *n*-BuLi in hexanes (1.51 M, 1.6 mL, 2.4 mmol) was added dropwise at 0 °C. A yellow suspension formed, which was allowed to warm to room temperature and stirred for an additional hour, before being added dropwise to a solution of TBDMSCl (403 mg, 2.67 mmol) in dry THF (3 mL) at -20 °C. After complete addition, the reaction was stirred for 1 h at 0 °C, then overnight at room temperature. The solvents were replaced with *n*-hexane (3 mL), and the mixture pushed through a syringe filter. The residue was washed once with hexane (3 mL), then the solvents were removed under vacuum to leave a colorless liquid.

b) Intentional synthesis: **4** (503 mg, 3.01 mmol) was dissolved in dry $Et_2O$ (3 mL). The solution was cooled to 0 °C and *n*-BuLi in hexanes (1.51 M, 2 mL, 3.02 mmol) was added dropwise. The resulting yellow suspension was stirred for 1 h, then the solvents were removed *in vacuo* and the product was isolated through recondensation (50 °C, 0.012 mbar). Yield: 401 mg (59.5%) of clear, colorless liquid.

$^1$H NMR ($C_6D_6$, 400 MHz): δ = 7.40 (d, 2 H, $^3J_{H-H}$ = 8.0 Hz, Ar-H), 7.02 (d, 2 H, $^3J_{H-H}$ = 7.7 Hz, Ar-H), 4.55 (t, 2 H, $^3J_{H-H}$ = 3.2 Hz, $GeH_2$), 2.11 (s, 3 H, Ar-$CH_3$), 1.38-1.46 (m, 2 H, $CH_2$), 1.22-1.31 (m, 2 H, $CH_2$), 1.01-1.07 (m, 2 H, $CH_2$), 0.81 (3, 3 H, $^3J_{H-H}$ = 7.3 Hz, $CH_3$) ppm; $^{13}$C{H} NMR ($C_6D_6$, 101 MHz) δ = 138.6, 135.3, 131.7, 129.4, 29.2, 26.0, 21.4, 13.9, 11.8 ppm. HRMS (DART): *m*/*z* calcd. for $C_{11}H_{17}Ge$ 223.0542 $[M - H]^+$, found 223.0555. EA calcd. For $C_{11}H_{18}Ge$: C: 59.27%, H: 8.14%. Found: C: 59.15%, H: 8.75%.

*t*-Bu(*p*-tolyl)$GeH_2$ (**24**)

**4** (542 mg, 3.3 mmol) was dissolved in dry *n*-pentane (4 mL) and cooled to -85 °C. While stirring with a glass bar, *t*-BuLi in *n*-pentane (1.9 M, 2 mL, 3.8 mmol) was added over 5 min. The cooling bath was removed and the yellow suspension allowed to warm to room temperature. It was stirred for another hour, then the mixture was filtrated through a cannula, the solvents were removed under reduced pressure, and the product was isolated through recondensation a (45 °C, $6.3*10^{-3}$ mbar) as clear, colorless liquid (0.27 g, 33%).

$^{1}$H NMR ($C_6D_6$, 400 MHz): δ = 7.41 (d, 2 H, $^{3}J_{H-H}$ = 7.9 Hz, Ar-H), 7.02 (d, 2 H, $^{3}J_{H-H}$ = 8.0 Hz, Ar-H), 4.57 (s, 2 H, $GeH_2$), 2.11 (s, 3 H, Ar-$CH_3$), 1.09 (s, 9 H, C-$CH_3$) ppm; $^{13}$C{H} NMR ($C_6D_6$, 101 MHz) δ = 138.7, 135.9, 131.5, 129.4, 29.0, 22.4, 21.4 ppm. MS (EI, 70 eV): *m*/*z*(%) = 224.1(10) $[M]^+$, 166.0(100) [M – *t*-Bu]$^+$, 91.1(50) $[C_7H_7]^+$, 57.1(56) $[C_4H_9]^+$.

Screening Reactions

All screening reactions followed the same general process: $ArGeH_3$ was dissolved in dry solvent and cooled to -40 °C. A slight excess of RLi solution (MeLi in $Et_2O$, *n*-Buli in hexanes, *sec*-BuLi in cyclohexane/hexane, *i*-BuLi in *n*-heptane, *t*-BuLi in *n*-pentane, PhLi in $Bu_2O$) was added dropwise while stirring with a glass stir bar. After complete addition, the reaction was first stirred for 30 min at -40 °C, then for another 90 min while being allowed to warm to room temperature. Then the reaction was cooled again to -40 °C, and TBDMSCl (1 M in THF) was added in excess as derivatization reagent for GC/MS analysis (note: while there are many cheaper and faster options for derivatization, TBDMSCl was chosen because the so produced compounds were useful precursors for (triarylsilyl)germanium trihydride synthesis). The solvents were replaced with *n*-pentane, the mixture was filtrated, and the resulting clear solution was analyzed on the GC/MS. Where only the silylated product was present, it was isolated through vacuum removal of the solvents, followed by recondensation. Table 10 shows which starting materials were used for each screening reaction, Table 11 lists the relative peak areas for all germanium containing compounds found in a GC/MS (EI, 70 eV) of each reaction mixture after the experiment. Compounds were identified either by their retention time ($t_R$) and fragmentation pattern.

Ar = *p*-tolyl: **4** ($t_R$ = 5.15 min): *m*/*z*(%) = 166.0(68) [M – $H_2$]$^+$, 91.9(100) $[C_7H_7]$. Me(*p*-tolyl)$GeH_2$ ($t_R$ = 6.10 min): *m*/*z*(%) = 182.0(28) $[M]^+$, 165.0(100) $[C_7H_7Ge]^+$, 91.1(53) $[C_7H_7]^+$. $Me_2$(*p*-tolyl)GeH ($t_R$ = 6.62 min): *m*/*z*(%) = 196(19) $[M]^+$, 181(100) [M – $CH_3$]$^+$, 165(24) $[C_7H_7Ge]^+$, 91.1(41) $[C_7H_7]^+$. *i*-Bu(*p*-tolyl)$GeH_2$ ($t_R$ = 8.05 min): *m*/*z*(%) = 222.1(6) [M – $H_2$]$^+$, 165.0(21) $[C_7H_7Ge]^+$, 132.0(69) [M – $C_7H_8$]$^+$, 91.1(100) $[C_7H_7]^+$. *sec*-Bu(*p*-tolyl)$GeH_2$ ($t_R$ = 8.08 min): *m*/*z*(%) = 224.1(7) $[M]^+$, 165.0(100) $[C_7H_7Ge]^+$, 91.1(53) $[C_7H_7]^+$. 15 ($t_R$ = 9.61 min): *m*/*z*(%) = 282.1(3) $[M]^+$, 166.0(19) $[C_7H_7GeH]^+$, 73.1(100) $[Me_3Si]^+$. *i*-$Bu_2$(*p*-tolyl)GeH ($t_R$ = 9.73 min): *m*/*z*(%) = 280.1(<1) $[M]^+$, 223.1(18) [M – $C_4H_9$]$^+$, 167.0(100) $[C_7H_7GeH_2]^+$, 91.1(21) $[C_7H_7]^+$.

phenyl(*p*-tolyl)$GeH_2$ ($t_R$ = 10.02 min): *m*/*z*(%) = 244.1(56) $[M]^+$, 165.0(99) $[C_7H_7Ge]^+$, 151.0(100) $[C_6H_5Ge]^+$, 91.1(100) $[C_7H_7]^+$. *p*-tolyl$_2GeH_2$ ($t_R$ = 10.63 min): *m*/*z*(%) = 257(28) $[M - H]^+$, 166(100) $[C_7H_7GeH]^+$, 91.1(99) $[C_7H_7]^+$. TBDMSGe(*i*-Bu, *p*-tolyl)H ($t_R$ = 10.92 min): *m*/*z*(%) = 338.2(6) $[M]^+$, 222.1(98) $[M - TBDMSH]^+$, 165(100) $[C_7H_7Ge]^+$, 73.1(96) $[Me_3Si]^+$. Me(*p*-tolyl$_2$)GeH ($t_R$ = 10.96 min): *m*/*z*(%) = 271.1(15) $[M - H]^+$, 257.1(100) $[M - CH_3]^+$, 180(61) $[M - C_7H_8]^+$, 165(78) $[C_7H_7Ge]$. TBDMSGe(phenyl, *p*-tolyl)H ($t_R$ = 12.64 min): *m*/*z*(%) 358.2(5) $[M]^+$, 280.0(1) $[M - C_6H_6]^+$, 242.0(100) $[M - TBDMSH]^+$, 167.1(20) $[C_7H_7GeH_2]^+$, 73.1(45) $[Me_3Si]^+$. phenyl$_2$(*p*-tolyl)GeH ($t_R$ = 13.08 min): *m*/*z*(%) = 319.1(20) $[M - H]^+$, 242.0(80) $[M - C_6H_6]^+$, 228(100) $[M - C_7H_8]^+$, 167.1(50) $[C_7H_7GeH_2]^+$, 151(53) $[C_6H_5Ge]^+$. *p*-tolyl$_3$GeH ($t_R$ = 13.98 min): *m*/*z*(%) = 347.1(15) $[M - H]^+$, 256.1(100) $[M - C_7H_8]^+$, 165.0(42) $[C_7H_7Ge]^+$, 91.1(32) $[C_7H_7]^+$.

<u>Ar = *o*-tolyl:</u> **3** ($t_R$ = 5.33): *m*/*z*(%) = 166(58) $[M]^+$, 150.9(9) $[M - CH_3]^+$, 91.1(100) $[C_7H_7]^+$. *n*-Bu(*o*-tolyl)$GeH_2$ ($t_R$ = 8.38 min): *m*/*z*(%) = 224.1(11) $[M]^+$, 165.0(100) $[C_7H_7Ge]^+$, 91.1(56) $[C_7H_7]^+$. *t*-Bu($C_2H_5$, *o*-tolyl)GeH ($t_R$ = 8.76 min): *m*/*z*(%) = 252.1(4) $[M]^+$, 193.0(21) $[C_9H_{11}Ge]^+$, 119.1(100) $[C_9H_{11}]^+$. *n*-Bu($C_2H_5$, *o*-tolyl)GeH ($t_R$ = 9.28 min): *m*/*z*(%) = 252.1(6) $[M]^+$, 195.0(14) $[M - C_4H_9]^+$, 165.0(3) $[C_7H_7Ge]^+$, 119.1(100) $[C_9H_{11}]^+$. TBDMSGe(*o*-tolyl)$H_2$ ($t_R$ = 9.69 min): *m*/*z*(%) = 282.1(4) $[M]^+$, 165.0(16) $[C_7H_7Ge]^+$, 115.1(19) $[TBDMS]^+$, 73.1(100) $[Me_3Si]^+$. *n*-Bu$_2$(*o*-tolyl)GeH ($t_R$ = 10.22 min): *m*/*z*(%) = 280.0(3) $[M]^+$, 223.1(28) $[M - C_4H_9]^+$, 167.0(100) $[C_7H_9]^+$, 91.1(33) $[C_7H_7]$. *o*-tolyl$_2GeH_2$ ($t_R$ = 10.58 min): *m*/*z*(%) = 258.1(24) $[M]^+$, 166.0(96) $[C_7H_8]^+$, 91.1(100) $[C_7H_7]^+$. *o*-tolyl$_2$($C_2H_5$)GeH ($t_R$ = 11.30 min): *m*/*z*(%) = 286.1(11) $[M]^+$, 194.0(6) $[C_9H_{12}Ge]^+$, 165.0(17) $[C_7H_7Ge]^+$, 119.1(100) $[C_9H_{11}]$, 91.1(31) $[C_7H_7]^+$.

<u>Ar = 2,6-xylyl:</u> **5** ($t_R$ = 6.59 min): *m*/*z*(%) = 180.0(34) $[M]^+$, 165.0(9) $[M - CH_3]^+$, 107.1(100) $[C_8H_{11}]^+$. Me(2,6-xylyl)$GeH_2$ ($t_R$ = 7.22 min): *m*/*z*(%) = 196(29) $[M]^+$, 179.0(100) $[C_8H_9Ge]^+$, 105.1(42) $[C_8H_9]^+$. $Me_2$(2,6-xylyl)$GeH_2$ ($t_R$ = 7.73 min): *m*/*z*(%) = 210.1(22) $[M]^+$, 195.0(100) $[M - CH_3]^+$, 178.9(15) $[C_8H_9Ge]^+$, 105.0(37) $[C_8H_9]^+$. *t*-Bu(2,6-xylyl)$GeH_2$ ($t_R$ = 8.62 min): *m*/*z*(%) = 238.1(10) $[M]^+$, 179.0(100) $[C_8H_9Ge]^+$, 105.1(56) $[C_8H_9]^+$. *n*-Bu(2,6-xylyl)$GeH_2$ ($t_R$ = 9.15 min): *m*/*z*(%) = 238.1(13) $[M]^+$, 179(100) $[C_8H_9Ge]^+$, 105.1(38) $[C_8H_9]^+$. TBDMSGe(2,6-xylyl)$H_2$ ($t_R$ = 10.40 min): *m*/*z*(%) = 296.1(4) $[M]^+$, 178.9(18) $[C_8H_9Ge]^+$, 73.1(100) $[Me_3Si]^+$. TBDMSGe(Me, 2,6-xylyl)$H_2$ ($t_R$ = 10.71 min): *m*/*z*(%) = 308.2(5) $[M]^+$, 194.0(64)

[M – TBDMSH]$^+$, 179.0(87) [$C_8H_9Ge$]$^+$, 73.1(100) [$Me_3Si$]$^+$. 2,6-xylyl$_2$GeH$_2$ ($t_R$ = 11.81 min): *m*/*z*(%) = 286.1(24) [M]$^+$, 180.0(100) [$C_8H_9GeH$]$^+$, 105.1(98) [$C_8H_9$]$^+$.

Ar = mesityl: **7** ($t_R$ = 7.40 min): *m*/*z*(%) = 194.1(23) [M]$^+$, 179.0(7) [M – $CH_3$]$^+$, 121.1(100) [$C_9H_{13}$]$^+$. Me(mesityl)GeH$_2$ ($t_R$ = 7.97 min): *m*/*z*(%) = 210.1(8) [M]$^+$, 193.0(28) [$C_9H_{11}Ge$]$^+$, 121.1(12) [$C_9H_{13}$]$^+$. TBDMSGe(mesityl)H$_2$ ($t_R$ = 10.90 min): *m*/*z*(%) = 310.1(4) [M]$^+$, 253.0(2) [M – $C_4H_9$]$^+$, 194(46) [$C_9H_{12}Ge$]$^+$, 73.1(100) [$Me_3Si$]$^+$. TBDMSGe(Me, mesityl)H $t_R$ = 11.16 min): *m*/*z*(%) = 324.1(6) [M]$^+$, 208.1(57) [$C_{10}H_{14}Ge$]$^+$, 193.0(100) [$C_9H_{11}Ge$]$^+$, 73.1(100) [$Me_3Si$]$^+$:

**Table 10:** List of screening reactions

| Nr. | $ArGeH_3$ | Base (amount) | Solvent (volume) |
|---|---|---|---|
| **S1** | ***4*** (3.4 mmol) | *i*-BuLi (1.7 M, 2 mL, 3.4 mmol) | Pentane (4 mL) |
| **S2** | ***4*** (3.1 mmol) | *sec*-BuLi (1.3 M, 2.4 mL, 3.1 mmol) | Pentane (4 mL) |
| **S3** | ***4*** (3.6 mmol) | MeLi (1.6 M, 2.4 mL, 3.8 mmol) | $Et_2O$ (5 mL) |
| **S4** | ***4*** (3.7 mmol) | *i*-BuLi (1.7 M, 2.2 mL, 3.7 mmol) | $Et_2O$ (5 mL) |
| **S5** | ***4*** (2.7 mmol) | *sec*-BuLi (1.3 M, 2.1 mL, 2.7 mmol) | $Et_2O$ (4 mL) |
| **S6** | ***4*** (3.5 mmol) | PhLi (1.9 M, 2.0 mL, 3.6 mmol) | $Et_2O$ (4 mL) |
| **S7** | ***4*** (3.6 mmol) | MeLi (1.6 M, 2.4 mL, 3.8 mmol) | THF (5 mL) |
| **S8** | ***4*** (3.7 mmol) | *i*-BuLi (1.7 M, 2.2 mL, 3.7 mmol) | THF (5 mL) |
| **S9** | ***4*** (3.7 mmol) | *sec*-BuLi (1.3 M, 2.8 mL, 3.6 mmol) | THF (5 mL) |
| **S10** | ***4*** (3.5 mmol) | PhLi (1.9 M, 2.0 mL, 3.8 mmol) | THF (4 mL) |
| **S11** | ***3*** (2.65 mmol) | *n*-BuLi (2.5 M, 1.2 mL, 3.00 mmol) | $Et_2O$ (4 mL) |
| **S12** | ***3*** (2.03 mmol) | *t*-BuLi (1.9 M, 1.2 mL, 2.28 mmol) | $Et_2O$ (3 mL) |
| **S13** | **6** (2.08 mmol) | MeLi (1.6 M, 1.4 mL, 2.24 mmol) | Pentane (4 mL) |
| **S14** | **6** (1.64 mmol) | *n*-BuLi (1.6 M, 0.7 mL, 1.12 mmol + 2.5 M, 0.5 mL, 1.25 mmol; total: 1.2 mL, 2.37 mmol) | Pentane (4 mL) |
| **S15** | **6** (1.87 mmol) | *t*-BuLi (1.9 M, 1 mL, 1.90 mmol) | Pentane (4 mL) |
| **S16** | **6** (1.74 mmol) | MeLi (1.6 M, 1.2 mL, 1.92 mmol) | $Et_2O$ (4 mL) |
| **S17** | **6** (2.88 mmol) | *n*-BuLi (1.6 M, 1.4 mL, 2.24 mmol + 2.5 M, 0.3 mL, 0.6 mmol; total. 1.7 mL, 2.84 mmol) | $Et_2O$ (4 mL) |
| **S18** | **6** (6.35 mmol) | *n*-BuLi (2.5 M, 2.6 mL, 6.50 mmol) | $Et_2O$ (5 mL) |
| **S19** | **6** (1.62 mmol) | *t*-BuLi (1.9 M, 0.9 mL, 1.71 mmol) | $Et_2O$ (3 mL) |
| **S20** | **6** (6.64 mmol) | *t*-BuLi (1.9 M, 3.6 mL, 6.84 mmol) | $Et_2O$ (5 mL) |
| **S21** | **6** (1.93 mmol) | MeLi (1.6 M, 1.4 mL 2.24 mmol) | THF (4 mL) |
| **S22** | **6** (1.84 mmol) | *n*-BuLi (2.5 M, 0.8 mL, 2.00 mmol) | THF (4 mL) |
| **S23** | **6** (2.78 mmol) | *t*-BuLi (1.9 M, 2.0 mL, 3.80 mmol) | THF (5 mL) |
| **S24** | **7** (1.63 mmol) | MeLi (1.6 M, 1.1 mL, 1.76 mmol) | $Et_2O$ (4 mL) |
| **S25** | **7** (1.67 mmol) | MeLi (1.6 M, 1.2 mL, 1.92 mmol) | THF (4 mL) |

**Table 11:** Relative GC area [%] for germanium containing products of screening reactions. Germanium free compounds omitted.

| Nr. | ArG | R(Ar)$GeH_2$ | TBDMSGe(Ar)$H_2$ | $R_2$ArGe | TBDMSGe(R, | $Ar_2GeH_2$ | Other Ge |
|---|---|---|---|---|---|---|---|
| **S1** | 12 | 7 | 26 | <1 | <1 | <1 | 4 |
| **S2** | 0 | 59 | 30 | 0 | 0 | 0 | 0 |
| **S3** | <1 | 55 | 0 | 26 | 0 | 0 | 0 |
| **S4** | 0 | 52 | 2 | 32 | 4 | 0 | 4 |
| **S5** | 5 | 64 | 24 | 0 | 0 | 0 | 0 |
| **S6** | 0 | 52 | 4 | 14 | 17 | 0 | 0 |
| **S7** | <1 | 42 | <1 | 9 | 0 | <1 | 2 |
| **S8** | 3 | 45 | 30 | 11 | 2 | 0 | 1 |
| **S9** | 3 | 20 | 71 | 0 | 0 | 0 | 0 |
| **S10** | <1 | 24 | 42 | 0 | 0 | 0 | 0 |
| **S11** | 0 | 79 | 7 | 1 | 0 | 0 | 2 |
| **S12** | 12 | 10 | 22 | 0 | 0 | 5 | 18* |
| **S13** | 2 | 22 | <1 | 2 | 0 | 0 | <1 |
| **S14** | 0 | 5 | 83 | 0 | 0 | 0 | 0 |
| **S15** | 8 | 8 | 15 | 0 | 0 | 6 | 3 |
| **S16** | 0 | 9 | 12 | 2 | 3 | 2 | <1 |
| **S17** | 38 | 0 | 0 | 0 | 0 | <1 | 2 |
| **S18** | 2 | 8 | 64 | 0 | 0 | 10 | 0 |
| **S19** | 38 | 0 | 0 | 0 | 0 | 3 | 1 |
| **S20** | 28 | 0 | 13 | 0 | 0 | 36 | 0 |
| **S21** | 2 | 0 | 90 | 0 | 0 | 0 | 0 |
| **S22** | 6 | 0 | 86 | 0 | 0 | 0 | 0 |
| **S23** | <1 | 0 | 100 | 0 | 0 | 0 | 0 |
| **S24** | 46 | 11 | 3 | 0 | 0 | 0 | 0 |
| **S25** | 3 | 0 | 67 | 0 | 4 | 0 | 0 |

*Very high number of “Other Ge” in **S12** due to *t*-Bu($C_2H_5$)$GeH_2$ (1%), *t*-Bu($C_2H_5$, *o*-tolyl)GeH (10%), *o*-tolyl$_2$($C_2H_5$)GeH (5%). The origin and position of the two additional carbon atoms is not clear. They are also present in much lower amounts in **S11**.

### 5.3.4 Nanoparticle Preparation

Ge@Ar *via* Microwave

For these experiments, a Microwave Synthesis Reactor Monowave 300 from Anton Paar was used. A microwave vial (10 mL) was charged with Ar$GeH_3$, solvent and, if specified, TMEDA. The vial was closed with a sealed cap and put into the microwave. The vial was heated to the target temperature as fast as possible, held there for the

indicated time, then cooled to 50 °C before being automatically vented to the atmosphere. The contents of the microwave vial were transferred into a Schlenk flask with a Pasteur pipette, and the vial was washed once with the solvent used for the reaction (5 mL). Then all volatiles were removed under vacuum (50 °C, 0.5 mbar) and collected in a separate flask for supernatant analysis. The colored residue was transferred into a glovebox for storage. Due to cleavage of varying amounts of aryl groups and the resulting non-stoichiometric material, yields are given as product weight divided by precursor weight. Calculated EA values are not provided for the same reason.

Ge@*o*-tolyl (microwave) (**25**):

**25a**: **3** (0.18 g, 1.1 mmol), dry DME (2 mL). 250 °C, 10 min. Yield: 0.010 g (5.6% w/w) of orange powder.

**25b**: **3** (0.16 g, 0.959 mmol), dry DME (1.5 mL), TMEDA (0.111 g, 0.959 mmol). 250 °C, 10 min. Yield: 0.016 g (10% w/w) of orange powder.

**25c**: **3** (0.192 g, 1.15 mmol), dry DME (2 mL), TMEDA (0.16 g, 1.3 mmol). 250 °C, 30 min. Yield: 0.031 g (16% w/w) of orange powder.

**25d**: **3** (0.450 g, 2.70 mmol), dry DME (4 mL), TMEDA (0.31 g, 2.7 mmol). 250 °C, 3x15 min. Yield: 0.100 g (22% w/w) of red powder.

**25e**: **3** (0.423 g, 1.54 mmol), dry DME (4 mL), TMEDA (0.31 g, 2.7 mmol). 260 °C, 2x15 min. Yield: 0.151 g (36% w/w) of red/brown powder.

**25f**: **3** (0.435 g, 2.61 mmol), dry toluene (4 mL), TMEDA (0.31 g, 2.7 mmol). ≤265 °C, 4x15 min. Yield: 0.242 g (56% w/w). EA found: C: 34.07%; H: 3.09% of red/brown powder.

**25g**: **3** (0.426 g, 2.55 mmol), dry diglyme (4 mL), TMEDA (0.31 g, 2.7 mmol). 270 °C, 2x15 min. Yield: 0.327 g (77% w/w) of black powder. EA found: C: 28.96%, H: 2.89%.

**25h**: **3**(0.418 g, 2.51 mmol), dry diglyme (4 mL), TMEDA (0.31 g, 2.7 mmol). 240 °C, 4x20 min. 0.290 g (69% w/w) of black powder. EA found: C: 29.47%, H: 3.04%.

**25i**: **3**(0.485 g, 2.88 mmol), dry diglyme (4 mL), TMEDA (0.31 g, 2.7 mmol). 300 °C, 2x10 min. Yield: 0.208 g (42% w/w) of black powder. EA found: C: 25.31%, H: 2.65%.

Ge@mesityl (microwave) (**26**):

**26a**: **7** (0.39 g, 2.0 mmol), dry diglyme (2.7 mL), TMEDA (0.23 g, 2.0 mmol). 270 °C, 2x15 min. Yield: 0.180 g (46%) of black powder. EA found: C: 14.56%, H: 2.53%.

**26b**: **7** (0.52 g, 2.7 mmol), dry diglyme (3.6 mL), TMEDA (0.31 g, 2.7 mmol). 210 °C, 2x15 min. Yield: 0.049 g (9.4%) of orange liquid.

Ge@Ar *via* reflux

A Schlenk tube was charged with $ArGeH_3$ and dry diglyme. If TMEDA was used, the volume of diglyme was reduced by the same amount to keep $ArGeH_3$ concentration consistent. An oil bath was pre-heated to 180 °C, then the Schlenk tube was submerged in it to start the reflux. The reaction was heated for the indicated time, after which the oil bath was removed. The flask was allowed to cool down a bit, then volatiles were removed under reduced pressure (50 °C, 0.5 mbar) and collected in a separate flask for supernatant analysis. The colored residue was transferred into a glovebox for storage. Due to cleavage of varying amounts of aryl groups and the resulting non-stoichiometric material, yields are given as product weight divided by precursor weight. Calculated EA values are not provided for the same reason.

Ge@*o*-tolyl (reflux) (**27**):

**27a**: **3** (0.44 g, 2.6 mmol), dry diglyme (3.6 mL), TMEDA (0.31 g, 2.7 mmol), 24 h. Yield: 211 mg (48% w/w) of orange powder. EA found: C: 36.92%, H: 3.73%.

**27b**: **3** (0.44 g, 2.6 mmol), dry diglyme (3.6 mL), TMEDA (0.31 g, 2.7 mmol), 70 h. Yield: 330 mg (75% w/w) of red powder. EA found: C: 35.70%, H: 3.70%.

**27c**: **3** (0.44 g, 2.6 mmol), dry diglyme (4 mL), 24 h. Yield: 83 mg (19% w/w) of orange powder. EA found: C: 39.27%, H: 4.08%.

**27d**: **3** (0.44 g, 2.6 mmol), dry diglyme (4 mL), 92 h. Yield: 260 mg (59% w/w) of brown powder. EA found: C: 33.63%, H: 3.18%.

**27e**: **3** (2.44 g, 14.6 mmol), dry diglyme (18 mL), TMEDA (1.54 g, 13.3 mL). Aliquots (1 mL) removed after 0 h (**27e$_0$**), 4 h (**27e$_4$**), 6 h (**27e$_6$**), 12 h (**27e$_{12}$**), 24 h (**27e$_{24}$**), 48 h (**27e$_{48}$**), 72 h (**27e$_{72}$**) and 120 h (**27e$_{120}$**). Volatiles were removed from each aliquot (30 °C, 0.1 mbar), after which the material was left as film on the flask walls ranging from pale yellow (**27e$_0$**) to deep red (**27e$_{120}$**) in color. A yield was not determined. EA$_{\mathbf{27e120}}$ found: C: 39.4%, H: 3.83%.

**27f**: **12** (0.44 g, 2.6 mmol), dry diglyme (3.6 mL), TMEDA (0.31 g, 2.7 mmol), 24 h. Yield: 234 mg (53% w/w) of orange powder. EA found: C: 37.96%, H: 3.74%.

**27g**: **3** (0.44 g, 2.6 mmol), dry diglyme (3.6 mL), TMEDA (0.31 g, 2.7 mmol), 8 h. Yield: 78 mg (18% w/w) of sticky yellow film on the flask walls.

Ge@2,6-xylyl (reflux) (**28**):

**28a**: **5** (0.421 mg, 2.33 mmol), dry diglyme (3.6 mL), TMEDA (0.31 g, 2.7 mmol), 92 h. Yield: 249 mg (59% w/w) of brown powder. EA found: C: 34.03%, H: 3.39%.

**28a**: **5** (435 mg, 2.41 mmol), dry diglyme (4 mL), 94 h. Yield: 93 mg (21% w/w) of black flakes.

Ge@mesityl (reflux) (**29**):

**29a**: **7** (0.52 g, 2.7 mmol), dry diglyme (3.6 mL), TMEDA (0.31 g, 2.7 mmol) 94 h. Yield: 283 mg (54% w/w) of brown powder. EA found: C: 37.18%, H: 4.51%.

**29b**: **7** (0.52 g, 2.7 mmol), dry diglyme (4 mL), 92 h. Yield: 54 mg (10% w/w) of black flakes. EA found: C: 28.7%, H: 3.83%.

**29c**: **7** (0.52 g, 2.7 mmol), dry diglyme (4 mL), TMEDA (0.31 g, 2.7 mmol) 24 h. Yield: Small amounts of brown liquid, weight not determined.

**29d**: **7** (0.52 g, 2.7 mmol), dry diglyme (4 mL), 192 h. Yield: 116 mg (22% w/w) of black powder. EA found: C: 25.2%, H: 3.35%.

Ge@*n*-butyl (**30**)

Attempt 1: Reflux: **8** (0.41 g, 3.1 mmol), dry diglyme (3.6 mL), TMEDA (0.31 g, 2.7 mmol), 24 h. No product obtained.

Attempt 2: Reflux: **8** (0.41 g, 3.1 mmol), dry diglyme (3.6 mL), TMEDA (0.31 g, 2.7 mmol), 72 h. No product obtained.

Attempt 3: Carius tube: **8** (0.41 g, 3.1 mmol), dry diglyme (3.6 mL), TMEDA (0.31 g, 2.7 mmol). 180 °C, 16 h. Yield: Orange material intermixed with O-ring plastic. Weight not determined.

Ge@TBDMS (**31**)

**21** (0.23 g, 1.20 mmol) was mixed with dry diglyme (2 mL) and TMEDA (0.16 g, 1.34 mmol) in a Schlenk flask with a reflux condenser and an overpressure bubbler (+0.1 bar). The mixture was heated to 120 °C for 3 h. At this point the reaction was stopped, because brown solids had begun precipitating. After the flask had cooled down again, volatiles were removed (room temperature, 0.1 mbar) leaving behind small amounts of brown powder. The collected volatile fraction was further concentrated for GC/MS analysis under vacuum (room temperature, 1.2 mbar).

Supernatant: MS (EI, 70 eV): *m*/*z*(%) = 378.1(0.1) $[M - 2\ H_2]^+$ (calcd. for $C_{12}H_{30}Ge_2Si_2$ 378.03), 190.0(9) $[TBDMSGeH]^+$, 115.1(11) $[TBDMS]^+$, 73.1(100) $[Me_3Si]^+$.

Ge@DTBMS (**32**)

**22** (0.100 g, 0.429 mmol) was mixed with dry diglyme (2 mL) and TMEDA (0.16 g, 1.3 mmol) in a Schlenk flask with a reflux condenser and an overpressure bubbler (+0.1 bar). The mixture was heated to 110 °C. A yellow color was noticeable within 1 h. After 3 h of heating, the mixture was a deep orange and solids had started precipitating. Heating was stopped and the flask left to cool down. Volatiles were then removed under reduced pressure (room temperature, 1 mbar), leaving behind small amounts of orange solids.

### 5.3.5 Nanoparticle modification

$H_2O_2$ etching of Ge@*o*-tolyl

A Schlenk tube was charged with **27e$_{120}$** (0.160 mg). $H_2O_2$ (0.165 mL, 30% w/w in $H_2O$, 1.61 mmol) was added, and the reaction was stirred for 90 min. The solution turned from red to orange over the duration. At this point the reaction was diluted with degassed $H_2O$ (2 mL), which caused precipitation of red powder, and stirred overnight. The powder had redissolved in the morning and the color of the solution had changed to yellow. The solvents were removed under vacuum and the solids resuspended in dry THF. The solution was filtrated through a cannula and THF was evaporated under reduced pressure to yield 98 mg of pale yellow powder.

Functionalization of Ge@*o*-tolyl with 3-chloro-1-propene (**33**)

A Schlenk flask was charged with dry THF (10 mL) and **27a** (0.05 g, 0.3 mmol). 3-chloro-1-propene (93 mg, 1.2 mmol) and AIBN (8 mg) where added and the reaction was refluxed overnight. Then the volatiles were removed under vacuum (room temperature, 0.1 mbar) to yield 32 mg of orange powder.

Annealing of Ge@*o*-tolyl

A sample of **27a** (40 mg) was transferred into a ceramic dish. The ceramic dish was put into a glass tube under nitrogen, which was put into a tube furnace (Carbolite GHA 12/600). The sample was heated to a temperature of 220 °C, 240 °C or 500 °C for 4 hours. After cooling back down to room temperature, the sample was transferred into a Schlenk tube and evacuated (room temperature, 0.01 mbar) to remove any potential degradation products.

# References


[1] R. P. Feynmann, *Caltech Engineering and Science* **1960**, *23*, 22.

[2] a) D. Guo, G. Xie, J. Luo, *J. Phys. D: Appl. Phys.* **2014**, *47*, 13001; b) I. Khan, K. Saeed, I. Khan, *Arabian J. Chem.* **2019**, *12*, 908; c) G. Schmid (Ed.) *Nanoparticles*. *From Theory to Application*, Wiley-VCH, Weinheim, **2006**; d) S. Horikoshi, N. Serpone in *Horikoshi, Serpone (Hg.) 2013 – Microwaves in Nanoparticle Synthesis*, pp. 1–24; e) K. Manojkumar, A. Sivaramakrishna, K. Vijayakrishna, *J. Nanopart. Res.* **2016**, *18*, 15.

[3] W. J. Stark, P. R. Stoessel, W. Wohlleben, A. Hafner, *Chem. Soc. Rev.* **2015**, *44*, 5793.

[4] a) H. Abbasinia, M. Heshmati, M. Yousefi, N. Najjar, H. Sadeghi, *ACS Appl. Bio Mater.* **2023**, *6*, 3768; b) I. B. Belyaev, I. V. Zelepukin, P. A. Kotelnikova, G. V. Tikhonowski, A. A. Popov, A. Y. Kapitannikova, J. Barman, A. N. Kopylov, D. N. Bratashov, E. S. Prikhozhdenko et al., *Adv. Sci. (Weinheim, Ger.)* **2024**, *11*, e2307060; c) S. Deb-Choudhury, S. Prabakar, G. Krsinic, J. M. Dyer, R. D. Tilley, *J. Agric. Food Chem.* **2013**, *61*, 7188; d) P. Dhakate, N. Kandhol, G. Raturi, P. Ray, A. Bhardwaj, A. Srivastava, L. Kaushal, A. Singh, S. Pandey, D. K. Chauhan et al., *Chemosphere* **2022**, *305*, 135165; e) K. A. S. Fernando, S. Sahu, Y. Liu, W. K. Lewis, E. A. Guliants, A. Jafariyan, P. Wang, C. E. Bunker, Y.-P. Sun, *ACS Appl. Mater. Interfaces* **2015**, *7*, 8363; f) F. Lin, M. Jia, Z. Sun, Z. Fu, *Scr. Mater.* **2020**, *186*, 298; g) A. M. Parambil, S. Rajan, P.-C. Huang, U. Shashikumar, P.-C. Tsai, P. Rajamani, Y.-C. Lin, V. K. Ponnusamy, *Environ. Res.* **2024**, *251*, 118541; h) A. Ratnadass, A. L. Llandres, F.-R. Goebel, O. Husson, J. Jean, A. Napoli, M. Sester, S. Joseph, *Sci. Total. Environ.* **2024**, *910*, 168545; i) S. A. A. Shah, M. H. Sayyad, J. Sun, Z. Guo, *J. Rare Earths* **2022**, *40*, 1651; j) V. Slynchuk, C. Schedel, M. Scheele, A. Schnepf, *Int. J. Mol. Sci.* **2023**, *24*; k) F. Wang, Y. Zhang, H. Li, W. Gong, J. Han, S. Jiang, D. Li, Z. Yao, *Food Chem.* **2025**, *463*, 141122; l) Y. Xu, P. Li, D. Cheng, C. Wu, Q. Lu, W. Yang, X. Zhu, P. Yin, M. Liu, H. Li et al., *J. Mater. Chem. B* **2020**, *8*, 10290.

[5] J. Hu, Q. Lu, C. Wu, M. Liu, H. Li, Y. Zhang, S. Yao, *Talanta* **2019**, *195*, 407.

[6] M. Vörös, S. Wippermann, B. Somogyi, A. Gali, D. Rocca, G. Galli, G. T. Zimanyi, *J. Mater. Chem. A* **2014**, *2*, 9820.

[7] S. Wu, C. Han, J. Iocozzia, M. Lu, R. Ge, R. Xu, Z. Lin, *Angew. Chem. Int. Ed. Engl.* **2016**, *55*, 7898.

[8] A. Khan, R. A. Gossage, D. A. Foucher, *Can. J. Chem.* **2010**, *88*, 1046.

[9] M.-L. Lechner, M. Trummer, I. Bräunlich, P. Smith, W. Caseri, F. Uhlig, *Appl. Organomet. Chem.* **2011**, *25*, 769.

[10] C. Zeppek, *Doctoral Thesis*, Graz University of Technology, Graz, **2015**.

[11] a) C. R. Dillard, E. H. McNeill, D. E. Simmons, J. B. Yeldell, *J. Am. Chem. Soc.* **1958**, *80*, 3607; b) C. Zeppek, R. C. Fischer, A. Torvisco, F. Uhlig, *Can. J. Chem.* **2014**, *92*, 556.

[12] C. Winkler, *J. Prakt. Chem.* **1887**, *36*, 177.

[13] G. T. Morgan, H. D. K. Drew, *J. Chem. Soc., Trans.* **1925**, *127*, 1760.

[14] D. L. Tabern, W. R. Orndorff, L. M. Dennis, *J. Am. Chem. Soc.* **1925**, *47*, 2039.

[15] W. R. Orndorff, D. L. Tabern, L. M. Dennis, *J. Am. Chem. Soc.* **1927**, *49*, 2512.

[16] C. A. Kraus, L. S. Foster, *J. Am. Chem. Soc.* **1927**, *49*, 457.

[17] C. A. Kraus, C. L. Brown, *J. Am. Chem. Soc.* **1930**, *52*, 4031.

[18] a) R. Schwarz, M. Lewinsohn, *Ber. dtsch. Chem. Ges. A/B* **1931**, *64*, 2352; b) R. Schwarz, W. Reinhardt, *Ber. dtsch. Chem. Ges. A/B* **1932**, *65*, 1743.

[19] H. Oikawa, *Nippon Kagaku Zasshi* **1963**, *84*, 453-458,A31.

[20] a) W. C. Butterman, J. D. Jorgenson, *Open-File Report* **2005**; b) "Germanium(IV) bromide. SDS", can be found under https://assets.thermofisher.com/DirectWebViewer/private/document.aspx?prd=ALFAA40219~~PDF~~MTR~~AGHS~~EN~~2024-03-30%2013:02:04~~Germanium(IV, **2024**.

[21] M. A. Chaubon, B. Dittrich, J. Escudié, H. Ramdane, H. Ranaivonjatovo, J. Satgé, *Synth. React. Inorg. Met.-Org. Chem.* **1997**, *27*, 519.

[22] J. K. Simons, E. C. Wagner, J. H. Müller, *J. Am. Chem. Soc.* **1933**, *55*, 3705.

[23] H. Bauer, K. Burschkies, *Ber. dtsch. Chem. Ges. A/B* **1932**, *65*, 956.

[24] M. Dakkouri, H. Kehrer, *Chem. Ber.* **1983**, *116*, 2041.

[25] K. Kühlein, W. P. Neumann, *Justus Liebigs Ann. Chem.* **1967**, *702*, 17.

[26] C. A. Kraus, C. L. Brown, *J. Am. Chem. Soc.* **1930**, *52*, 3690.

[27] a) M. Wolf, A. Falk, M. Flock, A. Torvisco, F. Uhlig, *J. Organomet. Chem.* **2017**, *851*, 143; b) P. Jutzi, B. Hielscher, *Organometallics* **1986**, *5*, 1201.

[28] A. Torvisco, M. Wolf, M. Traxler, D. Gudat, F. Uhlig, *Mendeleev Commun.* **2022**, *32*, 22.

[29] M. L. Amadoruge, E. K. Short, C. Moore, A. L. Rheingold, C. S. Weinert, *J. Organomet. Chem.* **2010**, *695*, 1813.

[30] a) H. Tanimoto, T. Nagao, Y. Nishiyama, T. Morimoto, F. Iseda, Y. Nagato, T. Suzuka, K. Tsutsumi, K. Kakiuchi, *Dalton Trans.* **2014**, *43*, 8338; b) O. G. Yarosh, *Russ. J. Gen. Chem.* **2002**, *72*, 1901; c) B. Wrackmeyer, S. Bayer, W. Milius, E. V. Klimkina, *J. Organomet. Chem.* **2018**, *865*, 80.

[31] J. Park, S. A. Batcheller, S. Masamune, *J. Organomet. Chem.* **1989**, *367*, 39.

[32] a) K. V. Zaitsev, A. A. Kapranov, Y. F. Oprunenko, A. V. Churakov, J. A. Howard, B. N. Tarasevich, S. S. Karlov, G. S. Zaitseva, *J. Organomet. Chem.* **2012**, *700*, 207; b) S. Pelzer, B. Neumann, H.-G. Stammler, N. Ignat'ev, B. Hoge, *Chemistry* **2016**, *22*, 4758; c) V. V. Bardin, *J. Organomet. Chem.* **2016**, *822*, 46; d) S. N. Bhattacharya, P. Raj, R. C. Srivastava, *J. Organomet. Chem.* **1976**, *105*, 45.

[33] F. Riedmiller, G. L. Wegner, A. Jockisch, H. Schmidbaur, *Organometallics* **1999**, *18*, 4317.

[34] A. Sekiguchi, H. Naito, C. Kabuto, H. Sakurai, *Nippon Kagaku Kaishi* **1994**, 248.

[35] Y. Inagaki, K. Yamaguchi, W. Setaka, *RSC Adv.* **2014**, *4*, 58624.

[36] S. P. Komanduri, F. A. Shumaker, K. D. Roewe, M. Wolf, F. Uhlig, C. E. Moore, A. L. Rheingold, C. S. Weinert, *Organometallics* **2016**, *35*, 3240.

[37] K. A. Kozeschkow, *Ber. dtsch. Chem. Ges. A/B* **1929**, *62*, 996.

[38] F. Rijkens, G. J. M. van der Kerk, *Recl. Trav. Chim. Pays-Bas* **1964**, *83*, 723.

[39] a) G. J. M. van der Kerk, F. Rijkens, M. J. Janssen, *Recl. Trav. Chim. Pays-Bas* **1962**, *81*, 764; b) R. Laurent, A. Laporterie, J. Dubac, J. Berlan, *Organometallics* **1994**, *13*, 2493.

[40] J. G. A. Luijten, F. Rijkens, *Recl. Trav. Chim. Pays-Bas* **1964**, *83*, 857.

[41] a) V. I. Zhun', I. V. Sbitneva, E. A. Chernyshev, *Russ. J. Gen. Chem.* **2005**, *75*, 867; b) K. M. Baines, K. A. Mueller, T. K. Sham, *Can. J. Chem.* **1992**, *70*, 2884.

[42] a) C. Janiak, M. Schwichtenberg, F. Ekkehardt Hahn, *J. Organomet. Chem.* **1989**, *365*, 37; b) P. T. Matsunaga, J. Kouvetakis, T. L. Groy, *Inorg. Chem.*

**1995**, *34*, 5103; c) O. M. Nefedov, S. P. Kolesnikov, V. I. Sheichenko, *Angew. Chem. Int. Ed. Engl.* **1964**, *3*, 508.

[43] E. G. Rochow, *J. Am. Chem. Soc.* **1947**, *69*, 1729.

[44] a) P. S. Poskozim, *J. Organomet. Chem.* **1968**, *12*, 115; b) L. Horvitz, E. A. Flood, *J. Am. Chem. Soc.* **1933**, *55*, 5055.

[45] N. N. Greenwood, *Chemistry of the Elements*, Elsevier-Butterworth-Heinemann, Amsterdam, **2010**.

[46] a) E. A. Roth, H. Gossenberger, J. A. Amick, *RCA Rev.* **1963**, *24*, 499; b) R. Venkatasubramanian, R. T. Pickett, M. L. Timmons, *J. Appl. Phys. (Melville, NY, U. S.)* **1989**, *66*, 5662; c) J. E. Ayers, S. K. Ghandhi, *J. Cryst. Growth* **1988**, *89*, 371.

[47] a) E. Woelk, D. V. Shenai-Khatkhate, R. L. DiCarlo, A. Amamchyan, M. B. Power, B. Lamare, G. Beaudoin, I. Sagnes, *J. Cryst. Growth* **2006**, *287*, 684; b) Y. Inuzuka, S. Ike, T. Asano, W. Takeuchi, O. Nakatsuka, S. Zaima, *Thin Solid Films* **2016**, *602*, 7; c) L. A. Keeling, L. Chen, C. Greenlief, *Surf. Sci.* **1998**, *400*, 1; d) S. Miyajima, Y. Yashiki, A. Yamada, M. Konagai, *Thin Solid Films* **2008**, *516*, 670; e) J. Pola, J. P. Parsons, R. Taylor, *Faraday Trans.* **1992**, *88*, 1637; f) C. Seneza, C. Berger, P. Sana, H. Witte, J. Bläsing, A. Dempewolf, A. Dadgar, J. Christen, A. Strittmatter, *Jpn. J. Appl. Phys.* **2022**, *61*, 15501; g) M. Todd, J. McMurran, J. Kouvetakis, D. J. Smith, *Chem. Mater.* **1996**, *8*, 2491.

[48] a) Y. Kobayashi, Y. Sunada, *Chem. Sci.* **2023**, *14*, 1065; b) M. G. Voronkov, K. A. Abzaeva in *PATAI'S Chemistry of Functional Groups*, *Vol. 1* (Ed.: S. Patai), Wiley, **1975**, pp. 1–130.

[49] E. Voegelen, *Z. Anorg. Chem.* **1902**, *30*, 325.

[50] C. A. Kraus, E. A. Flood, *J. Am. Chem. Soc.* **1932**, *54*, 1635.

[51] a) S. N. Glarum, C. A. Kraus, *J. Am. Chem. Soc.* **1950**, *72*, 5398; b) G. K. Teal, C. A. Kraus, *J. Am. Chem. Soc.* **1950**, *72*, 4706.

[52] A. E. Finholt, A. C. Bond, H. I. Schlesinger, *J. Am. Chem. Soc.* **1947**, *69*, 1199.

[53] a) O. H. Johnson, W. H. Nebergall, *J. Am. Chem. Soc.* **1949**, *71*, 1720; b) O. H. Johnson, D. M. Harris, *J. Am. Chem. Soc.* **1950**, *72*, 5564; c) R. J. Cross, F. Glockling, *J. Organomet. Chem.* **1965**, *3*, 146; d) F. E. Brinckman, F. Stone, *J. Inorg. Nucl. Chem.* **1959**, *11*, 24; e) R. Fuchs, H. Gilman, *J. Org. Chem.* **1958**, *23*, 911; f) R. West, *J. Am. Chem. Soc.* **1952**, *74*, 4363.

[54] R. J. Cross, F. Glockling, *J. Chem. Soc.* **1964**, 4125.

[55] A. Torvisco, F. Uhlig, D. Scheschkewitz in *Smart Inorganic Polymers* (Eds.: E. Hey-Hawkins, M. Hissler), Wiley, **2019**, pp. 61–84.

[56] M. G. Voronkov, A. N. Egorochkin in *PATAI'S Chemistry of Functional Groups*, *Vol. 1* (Ed.: S. Patai), Wiley, **1975**, pp. 131–168.

[57] J. R. Durig, J. B. Turner, *J. Phys. Chem.* **1972**, *76*, 1558.

[58] P. Rivière, M. Rivière-Baudet, A. Castel, J. Satgé, E. A. Lavabre, *Synth. React. Inorg. Met.-Org. Chem.* **1987**, *17*, 539.

[59] a) M. L. Amadoruge, J. A. Golen, A. L. Rheingold, C. S. Weinert, *Organometallics* **2008**, *27*, 1979; b) H. Arii, N. Watanabe, K. Mochida, T. Kawashima, *Eur. J. Inorg. Chem.* **2012**, *2012*, 4791; c) S.-J. Hsiang, P. G. Hayes, *Chemistry* **2024**, *30*, e202302925; d) S. P. Komanduri, F. A. Shumaker, S. A. Hallenbeck, C. J. Knight, C. H. Yoder, B. A. Buckwalter, C. P. Dufresne, E. J. Fernandez, C. A. Kaffel, R. E. Nazareno et al., *J. Organomet. Chem.* **2017**, *848*, 104.

[60] A. Castel, P. Rivière, J. Satgé, D. Desor, *J. Organomet. Chem.* **1992**, *433*, 49.

[61] W. Lin, L. You, W. Yuan, C. He, *ACS Catal.* **2022**, *12*, 14592.

[62] J. M. Meyer, A. L. Allred, *J. Phys. Chem.* **1968**, *72*, 3043.

[63] Vo-Kim-Yen, Z. Papoušková, J. Schraml, V. Chvalovský, *Collect. Czech. Chem. Commun.* **1973**, *38*, 3167.

[64] M. N. Bochkarev, L. P. Maiorova, S. P. Korneva, L. N. Bochkarev, N. S. Vyazankin, *J. Organomet. Chem.* **1974**, *73*, 229.

[65] S. E. Skobeleva, A. N. Egorochkin, S. Khorshev, S. Ratushnaya, P. Rivière, J. Satgé, S. Richelme, A. Cazes, *J. Organomet. Chem.* **1979**, *182*, 1.

[66] F. Cosledan, A. Castel, P. Rivière, J. Satgé, M. Veith, V. Huch, *Organometallics* **1998**, *17*, 2222.

[67] M. Unno, Y. Kawai, H. Matsumoto, *Heteroat. Chem.* **2001**, *12*, 238.

[68] G. H. Spikes, J. C. Fettinger, P. P. Power, *J. Am. Chem. Soc.* **2005**, *127*, 12232.

[69] T. Matsumoto, Y. Matsui, M. Ito, K. Tatsumi, *Chem. - Asian J.* **2008**, *3*, 607.

[70] F. Diab, F. S. W. Aicher, C. P. Sindlinger, K. Eichele, H. Schubert, L. Wesemann, *Chemistry* **2019**, *25*, 4426.

[71] K. V. Zaitsev, Y. F. Oprunenko, A. V. Churakov, G. S. Zaitseva, S. S. Karlov, *Main Group Met. Chem.* **2014**, *37*.

[72] C. A. Kraus, W. K. Nelson, *J. Am. Chem. Soc.* **1934**, *56*, 195.

[73] J. G. Milligan, C. A. Kraus, *J. Am. Chem. Soc.* **1950**, *72*, 5297.

[74] H. Gilman, C. W. Gerow, *J. Am. Chem. Soc.* **1955**, *77*, 4675.

[75] E. J. Spanier, A. G. MacDiarmid, *Inorg. Chem.* **1963**, *2*, 215.

[76] a) H. Bürger, U. Goetze, *Angew. Chem. Int. Ed. Engl.* **1968**, *7*, 212; b) F. Fehér, P. Plichta, R. Guillery, *Tetrahedron Lett.* **1970**, *11*, 4443; c) M. Kumada, T. Kondo, K. Mimura, M. Ishikawa, K. Yamamoto, S. Ikeda, M. Kondo, *J. Organomet. Chem.* **1972**, *43*, 293; d) A. G. Brook, F. Abdesaken, H. Söllradl, *J. Organomet. Chem.* **1986**, *299*, 9; e) S. P. Mallela, Y. Saar, S. Hill, R. A. Geanangel, *Inorg. Chem.* **1999**, *38*, 2957.

[77] L.-C. Pop, N. Kurokawa, H. Ebata, K. Tomizawa, T. Tajima, M. Saito, *Eur. J. Inorg. Chem.* **2017**, *2017*, 4969.

[78] M. Nanjo, T. Oda, K. Mochida, *J. Organomet. Chem.* **2003**, *672*, 100.

[79] M. Ishifune, S. Kashimura, Y. Kogai, Y. Fukuhara, T. Kato, H.-B. Bu, N. Yamashita, Y. Murai, H. Murase, R. Nishida, *J. Organomet. Chem.* **2000**, *611*, 26.

[80] a) C. Drost, P. B. Hitchcock, M. F. Lappert, *Organometallics* **2002**, *21*, 2095; b) M. Kira, T. Iwamoto, S. Ishida, H. Masuda, T. Abe, C. Kabuto, *J. Am. Chem. Soc.* **2009**, *131*, 17135; c) Y. Suzuki, T. Sasamori, J.-D. Guo, N. Tokitoh, *Chemistry* **2018**, *24*, 364.

[81] T. J. Barton, C. R. Tully, *J. Org. Chem.* **1978**, *43*, 3649.

[82] L. J. Tyler, L. H. Sommer, F. C. Whitmore, *J. Am. Chem. Soc.* **1947**, *69*, 981.

[83] L. H. Sommer, L. J. Tyler, *J. Am. Chem. Soc.* **1954**, *76*, 1030.

[84] H. K. Sharma, F. Cervantes-Lee, L. Párkányi, K. H. Pannell, *Organometallics* **1996**, *15*, 429.

[85] a) T. Iwamoto, J. Okita, C. Kabuto, M. Kira, *J. Am. Chem. Soc.* **2002**, *124*, 11604; b) T. Iwamoto, D. Yin, S. Boomgaarden, C. Kabuto, M. Kira, *Chem. Lett.* **2008**, *37*, 520; c) M. Kira, T. Iwamoto, T. Maruyama, C. Kabuto, H. Sakurai, *Organometallics* **1996**, *15*, 3767.

[86] M. P. Doyle, C. T. West, *J. Am. Chem. Soc.* **1975**, *97*, 3777.

[87] N. Wiberg, C.-K. Kim, *Chem. Ber.* **1986**, *119*, 2980.

[88] W. Uhlig, *J. Organomet. Chem.* **1991**, *409*, 377.

[89] a) V. Y. Lee, Y. Ito, O. A. Gapurenko, R. M. Minyaev, H. Gornitzka, A. Sekiguchi, *J. Am. Chem. Soc.* **2020**, *142*, 16455; b) V. Y. Lee, Y. Ito, O. A. Gapurenko, A. Sekiguchi, V. I. Minkin, R. M. Minyaev, H. Gornitzka, *Angew.*

*Chem. Int. Ed. Engl.* **2015**, *54*, 5654; c) V. Y. Lee, Y. Ito, H. Yasuda, K. Takanashi, A. Sekiguchi, *J. Am. Chem. Soc.* **2011**, *133*, 5103; d) V. Y. Lee, H. Yasuda, M. Ichinohe, A. Sekiguchi, *Angew. Chem. Int. Ed.* **2005**, *44*, 6378; e) A. Sekiguchi, R. Izumi, S. Ihara, M. Ichinohe, V. Y. Lee, *Angew. Chem. Int. Ed.* **2002**, *41*, 1598.

[90] V. Y. Lee, M. Ichinohe, A. Sekiguchi, N. Takagi, S. Nagase, *J. Am. Chem. Soc.* **2000**, *122*, 9034.

[91] K. McNeice, V. Y. Lee, A. Sekiguchi, *Organometallics* **2011**, *30*, 4796.

[92] J. H. Warner, R. D. Tilley, *Nanotechnology* **2006**, *17*, 3745.

[93] J. P. Wilcoxon, P. P. Provencio, G. A. Samara, *Phys. Rev. B* **2001**, *64*.

[94] R. Hayashi, M. Yamamoto, K. Tsunetomo, K. Kohno, Y. Osaka, H. Nasu, *Jpn. J. Appl. Phys.* **1990**, *29*, 756.

[95] Y. Nakamura, K. Watanabe, Y. Fukuzawa, M. Ichikawa, *Appl. Phys. Lett.* **2005**, *87*.

[96] D. A. Ruddy, J. C. Johnson, E. R. Smith, N. R. Neale, *ACS Nano* **2010**, *4*, 7459.

[97] S. Takeoka, M. Fujii, S. Hayashi, K. Yamamoto, *Phys. Rev. B* **1998**, *58*, 7921.

[98] S. Prabakar, A. Shiohara, S. Hanada, K. Fujioka, K. Yamamoto, R. D. Tilley, *Chem. Mater.* **2010**, *22*, 482.

[99] T. N. Lambert, N. L. Andrews, H. Gerung, T. J. Boyle, J. M. Oliver, B. S. Wilson, S. M. Han, *Small* **2007**, *3*, 691.

[100] G. S. Armatas, M. G. Kanatzidis, *Nano Lett.* **2010**, *10*, 3330.

[101] a) P. C. Joshi, A. T. Voutsas, US2009217968 (A1), **5/18/2009**; b) Z. C. Holman, C.-Y. Liu, U. R. Kortshagen, *Nano Lett.* **2010**, *10*, 2661.

[102] D.-J. Xue, J.-J. Wang, Y.-Q. Wang, S. Xin, Y.-G. Guo, L.-J. Wan, *Adv. Mater. (Weinheim, Ger.)* **2011**, *23*, 3704.

[103] a) Y.-H. Ma, C.-P. Huang, J.-S. Tsai, M.-Y. Shen, Y.-K. Li, L.-Y. Lin, *Toxicol. Lett.* **2011**, *207*, 258; b) H. Yin, H.-H. Cai, J.-Y. Cai, J.-W. Teng, P. Yang, *Mater. Lett.* **2013**, *109*, 108.

[104] S. Bhattacharjee, I. M. C. M. Rietjens, M. P. Singh, T. M. Atkins, T. K. Purkait, Z. Xu, S. Regli, A. Shukaliak, R. J. Clark, B. S. Mitchell et al., *Nanoscale* **2013**, *5*, 4870.

[105] B. F. P. McVey, S. Prabakar, J. J. Gooding, R. D. Tilley, *Chempluschem* **2017**, *82*, 60.

[106] G. Shao, D. A. H. Hanaor, J. Wang, D. Kober, S. Li, X. Wang, X. Shen, M. F. Bekheet, A. Gurlo, *ACS Appl. Mater. Interfaces* **2020**, *12*, 46045.

[107] a) C. K. Chan, X. F. Zhang, Y. Cui, *Nano Lett.* **2008**, *8*, 307; b) S. Fugattini, U. Gulzar, A. Andreoli, L. Carbone, M. Boschetti, P. Bernardoni, M. Gjestila, G. Mangherini, R. Camattari, T. Li et al., *Electrochim. Acta* **2022**, *411*, 139832; c) H. Liu, T. Wu, L. Zhang, X. Wang, H. Li, S. Liu, Q. Zhang, X. Zhang, H. Yu, *ACS Nano* **2022**, *16*, 14402; d) M.-H. Park, K. Kim, J. Kim, J. Cho, *Adv. Mater. (Weinheim, Ger.)* **2010**, *22*, 415; e) D.-J. Xue, S. Xin, Y. Yan, K.-C. Jiang, Y.-X. Yin, Y.-G. Guo, L.-J. Wan, *J. Am. Chem. Soc.* **2012**, *134*, 2512.

[108] a) S. Sato, T. Ikeda, K. Hamada, K. Kimura, *Solid State Commun.* **2009**, *149*, 862; b) J. Liu, C. Liang, Z. Tian, S. Zhang, G. Shao, *Sci. Rep.* **2013**, *3*.

[109] J. Hecht, J. D. Eversole, H. P. Broida, *J. Appl. Phys. (Melville, NY, U. S.)* **1977**, *48*, 1503.

[110] Y. Saito, S. Yatsuya, K. Mihama, R. Uyeda, *Jpn. J. Appl. Phys.* **1978**, *17*, 291.

[111] a) T. Imura, M. Tashiro, T. Ohbiki, H. Terauchi, A. Hiraki, K. Tsuji, S. Minomura, *Jpn. J. Appl. Phys.* **1983**, *22*, L505; b) K. Kohno, T. Nakashita, T. Iwaoka, T. Imura, Y. Osaka, *Jpn. J. Appl. Phys.* **1984**, *23*, L674; c) S. Hayashi, M. Fujii, K. Yamamoto, *Jpn. J. Appl. Phys.* **1989**, *28*, L1464.

[112] a) Y. Maeda, N. Tsukamoto, Y. Yazawa, Y. Kanemitsu, Y. Masumoto, *Appl. Phys. Lett.* **1991**, *59*, 3168; b) Y. Kanemitsu, H. Uto, Y. Masumoto, Y. Maeda, *Appl. Phys. Lett.* **1992**, *61*, 2187.

[113] X.-X. Qu, K.-J. Chen, X.-F. Huang, Z.-F. Li, D. Feng, *Appl. Phys. Lett.* **1994**, *64*, 1656.

[114] J. R. Heath, J. J. Shiang, A. P. Alivisatos, *J. Chem. Phys.* **1994**, *101*, 1607.

[115] a) D. C. Lee, J. M. Pietryga, I. Robel, D. J. Werder, R. D. Schaller, V. I. Klimov, *J. Am. Chem. Soc.* **2009**, *131*, 3436; b) H. W. Chiu, S. M. Kauzlarich, *Chem. Mater.* **2006**, *18*, 1023; c) E. Muthuswamy, A. S. Iskandar, M. M. Amador, S. M. Kauzlarich, *Chem. Mater.* **2013**, *25*, 1416; d) E. Fok, M. Shih, A. Meldrum, J. G. C. Veinot, *Chem. Commun. (Cambridge, U. K.)* **2004**, 386.

[116] a) H. Gerung, S. D. Bunge, T. J. Boyle, C. J. Brinker, S. M. Han, *Chem. Commun. (Cambridge, U. K.)* **2005**, 1914; b) D. Gerion, N. Zaitseva, C. Saw, M. F. Casula, S. Fakra, T. van Buuren, G. Galli, *Nano Lett.* **2004**, *4*, 597; c) X. Lu, B. A. Korgel, K. P. Johnston, *Nanotechnology* **2005**, *16*, S389-94.

[117] N. Zaitseva, Z. R. Dai, C. D. Grant, J. Harper, C. Saw, *Chem. Mater.* **2007**, *19*, 5174.

[118] a) E. J. Henderson, C. M. Hessel, J. G. C. Veinot, *J. Am. Chem. Soc.* **2008**, *130*, 3624; b) E. J. Henderson, M. Seino, D. P. Puzzo, G. A. Ozin, *ACS Nano* **2010**, *4*, 7683; c) H. Yang, X. Yao, X. Wang, S. Xie, Y. Fang, S. Liu, X. Gu, *J. Phys. Chem. B* **2003**, *107*, 13319.

[119] a) X. Ma, F. Wu, S. M. Kauzlarich, *J. Solid State Chem.* **2008**, *181*, 1628; b) R. S. Tanke, S. M. Kauzlarich, T. E. Patten, K. A. Pettigrew, D. L. Murphy, M. E. Thompson, H. W. H. Lee, *Chem. Mater.* **2003**, *15*, 1682; c) B. R. Taylor, S. M. Kauzlarich, G. R. Delgado, H. W. H. Lee, *Chem. Mater.* **1999**, *11*, 2493.

[120] V. Slynchuk, M. Hodas, D. Naglav-Hansen, F. Schreiber, A. Schnepf, *Main Group Met. Chem.* **2021**, *44*, 243.

[121] a) C. J. Scheuermann, *Chem. - Asian J.* **2010**, *5*, 436; b) S. S. Hupp, H. E. Swift, *Ind. Eng. Chem. Prod. Res. Dev.* **1979**, *18*, 117.

[122] J. Pau, A. J. Lough, R. S. Wylie, R. A. Gossage, D. A. Foucher, *Chemistry* **2017**, *23*, 14367.

[123] S. Reischauer, *Master's Thesis*, Graz University of Technology, Graz, **2018**.

[124] I. Ojima, S.-I. Inaba, T. Kogure, Y. Nagai, *J. Organomet. Chem.* **1973**, *55*, C7-C8.

[125] C. Aitken, J. F. Harrod, E. Samuel, *J. Organomet. Chem.* **1985**, *279*, C11-C13.

[126] C. Aitken, J. F. Harrod, A. Malek, E. Samuel, *J. Organomet. Chem.* **1988**, *349*, 285.

[127] a) L. S. Chang, J. Y. Corey, *Organometallics* **1989**, *8*, 1885; b) C. Aitken, J. P. Barry, F. Gauvin, J. F. Harrod, A. Malek, D. Rousseau, *Organometallics* **1989**, *8*, 1732.

[128] N. Choi, M. Tanaka, *J. Organomet. Chem.* **1998**, *564*, 81.

[129] a) S. M. Thompson, U. Schubert, *Inorg. Chim. Acta* **2003**, *350*, 329; b) K. Schittelkopf, R. C. Fischer, S. Meyer, P. Wilfling, F. Uhlig, *Appl. Organomet. Chem.* **2010**, *24*, 897; c) J. Y. Corey, *Chem. Rev. (Washington, DC, U. S.)* **2011**, *111*, 863; d) S. Deeken, S. Proch, E. Casini, H. F. Braun, C. Mechtler, C. Marschner, G. Motz, R. Kempe, *Inorg. Chem.* **2006**, *45*, 1871; e) H. K. Sharma, R. Arias-Ugarte, A. J. Metta-Magana, K. H. Pannell, *Angew. Chem. Int. Ed. Engl.* **2009**, *48*, 6309.

[130] R. Waterman, *Chem. Soc. Rev.* **2013**, *42*, 5629.

[131] W. P. Neumann, K. König, *Justus Liebigs Ann. Chem.* **1964**, *677*, 1.

[132] C. P. Sindlinger, A. Stasch, H. F. Bettinger, L. Wesemann, *Chem. Sci.* **2015**, *6*, 4737.

[133] A. Feigl, I. Chiorescu, K. Deller, S. U. H. Heidsieck, M. R. Buchner, V. Karttunen, A. Bockholt, A. Genest, N. Rösch, B. Rieger, *Chemistry* **2013**, *19*, 12526.

[134] P. Schmid, *Master's Thesis*, Graz University of Technology, Graz, **2020**.

[135] J. E. Drake, W. L. Jolly, *J. Chem. Soc.* **1962**, 2807.

[136] P. C. Angus, S. R. Stobart, *J. Chem. Soc., Chem. Commun.* **1973**, 127a.

[137] A. Marchand, P. Gerval, P. Riviere, J. Satge, *J. Organomet. Chem.* **1978**, *162*, 365.

[138] M. Wolf, *Doctoral Thesis*, Graz University of Technology, Graz, **2017**.

[139] K. B. Clark, D. Griller, *Organometallics* **1991**, *10*, 746.

[140] S. R. Whittleton, R. J. Boyd, T. B. Grindley, *Can. J. Chem.* **2009**, *87*, 974.

[141] M. Traxler, *Master's Thesis*, Graz University of Technology, Graz, **2019**.

[142] A. Torvisco, F. Uhlig in *Organogermanium Compounds* (Ed.: V. Y. Lee), Wiley, **2023**, pp. 277–298.

[143] a) W. Schlenk, W. Schlenk, *Ber. dtsch. Chem. Ges. A/B* **1929**, *62*, 920; b) C. Honacker, Z.-W. Qu, J. Tannert, M. Layh, A. Hepp, S. Grimme, W. Uhl, *Dalton Trans.* **2016**, *45*, 6159.

[144] T. Hafner, A. Torvisco, M. Traxler, M. Wolf, F. Uhlig, *Z. Anorg. Allg. Chem.* **2020**, *646*, 1876.

[145] P. Schmid, K. Bartl, R. Saf, T. Sasamori, V. Y. Lee, F. Uhlig, *Organometallics* **2025**, *44*, 1000.

[146] a) S. Sharma, N. Caballero, H. Li, K. H. Pannell, *Organometallics* **1999**, *18*, 2855; b) H. Basch, *Inorg. Chim. Acta* **1996**, *252*, 265.

[147] a) Y. Goldshtein, Y. Glagovsky, B. Tumanskii, N. Fridman, D. Bravo-Zhivotovskii, Y. Apeloig, *Angew. Chem. Int. Ed.* **2022**, *61*; b) V. Y. Lee, *Eur. J. Inorg. Chem.* **2022**, *2022*; c) V. Y. Lee, K. McNeice, Y. Ito, A. Sekiguchi, *Chem. Commun. (Cambridge, U. K.)* **2011**, *47*, 3272.

[148] V. Y. Lee, M. Ichinohe, A. Sekiguchi, *J. Organomet. Chem.* **2003**, *685*, 168.

[149] V. Y. Lee, H. Yasuda, M. Ichinohe, A. Sekiguchi, *J. Organomet. Chem.* **2007**, *692*, 10.

[150] W. A. Dutton, M. Onyszchuk, *Inorg. Chem.* **1968**, *7*, 1735.

[151] A. Castel, P. Riviere, J. Satge, H. Y. Ko, *Organometallics* **1990**, *9*, 205.

[152] O. H. Johnson, D. M. Harris, *J. Am. Chem. Soc.* **1950**, *72*, 5566.

[153] H. Gilman, C. W. Gerow, *J. Am. Chem. Soc.* **1956**, *78*, 5435.

[154] a) J. K. Simons, *J. Am. Chem. Soc.* **1935**, *57*, 1299; b) T. W. Swaddle, *Doctoral Thesis*, University of Leicester (United Kingdom), England, **1961**.

[155] W. H. Nebergall, *J. Am. Chem. Soc.* **1950**, *72*, 4702.

[156] P. Schmid, B. Bitschnau, M. Finšgar, I. Letofsky-Papst, J. Rattenberger, R. Saf, F. Uhlig, A. Torvisco, *Chemistry* **2024**, *30*, e202401382.

[157] P. Riviere, J. Satge, D. Soula, *J. Organomet. Chem.* **1974**, *72*, 329.

[158] P. Rivière, J. Satgé, *Synth. React. Inorg. Met.-Org. Chem.* **1972**, *2*, 57.

[159] P. Rivière, A. Castel, J. Satgé, *J. Am. Chem. Soc.* **1980**, *102*, 5413.

[160] J.-J. Maudrich, F. Diab, S. Weiß, M. Widemann, T. Dema, H. Schubert, K. M. Krebs, K. Eichele, L. Wesemann, *Inorganic chemistry* **2019**, *58*, 15758.

[161] A. Caise, J. Hicks, A. Heilmann, S. Aldridge, *Chem. Commun. (Cambridge, U. K.)* **2023**, *59*, 7251.

[162] P. Rivière, A. Castel, J. Satgé, D. Guyot, *J. Organomet. Chem.* **1984**, *264*, 193.

[163] a) J. Wang, G. Wang, J. Zhao, *Phys. Rev. B* **2001**, *64*; b) S. Shi, Y. Liu, C. Zhang, B. Deng, G. Jiang, *Comput. Theor. Chem.* **2015**, *1054*, 8; c) Z. Mahdavifar, M. Afshari, A. Bagheri, A. Arab, *Polyhedron* **2021**, *193*, 114874.

[164] T. L. Barr, M. Mohsenian, L. M. Chen, *Applied Surface Science* **1991**, *51*, 71.

[165] a) T. Hanrath, B. A. Korgel, *J. Am. Chem. Soc.* **2004**, *126*, 15466; b) Y. Wang, U. Ramesh, C. K. A. Nyamekye, B. J. Ryan, R. D. Nelson, A. M. Alebri, U. H. Hamdeh, A. Hadi, E. A. Smith, M. G. Panthani, *Chem. Commun.* **2019**, *55*, 6102; c) M. A. Hossain, M. Javadi, H. Yu, A. N. Thiessen, N. Ikpo, A. O. Oliynyk, J. G. C. Veinot, *Nanoscale* **2020**, *12*, 6271.

[166] A. S. Almuslem, A. N. Hanna, T. Yapici, N. Wehbe, E. M. Diallo, A. T. Kutbee, R. R. Bahabry, M. M. Hussain, *Appl. Phys. Lett.* **2017**, *110*.

[167] A. Dopilka, A. Childs, S. Bobev, C. K. Chan, *Chem. Mater.* **2020**, *32*, 9444.

[168] S. Kim, B. Walker, S. Y. Park, H. Choi, S.-J. Ko, J. Jeong, M. H. Yun, J. C. Lee, D. S. Kim, J. Y. Kim, *Nanoscale* **2014**, *6*, 10156.

[169] Bruker, *APEX2 and SAINT*, Bruker ACS Inc., Madison, Wisonsin, USA, **2012**.

[170] G. M. Sheldrick, *CELL_Now*, Universität Göttingen, Germany, **2008**.

[171] a) R. H. Blessing, *Acta Crystallogr., Sect. A:Found. Crystallogr.* **1995**, *51 ( Pt 1)*, 33; b) G. M. Sheldrick, *SADABS, Version 2.10, Siemens Area Detector Correction*, Universität Göttingen, Germany, **2003**.

[172] G. M. Sheldrick, *Acta Crystallogr., Sect. A:Found. Adv.* **2015**, *71*, 3.

[173] a) G. M. Sheldrick, *Acta Crystallogr., Sect. A:Found. Crystallogr.* **1990**, *46*, 467; b) G. M. Sheldrick, *SHELXS97*, Universität Göttingen, Germany, **1997**; c) G. M. Sheldrick, *Acta Crystallogr., Sect. A:Found. Crystallogr.* **2008**, *64*, 112; d) G. M. Sheldrick, *Acta Crystallogr., Sect. C:Struct. Chem.* **2015**, *71*, 3.

[174] C. B. Hübschle, G. M. Sheldrick, B. Dittrich, *J. Appl. Crystallogr.* **2011**, *44*, 1281.

[175] a) A. L. Spek, *J. Appl. Crystallogr.* **2003**, *36*, 7; b) A. L. Spek, *Acta Crystallogr., Sect. D:Biol. Crystallogr.* **2009**, *65*, 148.

[176] C. F. Macrae, I. J. Bruno, J. A. Chisholm, P. R. Edgington, P. McCabe, E. Pidcock, L. Rodriguez-Monge, R. Taylor, J. van de Streek, P. A. Wood, *J. Appl. Crystallogr.* **2008**, *41*, 466.

[177] H. Putz, K. Brandenburg, *Diamond - Crystal and Molecular Structure Visualization*, Crystal Impact, Bonn, Germany.

[178] F. H. Allen, O. Johnson, G. P. Shields, B. R. Smith, M. Towler, *J. Appl. Crystallogr.* **2004**, *37*, 335.

[179] S. P. Westrip, *J. Appl. Crystallogr.* **2010**, *43*, 920.

[180] O. V. Dolomanov, L. J. Bourhis, R. J. Gildea, J. A. K. Howard, H. Puschmann, *J. Appl. Crystallogr.* **2009**, *42*, 339.

[181] F. Menges, *Spectragryph - optical spectroscopy software*, **2020**.

[182] B. L. L. Réant, V. E. J. Berryman, A. R. Basford, L. E. Nodaraki, A. J. Wooles, F. Tuna, N. Kaltsoyannis, D. P. Mills, S. T. Liddle, *J. Am. Chem. Soc.* **2021**, *143*, 9813.

[183] E. J. Corey, H. Cho, C. Rücker, D. H. Hua, *Tetrahedron Lett.* **1981**, *22*, 3455.

# Appendix

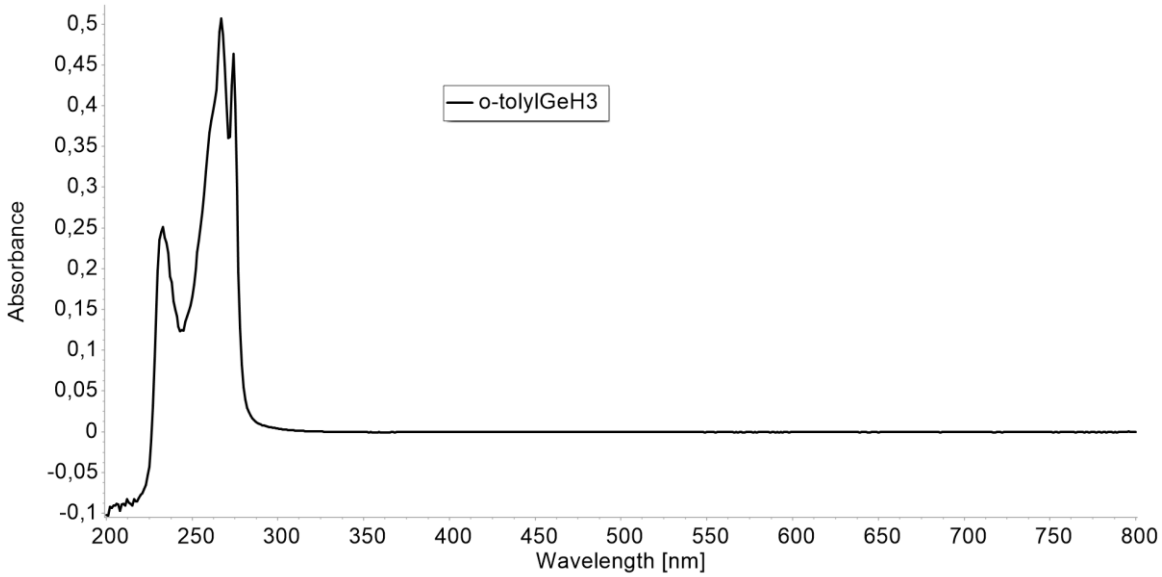


**Figure 51:** UV/Vis spectrum of **3** in THF. c=1.83 mg/L.

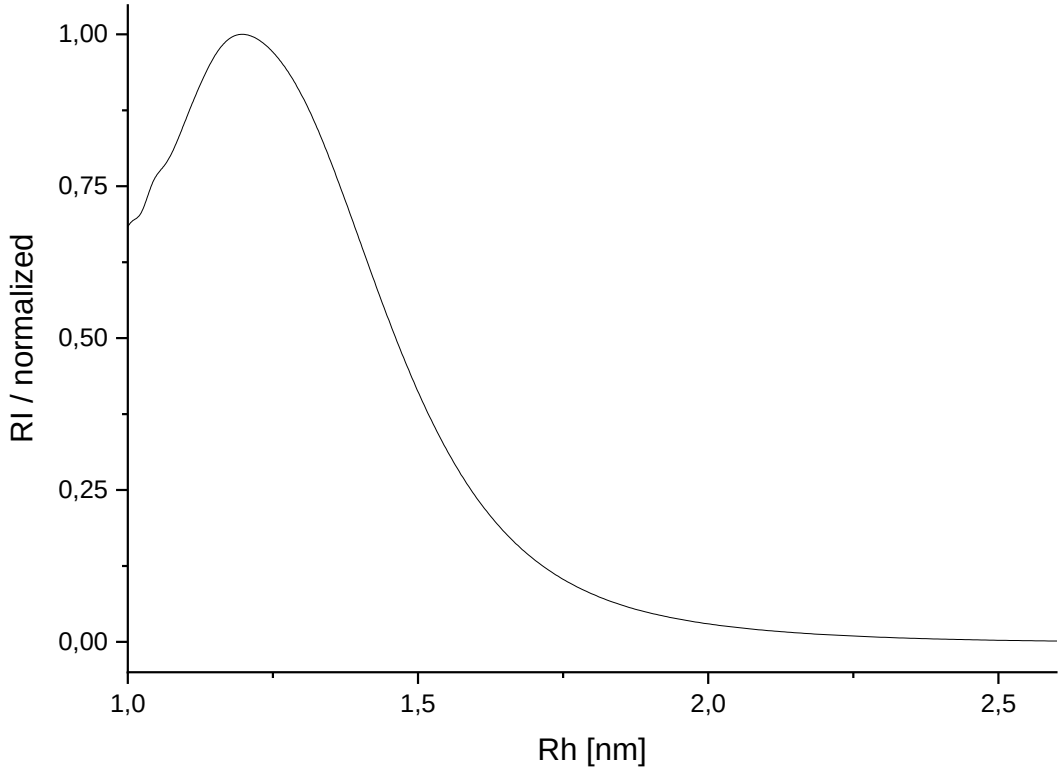


**Figure 52:** GPC elution curve for **27g** dispersed in THF

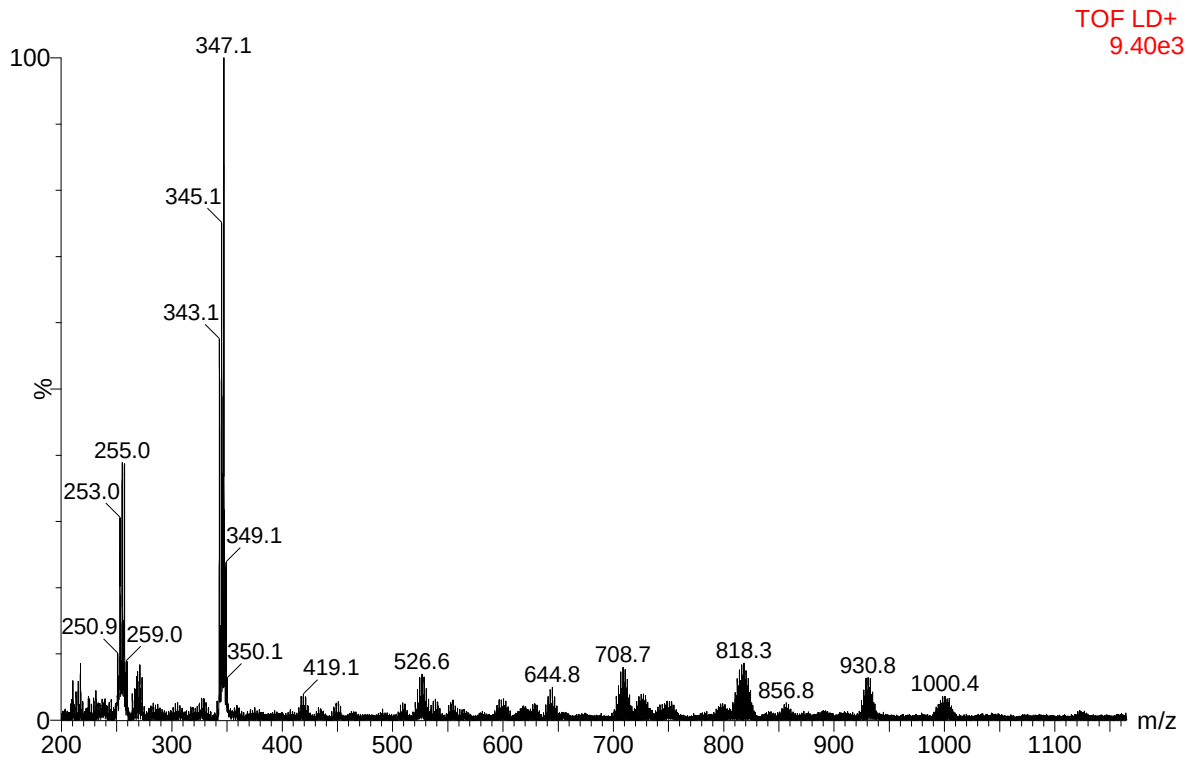


**Figure 53:** Reflectron mode TOF-MS of **27g**

**Table 12:** Crystallographic data and details of measurements for compounds **9** and 7 Mo Kα (λ=0.71073Å). R1= Σ/ |Fo|- |Fc|/|Σ|Fd; wR2 = [Σw(Fo2-F22)2/Σw(Fo2)2]1/2

| **Compound** | **AT1165 - 2,4,6-** | **AT1168 - 2,4,6-mesitylGeH3** |
|---|---|---|
| Formula | $C_9H_{11}Cl_3Ge$ | $C_9H_{14}Ge$ |
| Fw (g $mol^{-1}$) | 298.12 | 194.79 |
| *a* (Å) | 7.0358(6) | 8.1103(8) |
| *b* (Å) | 8.3017(7) | 7.0333(7) |
| *c* (Å) | 10.5145(9) | 8.3740(9) |
| *α* (°) | 73.172(3) | 90 |
| *β* (°) | 75.640(3) | 104.400(4) |
| *γ* (°) | 85.454(3) | 90 |
| *V* ($Å^3$) | 569.46(8) | 462.66(8) |
| *Z* | 2 | 2 |
| Crystal size (mm) | 0.16 × 0.14 × 0.12 | 0.17 × 0.15 × 0.09 |
| Crystal habit | Block, colourless | Block, colourless |
| Crystal system | Triclinic | Monoclinic |
| Space group | *P*-1 | $P2_1/m$ |
| $d_{calc}$ ( Mg $m^{-3}$) | 1.739 | 1.398 |
| *μ* ($mm^{-1}$) | 3.35 | 3.24 |
| *T* (K) | 100(2) | 100(2) |
| 2*θ* range (°) | 2.6–33.2 | 2.5–33.3 |
| *F*(000) | 296 | 200 |
| $T_{min}$, $T_{max}$ | 0.550, 0.747 | 0.622, 0.747 |
| $R_{int}$ | 0.047 | 0.076 |
| No. of measured, independent and observed [$I > 2\sigma(I)$] reflections | 51532, 4332, 4172 | 14507, 871, 841 |
| independent reflections | 4332 | 871 |
| No. of parameters, | 121, 0 | 95, 2 |
| Δρmax, Δρmin(e $Å^{-3}$) | 0.79, -0.43 | 0.50, -0.60 |
| R1, wR2 (all data) | R1 = 0.0183<br>wR2 = 0.0465 | R1 = 0.0301<br>wR2 = 0.0807 |
| R1, wR2 (>2*σ*) | R1 = 0.0171<br>wR2 = 0.0458 | R1 = 0.0294<br>wR2 = 0.0799 |

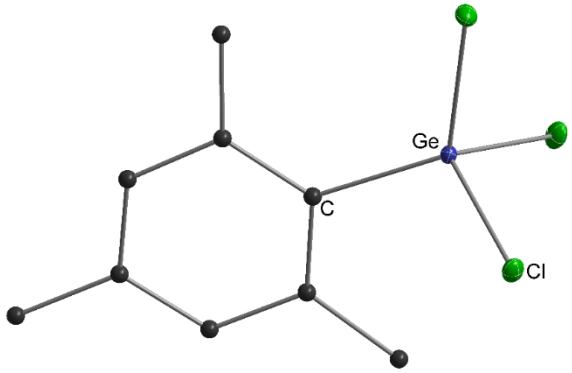


**Figure 54:** Crystal structure diagram for **9**. All non-carbon atoms shown as 30% shaded ellipsoids. Hydrogen atoms omitted for clarity.

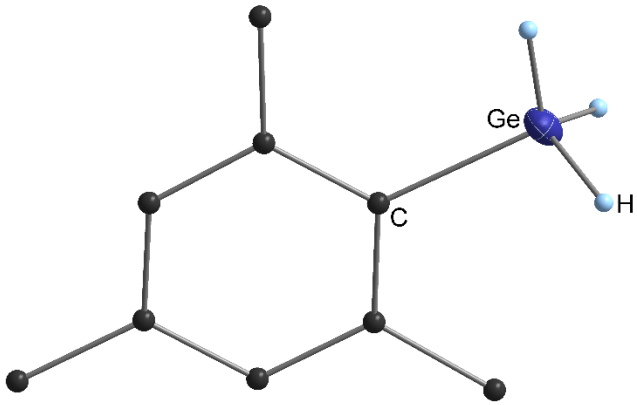


**Figure 55:** Crystal structure diagram for **7**. All non-carbon atoms shown as 30% shaded ellipsoids. Hydrogen atoms not metal-bound omitted for clarity.

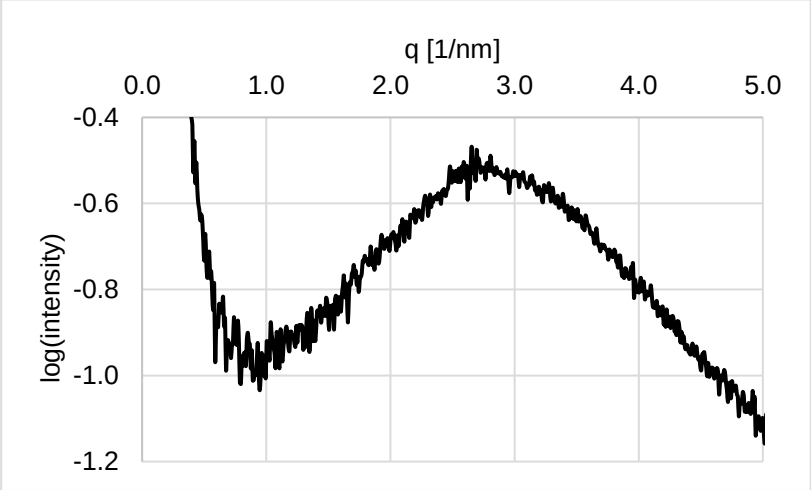


**Figure 56:** Powder SAXS curve of **25d**

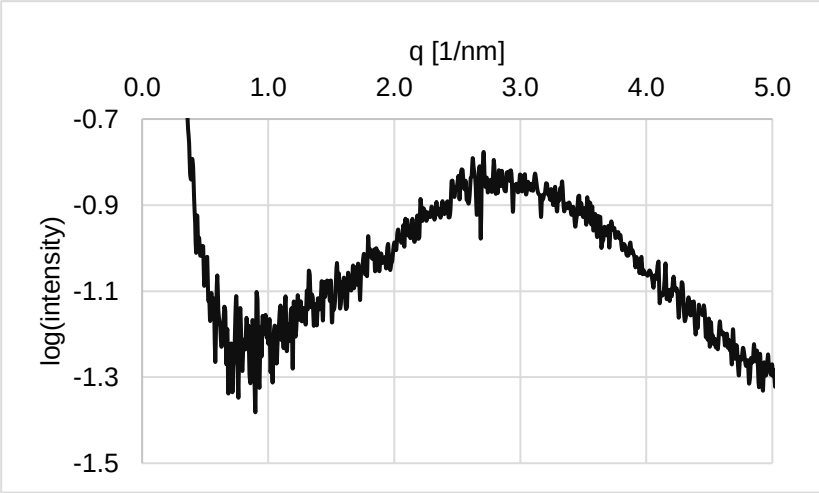


**Figure 57:** Powder SAXS curve of **25e**

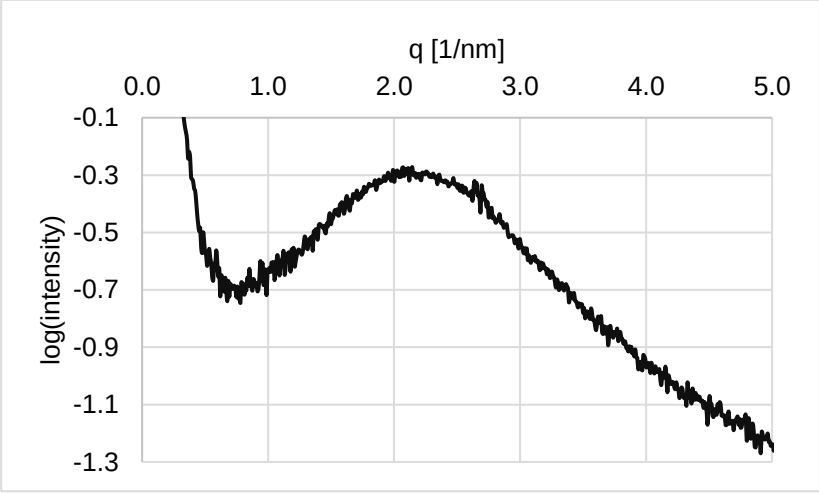


**Figure 58:** Powder SAXS curve of **25f**

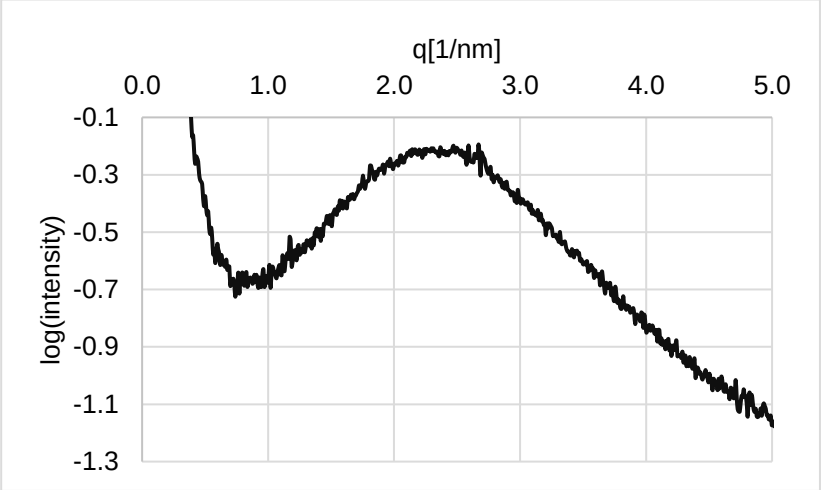


**Figure 59:** Powder SAXS curve of **25g**

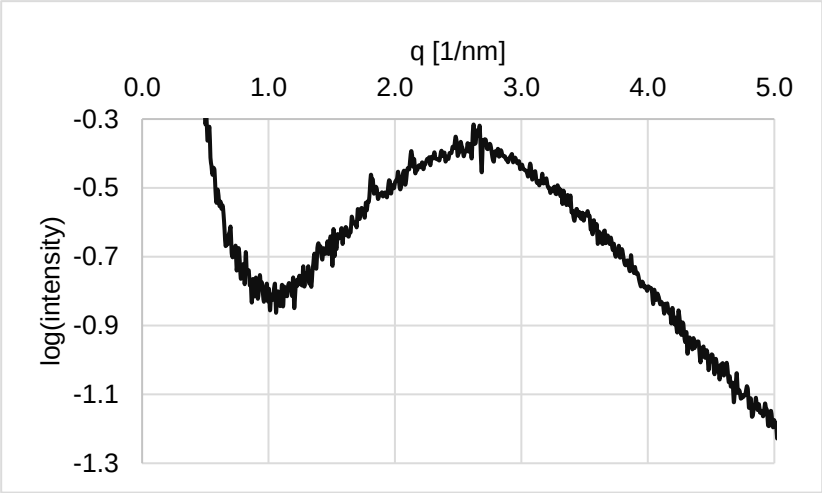


**Figure 60:** Powder SAXS curve of **25h**

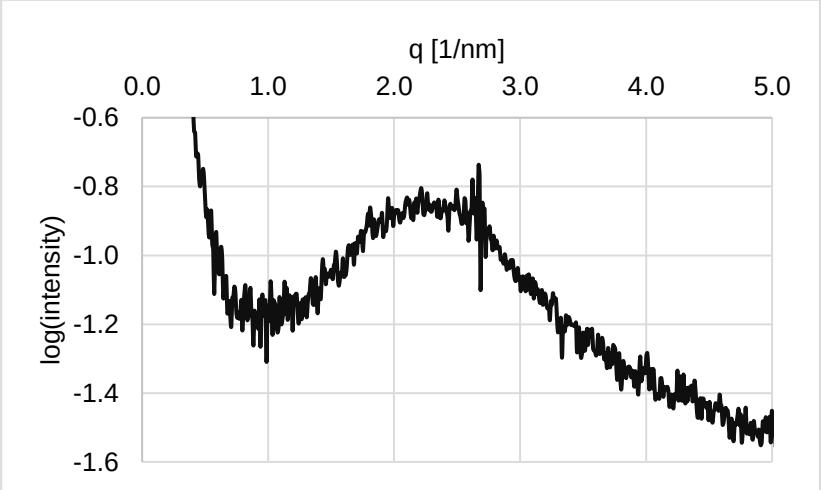


**Figure 61:** Powder SAXS curve of **25i**

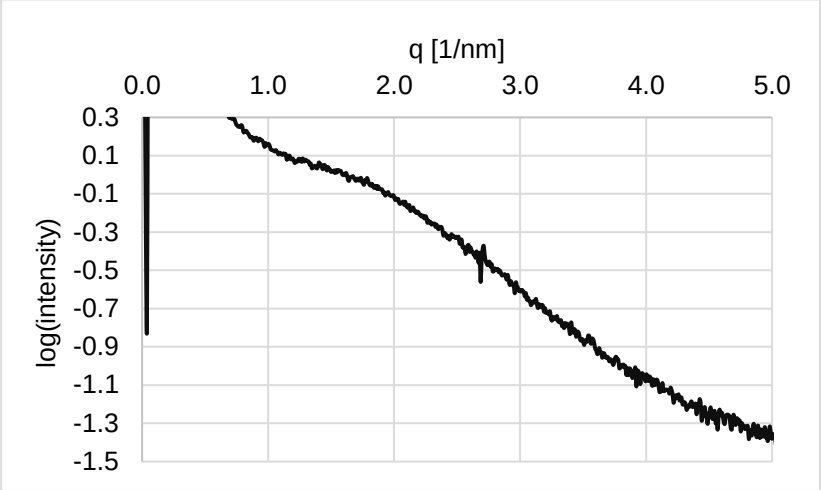


**Figure 62:** Powder SAXS curve of **26a**

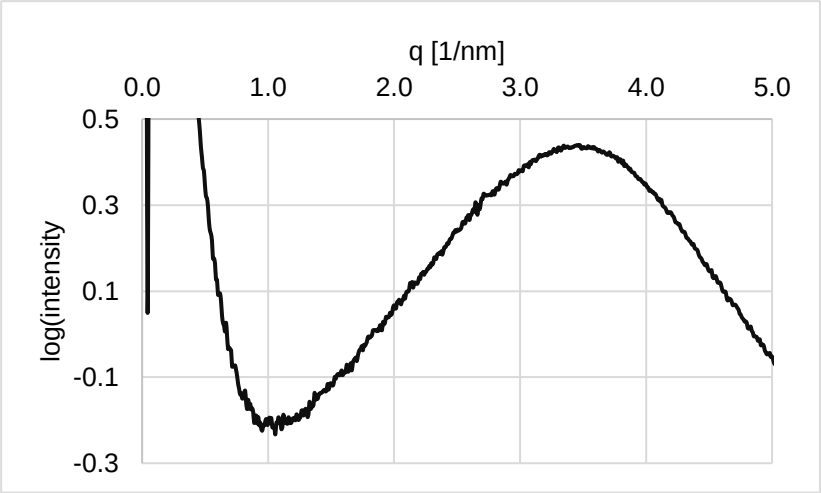


**Figure 63:** Powder SAXS curve of **27b**

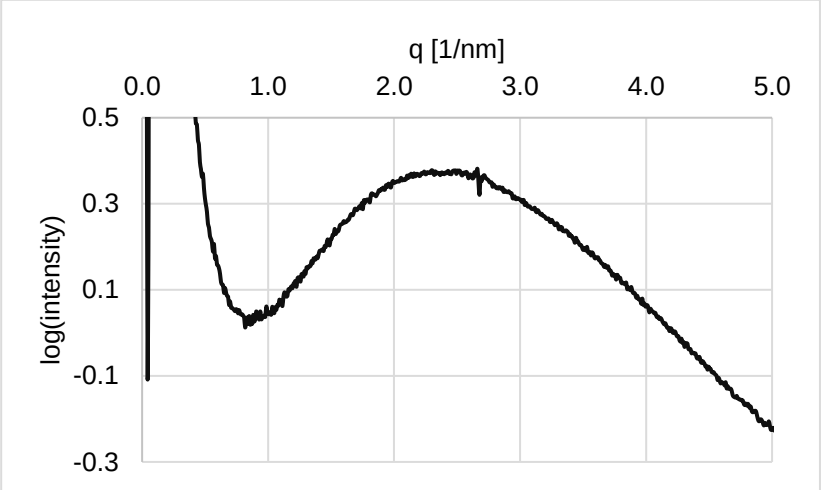


**Figure 64:** Powder SAXS curve of **27d**

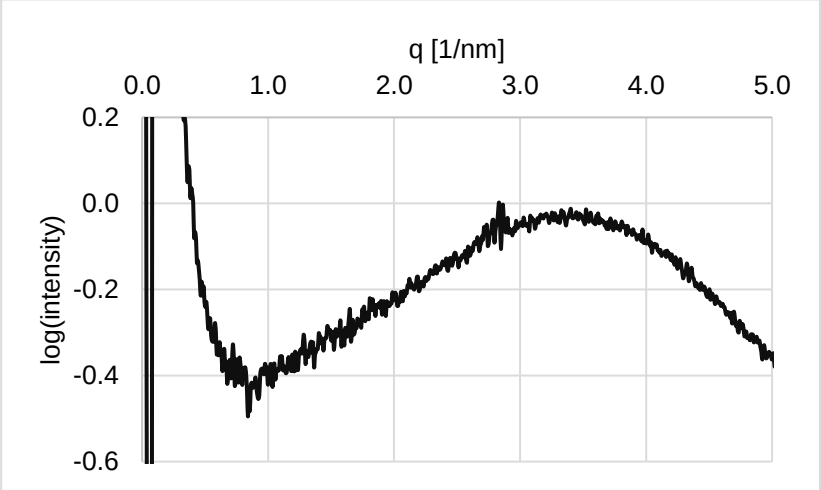


**Figure 65:** Powder SAXS curve of **27e$_{120}$**

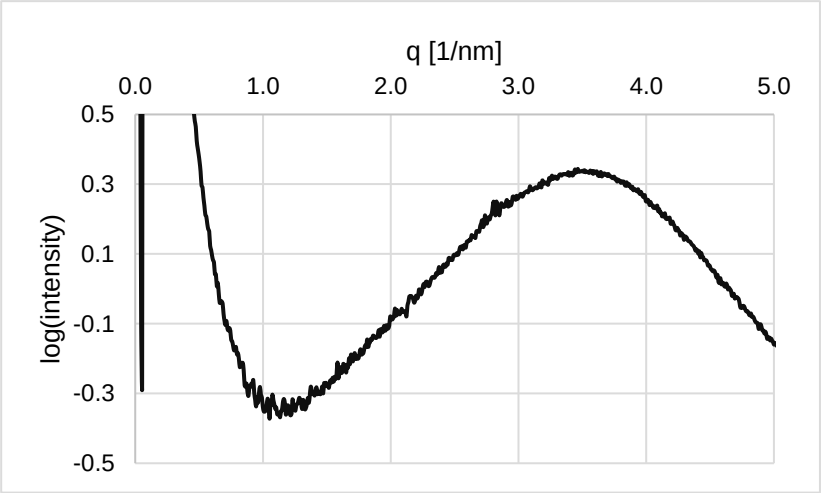


**Figure 66:** Powder SAXS curve of **27f**

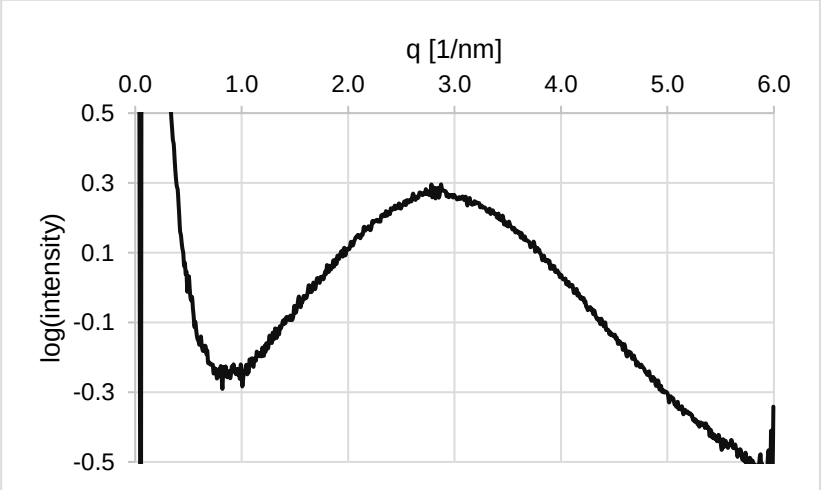


**Figure 67:** Powder SAXS curve of **28a**

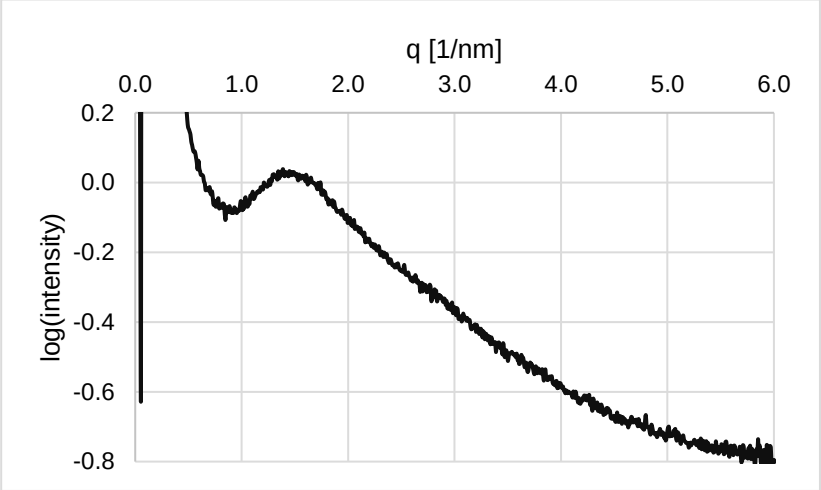


**Figure 68:** Powder SAXS curve of **28b**

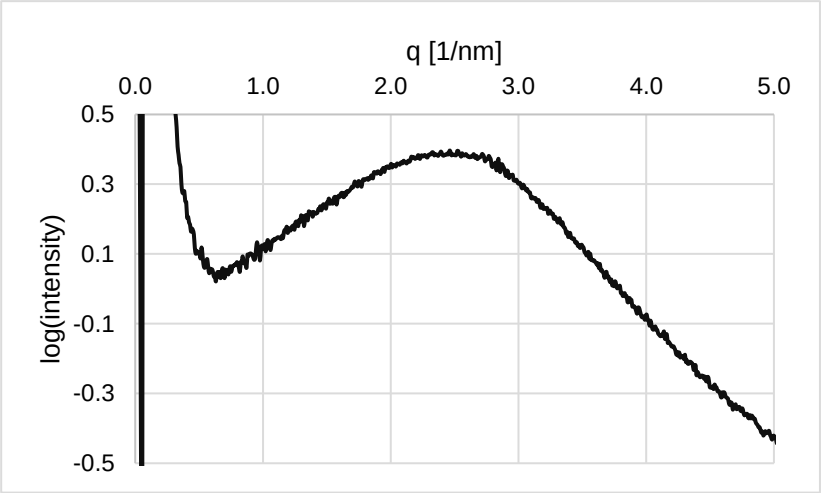


**Figure 69:** Powder SAXS curve of **29a**

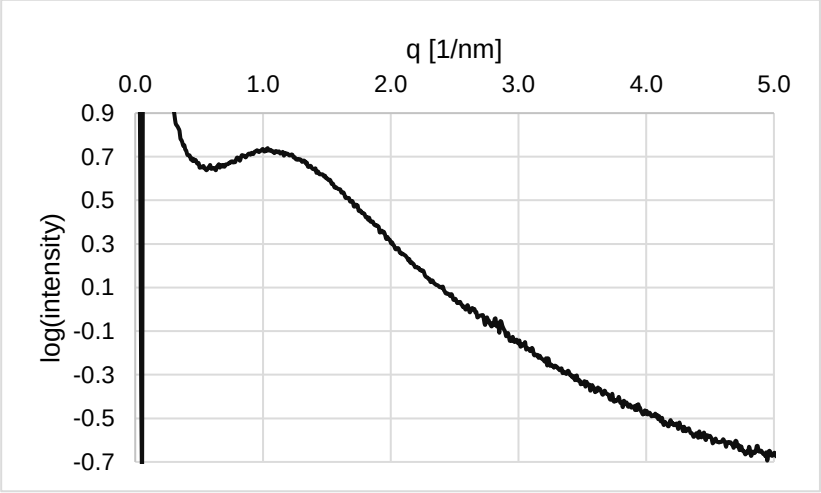


**Figure 70:** Powder SAXS curve of **29b**

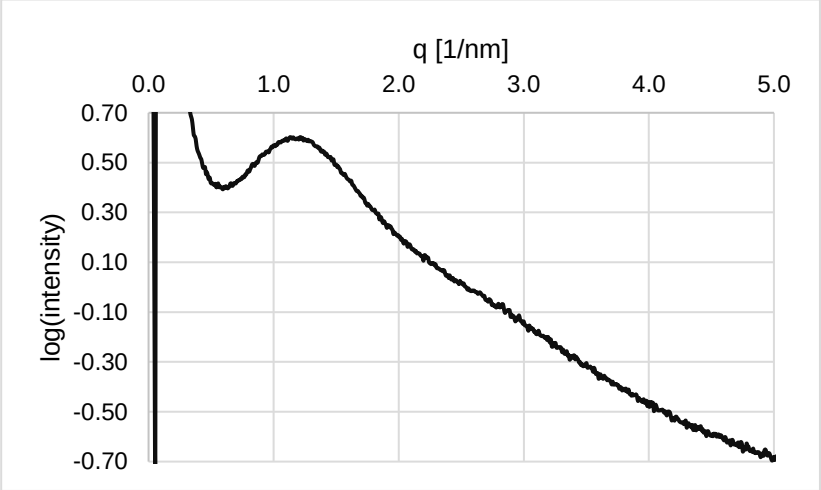


**Figure 71:** Powder SAXS curve of **29d**

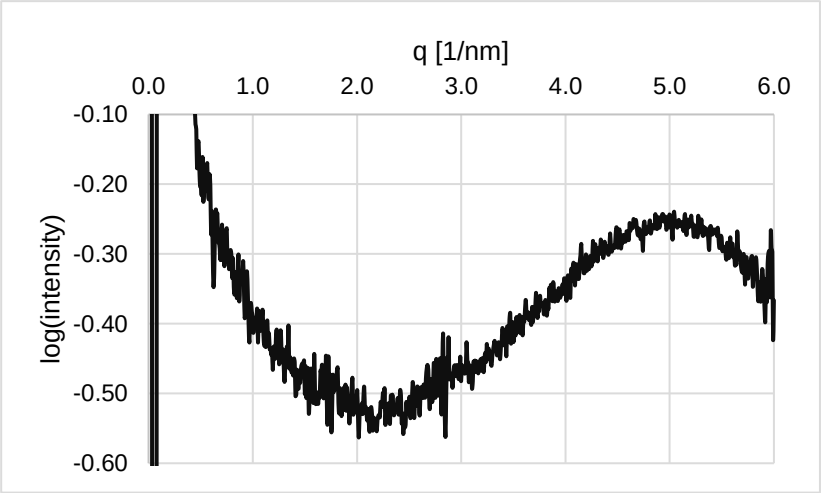


**Figure 72:** Powder SAXS curve of **27e$_{120}$** after etching with $H_2O_2$